Contributions to Network Planning and Operation of Flex-Grid/SDM Optical Core Networks

by

Rubén Rumipamba-Zambrano

A thesis submitted in fulfillment for the degree of Doctor of Philosophy

in the

Broadband Communications Research Group (CBA)

Computer Architecture Department (DAC)

February 2019

Contents

List of Figures

List of Tables

Abbreviations and Symbols

Abbreviations

ACO	Ant Colony Optimization
A/D	Add/Drop
ASE	Amplified Spontaneous Emission
AWG	Arrayed Waveguide Grating
AoD	Architecture on Demand
B&S	Broadcast-and-Select
BBP	Bandwidth Blocking Probability
BLSA	Balanced Load Spectrum Allocation
BV-OXC	Bandwidth Variable Optical Cross Connect
BVT	Bandwidth Variable Transponder
BF	Best-Fit
CapEx	Capital Expenditures
DAC	Digital-to-Analog Converter
DCN	Data Center Networks
DP	Dual-Polarization
DSDM	Dense Space Division Multiplexing
DSP	Digital Signal Processing
DT12	12-node Deutsche Telekom Optical Network
EDFA	Erbium-doped Fiber Amplifier
EGN	Enhanced Gaussian noise
EON	Elastic Optical Network
EON16	16-node European Optical Network
e2e-grooming	end-to-end spatial traffic grooming
F	Set of frequency slots per spatial channel
FF	First-Fit
FEC	Forward Error Correction
FJoS	Fractional Joint Switching
FMF	Few-Mode Fiber
FM-MCF	Few-Mode Multi-Core Fiber
FNB	Fully Non-Blocking
FS	Frequency Slot
FSA	Full Space Assignment
GB	Guard Band

GN	Gaussian noise
GER	50-node GERmany optical network
GoS	Grade-of-Service
GMPLS	Generalized Multi-protocol Label Switching
GRASP	Greedy Randomized Adaptive Search Procedure
HT	Holding Time
IAT	Inter-Arrival Time
ICXT	Inter-Core crosstalk
ILS	Iterated Local Search
InS with LC	Independent Switching with Lane Change support
InS w/o LC	Independent switching without Lane Change support
I2	Internet 2
JoS	Joint Switching
L	Offered Load
LC	Lane Change
LISA	Lowest Indexed Spectrum Allocation
LF	Last-Fit
LS	Local Search
MC	Multi-Carrier
MCF	Multi-Core Fiber
MIMO	Multiple-Input Multiple-Output
MF	Multi-Fiber
MMF	Multi-Mode Fiber
MRSA	Maximum Reuse Spectrum Allocation
NETCONF	Network Configuration
NFDM	Non-linear Frequency-Division Multiplexed
NLI	Non-Linear Interference
NP	Non-deterministic Polynomial
NSF15	15-node National Science Foundation optical network
NWDM	Nyquist-Wavelength Division Multiplexing
OAM	Operation, Administration, and Maintenance
OC	Optical Carrier
OpEx	Operational Expenditures
OSNR	Optical Signal-to-Noise-Ratio
PM	Polarization Multiplexing
POL	12-node POLand optical network

PON	Passive Optical Network
PSA	Partial Space Assignment
RA	Resource Allocation
RF	Random-Fit
R&S	Route-and-Select
ROADM	Reconfigurable Optical Add Drop Multiplexer
RMMSA	Route, Modulation Format, MIMO, Space and Spectrum Assignment
RMSSA	Route, Modulation Format, Space and Spectrum Assignment
RSA	Route, Spectrum Assignment
RSSA	Route, Space and Spectrum Assignment
RTSSA	Route, Transponder, Space and Spectrum Assignment
RWA	Routing and Wavelength Assignment
SA	Simulated Annealing
Sb-Ch	Sub-Channel
SC	Single-Carrier
SCC	Space Continuity Constraint
SCh	Super-Channel
SDM	Space Division Multiplexing
SDM-ROADM	SDM-capable ROADM
SDN	Software Defined Networks
SE	Spectral Efficiency
SMF	Single Mode Fiber
SNR	Signal-to-Noise-Ratio
SP	Shortest Path
Spa-SCh	Spatial Super-Channel
Spe-SCh	Spectral Super-Channel
S2-SCh	Spectral-Spatial Super-Channel
SP	Shortest Path
SS-FON	Spectrally-Spatially Flexible Optical Network
SSS	Spectrum Selective Switch
TP	Traffic Profile
TR	Transmission Reach
TRx	Transceiver
TS	Tabu Search

T7S	Top 7 Spain
US26	26-node US Optical Network
WDM	Wavelength Division Multiplexing
WSSA	Weighted Spectral and Spatial Allocation
YANG	Yet Another Next Generation

Symbols

α	Weighting parameter in WSSA method
α_i	Highest α which yields the same throughput as $\alpha = 0$
α_{opt}	Weighting parameter which yields the highest throughput
b	Function that weights spectral and spatial resources
β	Set of b values
d	Demand
$\mathcal{D}$	Set of demands d
Δ_f	Bandwidth per spatial channel necessary to allocate an Spa-SCh, including guard-bands
Δ_{f_c}	Central frequency granularity
Δ_{Sb}	Sb-Ch spectral width (occupied bandwidth per Sb-Ch)
e	Network link
$\mathcal{E}$	Set of unidirectional network links e
$\mathcal{F}$	Set of frequency slots
f_c	Central frequency
γ	Cooling rate
G	Size of group of spatial channels for FJoS
h_p	Number of hops of path p
K	Number of candidate physical paths over which a lightpath can be established
$\mathcal{L}_e$	Lightpaths traversing link e
$\mathcal{L}_e^f$	Lightpaths traversing link e and using FS f
lp	Lightpath
Lp	Set of active lightpaths
$Lp_{s,t}$	Set of active lightpaths with source node s and destination node t
M	Set of modulation formats
m_l	Modulation format assigned to lightpath l

m_{TRx}	Number of active transceivers
n	Number of bits per symbol
η	Maximum number of lightpaths with MIMO
$\mathcal{N}$	Set of network nodes
n_{fs}	Number of frequency slots needed to serve *d*
n_{OC}	Number of optical carriers needed to serve *d*
$\overline{n_{OC}}$	Mean number of optical carriers needed to serve *d*
n_s	Number of spatial channels needed to serve *d*
n_t	Number of FSs occupied by transponder t
$\overline{n_{TRx}}$	Mean number of transceivers per super-channel
Ω	Set of candidate super-channel configurations
$\mathcal{O}_t$	Set of all pre-computed candidate optical channels for transponder t
Φ	Objective function
Φ_{MCF}	Objective function for MCF
Φ_{MF}	Objective function for MF
ψ	Objective function worsening
p	Routing path
P_{acc}	Acceptance probability
$\mathcal{P}_d$	Feasible candidate paths for demand *d*
R_B	Baud-rate
R_B^{max}	Maximum operational baud-rate
r_d	Requested bit-rate of demand *d*
S	Spatial channel count
s_d	Source node of demand *d*
t	Transponder
$\mathcal{T}$	Set of transponders t
t_d	Destination node of demand *d*
μ	Mean bit-rate per connection
ω	Current solution
ω'	Neighboring solution
ω^*	Incumbent solution
W	Frequency Slot width
z_p	Length of path p

Summary

The ever demanding bandwidth requirements for supporting emerging telecom services such as ultra-high-definition video streaming, cloud computing, connected car, virtual/augmented reality, etc., bring to the fore the necessity to upgrade continuously the technology behind transport networks in order to keep pace with this exponential traffic growth. Thus, everything seems to indicate that fixed-grid Wavelength-Division Multiplexed (WDM) networks will be upgraded by adopting a flexible-grid, thus providing finer bandwidth allocation granularities, and therefore, increasing the Grade-of-Service by packing more information in the same spectral band of standard Single-Mode Fibers (SMFs). Nevertheless, unfortunately, the fundamental Shannon's limit of SMFs is rapidly approaching, and, then, the research efforts to increase the SMFs' capacity will be useless.

One solution to overcome this *capacity crunch* effect is to enable one extra dimension in addition to the frequency one, namely, the spatial dimension, thus deploying S parallel paths in order to multiply, in the best case, by S the capacity of SMF-based networks. However, additionally, it is necessary to decrease the cost and energy per bit in order to provide economically attractive solutions. For this purpose, a smooth upgrade path has to be carried out as new integrated devices and system components are developed for Space Division Multiplexing (SDM).

This thesis is concentrated on the planning and operation of the combined flexible WDM and SDM networks (i.e., Flex-Grid/SDM networks) proposing several strategies aimed at optimizing network resources usage with hardware complexity analysis. For this purpose, firstly, network problems are carefully studied and stated, and then, mathematical and/or heuristic algorithms are designed and implemented in an optical network simulator.

Specifically, after an introduction to the thesis, chapter 2 presents the background and related work. Next, chapter 3 concentrates on the study of spatially fixed Flex-Grid/SDM networks, i.e., when a rigid number of spatial channels are reserved per allocated traffic demand. In its turn, chapter 4 studies the case of Spectrally-Spatially Flexible Optical Networks (SS-FONs), as the ones providing the upper-bound network capacity. Costs and hardware requirements implied on providing this flexibility are analyzed. Network nodes aimed at reducing the cost of SS-FONs are presented and evaluated in chapter 5. Finally, this thesis ends with the presentation of the main contributions and future research work in chapter 6.

It shall be mentioned that this thesis has been mainly carried out in the framework of the projects SUNSET and ALLIANCE founded by the Spanish Ministry of Economy and Competitiveness under contracts TEC2017-90034-C2-1-R and TEC2017-90034-C2-2-R, respectively.

Resumen

La demanda de ancho de banda cada vez más exigente para soportar servicios de telecomunicación emergentes tales como la transmisión de video de alta calidad, computación en la nube, vehículo conectado, realidad virtual/aumentada, etc.…, ha puesto de manifiesto la necesidad de actualizar constantemente la tecnología detrás de las redes de transporte óptico con la finalidad de ir a la par de este incremento exponencial del tráfico. De esta manera, todo parece indicar que las redes basadas en la multiplexación por division de longitud de onda (Wavelength Division Multiplexing, WDM) de ancho espectral fijo serán actualizadas adoptando un ancho de banda espectral flexible, que ofrece asignaciones de ancho de banda con granularidad más fina acorde a las demandas de tráfico; y por lo tanto, incremanta el Grado de Servicio de la red, ya que se permite acomodar mayor información en la misma banda espectral de las fibras monomodo (Single Mode Fibers, SMFs). Sin embargo, desafortunadamente, el límite de Shannon de las fibras monomodo se está aproximando cada vez más, y cuando esto ocurra las investigaciones para incrementar la capacidad de las fibras monomodo serán infructuosas.

Una posible solución para superar este colapso de las fibras monomodo es habilitar la dimensión espacial a más de la frecuencial, desplegando S caminos paralelos con la finalidad de multiplicar por S (en el mejor de los casos) la capacidad de las fibras monomodo. No obstante, es necesario disminuir el costo y la energía por bit con la finalidad de proveer soluciones comerciales atractivas. Para tal propósito debe llevarse a cabo una actualización moderada conforme nuevos dispositivos y componentes integrados son desarrollados para la implementación de la tecnología basada en la multiplexación por división de espacio (Space Division Multiplexing, SDM).

Esta tesis se concentra en la planificación y operación de la combinación de las redes WDM flexibles y SDM (es decir, de las redes Flex-Grid/SDM) proponiendo varias estrategias dirigidas a optimizar el uso de los recursos de red junto con el análisis de la complejidad del hardware que viene acompañada. Para este fin, primeramente, los problemas de red son cuidadosamente estudiados y descritos. A continuación, se han diseñado e implementado algoritmos basados en programación lineal entera o heurísticas en un simulador de redes ópticas.

Después de una introducción inicial, el capítulo 2 de esta tesis presenta el marco teórico sobre los conceptos tratados y los trabajos publicados anteriormente. A continuación, el capítulo 3 se concentra en el estudio de las redes Flex-Grid/SDM con la dimensión espacial rígida; es decir, cuando un número fijo de canales espaciales son reservados por cada demanda de tráfico establecida. Por su parte, el capítulo 4 estudia las redes Flex-Grid/SDM considerando flexibilidad tanto en el dominio espacial como espectral (Spectrally and Spatially Flexible Optical Networks, SS-FONs), las cuales proveerían la capacidad máxima de las redes SDM. Adicionalmente, los

costos y requerimientos de hardware implicados en la provisión de esta flexibilidad son analizados. El capítulo 5 presenta la evaluación de nodos orientados a reducir los costos de las SS-FONs. Finalmente, el capítulo 6 expone las principales contribuciones y las posibles líneas de trabajo futuro.

Cabe mencionar que esta tesis ha sido principalmente llevada cabo dentro de los proyectos SUNSET y ALLIANCE financiadas por el Ministerio de Economía y Competividad de España bajo los contratos TEC2017-90034-C2-1-R y TEC2017-90034-C2-2-R, respectivamente.

Resum

Els requisits incessants d'ample de banda per al suport de nous serveis de telecomunicació, com poden ser la difusió en directe de vídeo de molt alta definició, la informàtica en el núvol, els cotxes intel·ligents connectats a la xarxa, la realitat virtual/augmentada, etc…, han exigit una millora contínua de les tecnologíes de les actuals xarxes de transport de dades. Tot sembla indicar que les xarxes de transport òptiques actuals, basades en la tecnologia de multiplexació per divisió de longitud d'ona (Wavelength Division Multiplexing, WDM) sobre un grid espectral rígid, hauran de ser reemplaçades per tecnologies òptiques més flexibles, amb una granularitat més fina a l'hora de suportar noves connexions, incrementat el grau de servei de les xarxes gràcies a aprofitament major de l'ample de banda espectral proporcionat per les fibres òptiques monomode (Single Mode Fibers, SMFs). Tanmateix, estem exhaurint ja la capacitat màxima de les fibres òptiques SMF segons ens indica el límit fonamental de Shannon. Per tant, qualsevol esforç enfocat a millorar la capacitat d'aquestes xarxes basades en SMFs pot acabar sent infructuós.

Una possible solució per superar aquestes limitacions de capacitat és explorar la dimensió espacial, a més de l'espectral, desplegant S camins en paral·lel per tal de multiplicar per S, en el millor cas, la capacitat de les SMFs. Tot i això, és necessari reduir el cost i el consum energètic per bit transmès, per tal de proporcionar solucions econòmicament viables. Amb aquest propòsit, pot ser necessària una migració progressiva, a mesura que es desenvolupen nous dispositius i components per aquesta nova tecnologia de multiplexació per divisió espacial (Spatial Division Multiplexing, SDM).

La present tesi es centra en la planificació i operació de xarxes òptiques de nova generació que combinin tecnologies de xarxa WDM flexible i SDM (és a dir, xarxes Flex-Grid/SDM), proposant estratègies per a l'optimització de l'ús dels recursos de xarxa i, en definitiva, el seu cost (CapEx). Amb aquest propòsit, s'analitzen en primer moment els problemes adreçats. Tot seguit, es dissenyen algorismes per tal de solucionar-los, basats en tècniques de programació matemàtica i heurístiques, els quals s'implementen i es proven en un simulador de xarxa òptica.

Després d'una introducció inicial, el capítol 2 d'aquesta tesi presenta tots els conceptes tractats i treballs relacionats publicats amb anterioritat. Tot seguit, el capítol 3 es centra en l'estudi de les xarxes Flex-Grid/SDM fixes en el domini espai, és a dir, on sempre es reserva un nombre rígid de canals espacials per qualsevol demanda suportada. El capítol 4 estudia les xarxes flexibles en els dominis espectrals i espacials (Spectrally-Spatially Flexible Optical Nextworks, SS-FONs), com aquelles que poden proporcionar una capacitat de xarxa màxima. En aquest context, s'analitzen els requeriments en termes de cost i hardware per tal de proporcionar aquesta flexibilitat. Llavors, en el capítol 6 es presenten opcions de node de xarxa capaces de reduir els

costos de les xarxes SS-FONs. Finalment, en el capítol 7 es repassen totes les contribucions de la tesi, així com posibles línies de treball futur.

Aquesta tesi s'ha desenvolupat en el marc dels projectes SUNSET i ALLIANCE, finançats pel Ministerio de Economía y Competitividad de España, amb referències TEC2017-90034-C2-1-R i TEC2017-90034-C2-2-R.

to my wife Tannia, my sons Matías and Leire for their love, great comprehension and support during this stage of our lifes,

to my parents and brothers, key pillars in the consecution of this goal.

Acknowledgments

First, I want to thank God for all His blessings, for making me strong in the adversity and the opportunity to achieve this goal.

Special thanks to my advisors Dr. Jordi Perelló and Dr. Salvatore Spadaro for all their technical support and guidance in the realization of this thesis as well as for the opportunity to be involved in the SUNSET and ALLIANCE research projects.

I would like to thank Dr. Joan M. Gené for his important scientific assistance in the initial studies of this thesis. Also, thanks to the Group of Optical Communications (GCO) from the Polytechnic University of Catalonia, especially to Albert Pagès and Fernando Agraz for their valuable discussions and assistance.

To the researchers Dr. Pablo Pavón-Mariño and Francisco J. Moreno-Muro from Technical University of Cartagena, Dr. Krzysztof Walkowiak and Piotr Lechowicz from Wroclaw University for their valuable collaboration and discussions during the elaboration of joint scientific articles of this thesis. I would like also to thank Dr. Raul Muñoz and Dr. Ramón Casellas from Centre Tecnològic de Telecomunicacions de Catalunya (CTTC) for the opportunity and guidance during my research stay in this prestigious research center.

To all my good teachers from my first steps in primary school until University for their important contributions in my professional formation and for encouraging me that every thing is possible with effort and honesty.

I want to express my gratitude to the *Secretaría Nacional de Educación Superior, Ciencia, Tecnología e Innovación* (SENESCYT) - Ecuador for the financial support by means of a full doctoral scholarship, without it, it would have been very hard to achieve this goal. Also, my recognize for its wise policy decision of investing in the human talent training. Finally, I want to thank the *Corporación Nacional de Telecomunicaciones* (CNT E.P.) - Ecuador for the granted work license in order to do my PhD.

Rubén Rumipamba Zambrano

February 2019

Chapter 1

1 Introduction

1.1 Motivation

The emerging telecommunications services require each time more bandwidth requirements. Indeed, all traffic load of access networks coming from Passive Optical Networks (PONs), Data Center Networks (DCNs), future 5G technology (with all its verticals), etc., has to be supported by core networks demanding each time more sophisticated fiber-optic-based systems. Thereby, core networks dimensioning is a crucial aspect; otherwise, they could become the bottleneck part of end-to-end services.

This vertiginous increment of bandwidth requirements follows a 10-fold exponential growth every 4 years [1]; but optical fibers, as any transmission medium, have finite and scarce resources to cope with it. Frequency/wavelength dimension has been one of the first explored physical dimensions to increase the capacity of fiber-optic communications. For instance, conventional linear Wavelength-Division Multiplexing (WDM) networks based on a fixed frequency grid have achieved transmissions up to 100 Gb/s per channel [2], while, recently, a record of 400 Gb/s has been achieved for the under research Non-linear Frequency-Division Multiplexed (NFDM) systems [3]. In order to go beyond WDM capacity, coping with heterogeneous traffic demands avoiding spectrum wastage, it has been proposed using flexible frequency grid arising the concept of Flex-Grid or Elastic Optical Networks (EONs) [4], [5], capable of multiplexing finer granularities than, e.g., 50-GHz-spaced WDM channels. Nowadays, the technology around Flex-Grid networks continues attracting the interest of the research community to optimize the spectrum usage as well as to solve the control and management of different bandwidth-variable network elements. Other explored physical dimensions are time, polarization and quadrature [6]. Nevertheless, the capacity of Single-Mode Fibers (SMFs) is rapidly approaching the theoretical limit (nonlinear Shannon) estimated at 100 Tb/s [1]. To overcome this limit, spatial dimension [7], [8] (as the only one pending to be explored) has gained enormous interest over the last years, thus achieving transmissions in the order of Pb/s [9].

The promising SDM technology relies on several candidates to be realized. For instance, on parallel SMFs, fibers with multiple cores within same cladding, fibers with a single-core transmitting multiple guided modes, and even fibers with multiple cores and modes per each. Each SDM fiber candidate has to deal with physical impairments, which limit its application

scope. Furthermore, new SDM-capable devices facilitating *integration* and *sharing* of system components are expected to be developed in order to reduce both Capital (CapEx) and Operational (OpEx) Expenditures.

In principle, frequency and spatial dimensions are orthogonal; however, their combination, namely, Flex-Grid/SDM networks is expected to be realized in the long-term horizon in the form of Spectrally-Spatially Flexible Optical Networks (SS-FONs) [10] to increase the Grade-of-Service (GoS) of core networks. However, as said, both technologies have to deal with several physical issues in order to reduce the energy and cost per bit, thus paving the way for attractive commercial solutions. For example, tunability, fine resolution, control, integration, Digital Signal Processing (DSP), physical-aware network planning and optimization algorithms, are some of the concerns subject to ongoing research efforts.

This PhD thesis is concentrated on the planning and operation of Flex-Grid/SDM optical core networks taking into account both fixed and flexible spatial dimension from the Resource Allocation (RA) point of view. Moreover, both SDM fibers with and without crosstalk are considered to propose various strategies aimed at optimizing spectral as well as hardware requirements, thus leading to also cost reductions.

1.2 Objectives

The main goal of this thesis is to study the RA problem in Flex-Grid/SDM networks dealing with different physical impairments specially related to SDM transmission medium. Specifically about SDM, in analogous way to frequency dimension, the spatial one can be operated either in a fixed or flexible manner. In this context, the planning and operation studies are specifically oriented to the following cases:

1. Spatially fixed Flex-Grid/SDM networks
2. Spectrally and spatially flexible optical networks
3. Spatial conversion for spectrally and spatially flexible optical networks

Each case study has several specific objectives as follows:

1. Spatially fixed Flex-Grid/SDM networks
1.1 To propose an spatial super-channel configuration
1.2 To evaluate the performance impact of spatial super-channel guard-band width
1.3 To analyze the scalability when a fixed spatial dimension is considered
1.4 To propose an spatial traffic grooming strategy
1.5 To apply Multiple-Input Multiple-Output (MIMO) assignment to counteract the negative effects of crosstalk

2.	**Spectrally and spatially flexible optical networks**
2.1	To analyze the scalability when flexible spatial dimension is considered
2.2	To evaluate the impact of super-channel configurations on the network performance and cost
3.	**Spatial conversion for spectrally and spatially flexible optical networks**
3.1	To analyze the SDM-capable Reconfigurable Optical Add/Drop Multiplexer (ROADM) configuration with/without spatial conversion
3.2	To evaluate the network performance and cost impact of spatial conversion

1.3 Methodology

This PhD thesis is carried out by simulating several network scenarios composed of different reference network topologies, traffic profiles, spectral and spatial resources, transponders, etc. Most the results of this thesis have been obtained with a Java-based ad-hoc simulator, while others with the Net2Plan simulator [11] in collaboration with researchers from the Technical University of Cartagena (UPCT). Fig. 1.1 shows the methodology carried out in the realization of this PhD thesis. Firstly, a given network problem is properly studied and stated. Then, it is mathematically formulated; or, directly, a specialized algorithm is proposed to solve it. Following the diagram of Fig. 1.1, designed algorithms are implemented in the ad-hoc simulator, specifically, in a first component called planning/operation tool by means of a heuristic or an Integer Linear Program (ILP) (optimization techniques presented in next chapter 2). In turn, these algorithms interact with a second component, namely, the network model representing all available network elements and resources. Moreover, they are responsible for properly changing the status of different network elements and resources for control, management or accounting purposes. If results are not what we are expecting or errors are found, then the proposed algorithms should be redesigned.

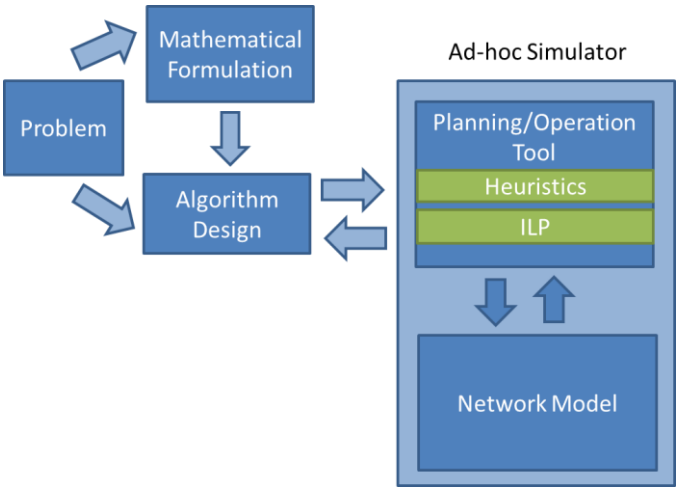

Fig. 1.1. PhD thesis methodology

The network model consists of a directed graph, where vertexes are the network nodes and edges are the network links. Different resources are associated to network elements. For example, spectral and spatial resources are components of network links, while transponders are components of network nodes. Each network element or resource is defined with different parameters. Some of them should provide access to query/modify/monitor their status during provisioning tasks.

It is worth mentioning that the network model of the developed ad-hoc simulator was initially validated by reproducing some previous works available in the literature.

1.4 Thesis Organization

The rest of this thesis is organized as follows.

Chapter 2 presents the background of Flex-Grid and SDM technologies. Specifically about SDM, different SDM fibers are discussed with emphasis on those considered in this thesis. Moreover, State-of-The-Art (SoTA) about network planning and operation of Flex-Grid/SDM networks is presented.

Chapter 3 concentrates on spatially fixed Flex-Grid/SDM optical networks addressing both network planning and operation scenarios. For network operation, firstly, the configuration of spatial super-channels is studied for Flex-Grid/SDM networks. Later on, the performance impact of the necessary Guard Bands (GBs) during spatial super-channel configuration is discussed. Due to spatial rigidity, some spectral-spatial resources could be wasted during provisioning tasks. To counteract this issue, a mechanism called end-to-end spatial traffic grooming enhances network throughput. Although this procedure improves spatial and spectrum usage, a spatial multiplicity increase does not always entail a throughput increment. Therefore, the relationship between spatial multiplicity and network throughput is also assessed for both SDM fibers with and without crosstalk. Finally, a mechanism called dynamic end-to-end spatial traffic grooming is proposed to exploit the huge capacity of spatially fixed Flex-Grid/SDM networks under several traffic conditions. Regarding network planning scenario, the last part of this chapter concentrates on the analysis of SDM fibers with crosstalk. To this end, firstly, the penalties introduced by crosstalk on the spectral resource requirements are analyzed. Then, in order to counteract this negative effect, MIMO processing is proposed to be assigned to the least amount of lightpaths, thus saving costs and computational complexity.

Chapter 4 concentrates on the operation of SS-FONs. For this purpose, firstly, different super-channel allocation options for SS-FONs are surveyed. Then, a cost-effective methodology to configure super-channels is proposed. Finally, the relationship between spatial multiplicity and network throughput under different super-channel allocation options is evaluated.

Chapter 5 focuses on the evaluation of SDM-capable ROADMs (hereinafter called SDM-ROADMs or simply nodes) performance without spatial conversion for SS-FONs in comparison to the ones where spatial conversion is supported. For this purpose, both network planning and operation scenarios are used to evaluate the impact of restricting the spatial conversion on network throughput and cost.

Finally, chapter 6 draws up the final discussion and future work of this PhD thesis.

Chapter 2

2 Background and related work

2.1 Flex-grid technology

Since early 1990s, the natural evolution of digital communications has led to the application of typical frequency-division multiplexing techniques of wireless systems to fiber-optic ones. The idea is to combine multiple connections (lightpaths) by assigning them different Frequency Slots (FSs) or wavelengths (colors). Initially the frequency grid, introduced by G.694.1 ITU-T recommendation in 2002, was exactly equal to 100 GHz (about 0.8 nm) for traditional WDM transport networks. Later on, in 2012 the second edition of such G.694.1 ITU-T recommendation [12] included a variety of channel spacing ranging from 12.5 GHz to 100 GHz and wider. That is, the minimum FS granularity is 12.5 GHz and the central frequency granularity is 6.25 GHz. In addition, the concept of flexible WDM grid (Flex-Grid) was incorporated stating that flexible spectrum ranges, in terms of an integer number of FSs, can be allocated to traffic demands. This allows dealing with mixed bit-rate and mixed modulation format transmission systems, thus optimizing the spectrum usage. To illustrate this, Fig. 2.1 shows the frequency grid for fixed (Fig. 2.1.a) and flexible (Fig. 2.1.b) WDM channels with FS width (W) equal to 12.5 GHz. As seen in Fig. 2.1.a, a fixed 50 GHz width is allocated to traffic demands regardless the required bandwidth, thus causing unutilized spectrum. In contrast, the allocated spectrum according to bandwidth requirements in multiples of 12.5 GHz is shown in Fig. 2.1.b. There, three traffic demands are allocated in a flexible manner by using 62.5 GHz (5 FSs), 12.5 GHz (1 FS) and 25 GHz (2 FSs), respectively, where central frequencies (f_c) are set-up with 6.25 GHz granularity (Δ_{f_c}).

One of the advantages of Flex-Grid technology is that ultra-high bit-rate transmissions are possible in the order of hundreds of Gb/s and even Tb/s by varying modulation format, baud-rate and/or number of Optical Carriers (OCs). The latter parameter allows forming Super-Channels (SChs) by concatenating multiple adjacent Sub-Channels (Sb-Chs). SChs are seen as a single entity and they are generated/detected by devices known as Bandwidth Variable Transponders (BVTs). Moreover, SChs are compactly switched at intermediate nodes called Bandwidth Variable Optical Cross Connects (BV-OXCs). In particular, BV-OXCs with additional capabilities of injecting/extracting optical channels originating/terminating at network nodes are implemented as ROADMs, based on Spectrum Selective Switches (SSSs).

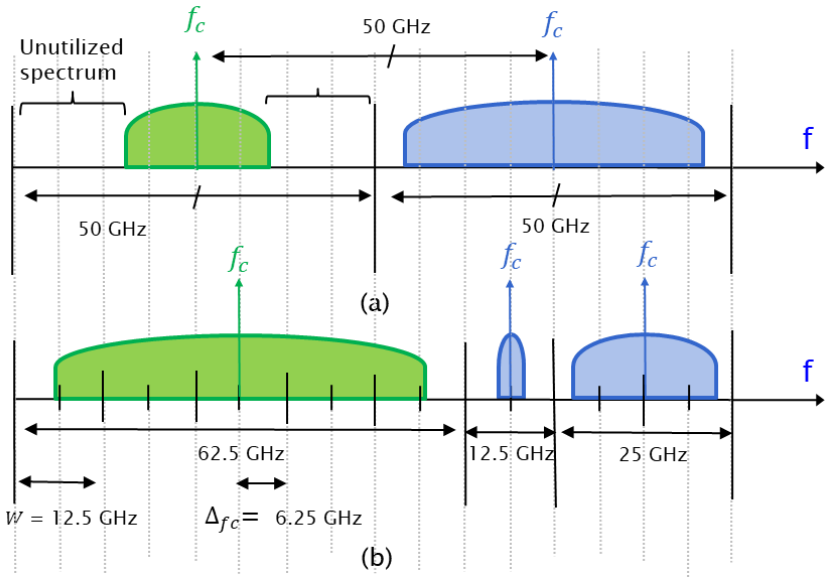

Fig. 2.1. Frequency grid for: (a) fixed and (b) flexible WDM channels.

Flex-Grid technology relies on the programmability of several transceiver (main component of BVTs, see Fig. 3.1) parameters such as modulation format (commonly adapted according to transmission distance), baud-rate, Forward Error Correction (FEC) overhead, launch-power, operational central frequency of tunable lasers, etc. All bandwidth-variable devices can be controlled and managed via software, e.g., by means a Software Defined Network (SDN) controller. In fact, several works available in the literature address the challenge of configuring/programing these enabling devices of Flex-grid technology according to traffic needs. For example, in [13], [14] Operation, Administration, and Maintenance (OAM) as well as control and management tasks of BVTs are proposed by means of Network Configuration (NETCONF) protocol and Yet Another Next Generation (YANG) model. In [15], an SDN-enabled sliceable BVT based on a Generalized Multi-protocol Label Switching (GMPLS) control plane is demonstrated, while [16] addresses the interoperability of multi-domain and multi-vendor EONs. Essentially, this work demonstrates the interoperation of several GMPLS/BGP-LS-based controllers for BVTs and BV-OXCs.

2.2 Space Division Multiplexing (SDM) technology

Although Flex-Grid technology proposes a better way to use the spectrum, the aggregate capacity per fiber cannot surpass the so-called non-linear Shannon's limit of 100 Tb/s [1], [17]. Indeed, estimations have shown that the current technology research reached this limit in 2011 (see Fig. 2.2), phenomenon known as *capacity crunch* [7]. The fact is that according to trends the traffic is multiplied by 10 every 4 years, as shown in Fig. 2.2. In order to go beyond 100 Tb/s the exploitation of the space dimension has been brought to the fore by the Space Division Multiplexing (SDM) technology [18].

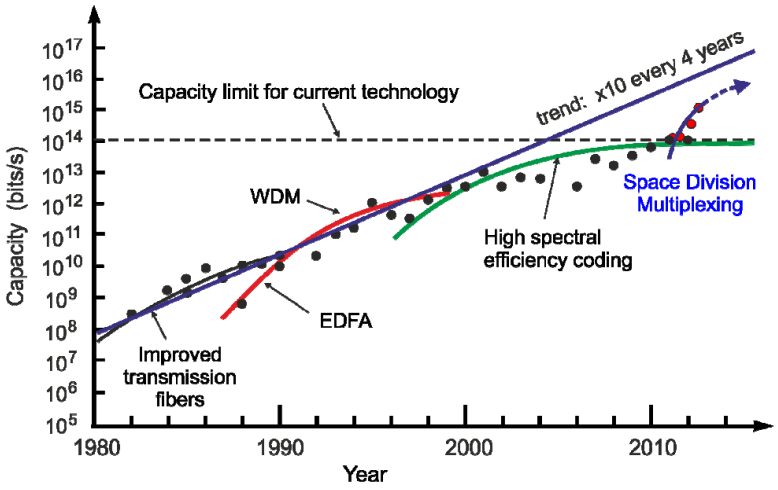

Fig. 2.2. Evolution of transmission capacity in optical fibers [1]

SDM is considered as the "next-frontier" of fiber optics, able to scale up the capacity of current WDM systems [18] and keep pace with the exponential traffic growth. Indeed, the enablement of S parallel optical paths multiplies by S the Spectral Efficiency (SE) instead of increasing the order of modulation formats. For instance, a system of 32 GBaud Dual-polarized (DP)-QPSK with 6 parallel optical paths would achieve an aggregate bit-rate of 768 Gb/s ($32 \cdot 2 \cdot 2 \cdot 6$) per channel. This means that the transmission would scale from 4 to 24 bits/symbol. Unfortunately, the alternative of increasing the order of modulation format is not scalable specially for long-haul communications because the use of regenerators would be mandatory due to limited transmission reach [19]. Moreover, advanced modulation formats would multiply transponder count by the number of regenerators plus one per connection. Hence, SDM seems to be the most promising solution for network capacity growth by packing more information into the limited ~5 THz bandwidth of single-band systems.

Although having parallel systems would potentially reduce the network cost, it is not yet the economically sustainable solution since S parallel systems yield S times the capacity at S times the cost and S times the power consumption. That is, the cost and energy per bit would be the same as today's single systems. Therefore, in addition to parallelization, *integration* and *sharing* of system components is necessary [6], [18], [20], [21]. In this regard, fiber design plays an important role. The straightforward SDM fiber solution is to upgrade current SMFs links to bundle of parallel SMFs, acting as a Multi-Fiber (MF) solution. However, novel designs [1], [22] are also attractive to facilitate SDM system integration, which are going to be presented in the following subsection.

2.2.1 SDM transmission medium

Spatial multiplicity can rely on different fiber designs shown in Fig. 2.3. As said before, already deployed MF (parallel SMF within the same fiber ribbon cable, see Fig. 2.3.a) infrastructures can

be leveraged by some telecom operators. However, new ways of exploiting the spatial dimension include the transmission of multiple guided modes over a single core, i.e., Multi-Mode Fiber (MMF). In addition, if only few modes are considered, these SDM fibers are referred to as Few-Mode Fibers (FMFs), as the case of Fig. 2.3.b. Another interesting design is to increase the core count within the same fiber cladding, namely, Multi-Core Fibers (MCFs, see Fig. 2.3.c and Fig. 2.3.d). Furthermore, if each of these cores transmits few modes, this kind of fibers is referred to as FM-MCFs.

Nevertheless, these novel fibers introduce a new impairment to deal with. Namely, the coupling between modes or cores has to be considered in order to determine if equalization based on end-to-end MIMO processing is necessary. In fact, MIMO equalization is mandatory for MMFs in order to undo the mode coupling. Meanwhile, coupling between cores, i.e., Inter-Core Cross Talk (ICXT), originating by the continuity of the electromagnetic field in adjacent dielectric regions [23], mainly depends on the distance between cores, called core pitch. Indeed, Saitoh *et al.* [24] classify MCFs in two categories, namely, weakly- (Fig. 2.3.c) and strongly-coupled MCFs (Fig. 2.3.d), basically by considering the core pitch (Λ) and coupling coefficient (κ). Weakly-coupled ones have a typical Λ higher than 30 μm and κ lower than 10^{-2} m^{-1}, keeping ICXT below -30 dB per 100 km (i.e., -50 dB/km) [25]. In contrast, strongly-coupled MCFs present lower Λ and higher κ values, mandating MIMO equalization.

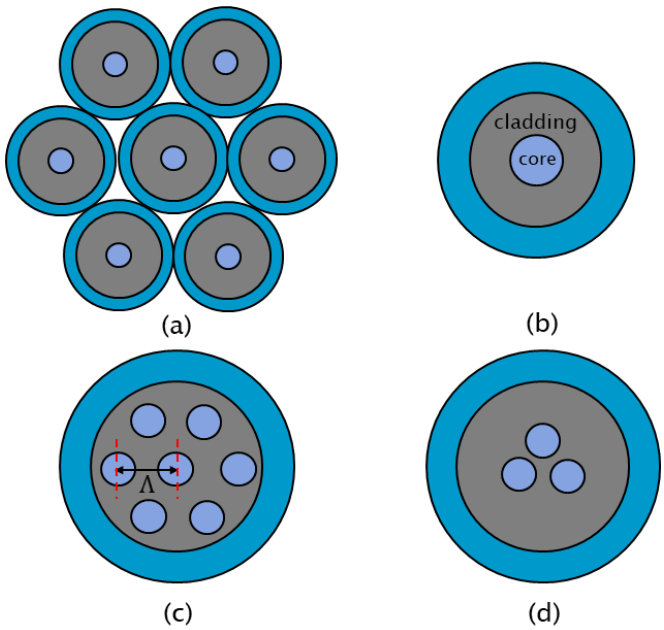

Fig. 2.3. Different SDM fibers (a) MF (bundle of SMFs), (b) Few-Mode Fiber (FMF), (c) weakly-coupled MCF, and (d) strongly-coupled MCF.

Weakly-coupled MCFs are particularly attractive, given their extremely low ICXT [26]–[31] that they introduce during the optical signal propagation, even with high core density, thus alleviating the need for MIMO equalization and, therefore, the complexity and cost of the receivers. Even

so, to further reduce ICXT, heterogeneous MCFs (cores with different characteristics) have been designed, which may be required for long-haul communications with core counts higher than 30 (Dense SDM –DSDM–) [32], [33]. Besides low ICXT, MCFs are economically attractive candidates to realize SDM as well [34], [35]. The interest reader can review more details about fabrication, theoretical analysis of physical impairments and applications of MCFs in [23].

2.3 Flex-Grid/SDM networks

As mentioned before, in order to overcome the capacity of current WDM networks the adoption of SDM technology is an attractive solution. Furthermore, the combination of Flex-Grid and SDM technologies allows optimizing the spectrum usage of each parallel optical path enabled by SDM. In this sense, Flex-Grid/SDM backbone networks, or the synonym term SDM-EONs, have gained enormous interest of the research community over the last years [36]–[38], in order to take full advantage of the vast amount of spectral resources, as spatial multiplicity increases. In particular, Flex-Grid/MCF networks have been advocated by many works in the literature as a promising implementation of SDM-EONs [39]–[45].

Fig. 2.4 shows a typical transparent[1] Flex-Grid/SDM network, basically, composed of SDM-ROADMs linked by SDM fibers and BVTs connected to Add/Drop (A/D) modules of SDM-ROADMs. In this scenario, optical amplifiers are implicit in between nodes typically for every fiber span of 80-100 kilometers, while signal regenerators are not considered in the context of this thesis. By doing a zoom to one SDM fiber link, we can appreciate the parallel S optical paths, each one identified by index i.

Typical traffic demands ask for an optical connection established in form of lightpath (lp) from one source node (s_d) to another destination node (t_d) and transmitting r_d b/s. That is, one demand d can be defined by a triplet (s_d, t_d, r_d). Over one active lightpath a virtual connection can be established, e.g., between two IP/MPLS nodes forming what is known a multilayer IP/MPLS over Flex-Grid/SDM network. Lightpaths, as stated before, are essentially defined in WDM networks by one routing path plus the *wavelength* (color) of the signal. When parallel optical paths are enabled by SDM and each one of them is independently used, the routing path should include an attribute with the sequence of s_i spatial channels used for OAM tasks.

In particular, SDM-ROADMs determine the form in how optical channels are switched and, therefore, how they have to be allocated. There are some node designs available in the literature, which are going to be explained in next subsection.

[1] Term used for network without wavelength conversion and all-optical transmission (i.e., without optical to electrical conversion).

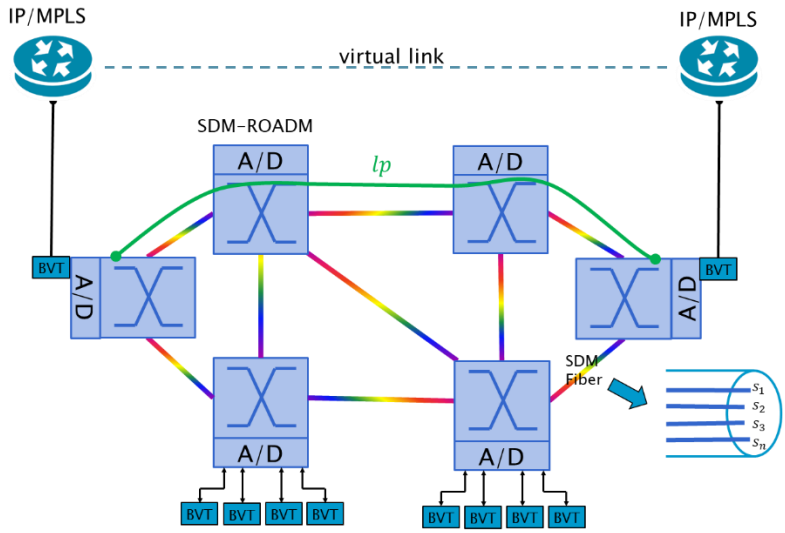

Fig. 2.4. Transparent Flex-Grid/SDM network

2.3.1 SDM-ROADM solutions

ROADMs are in charge of automatically adding, dropping or bypassing (transparent switching) lightpaths in Flex-Grid networks. The ROADM design includes SSS devices, which are able to switch any FS at any of its input ports, to any of its outputs ports [46]. The SSSs are the most expensive elements in the ROADM design.

ROADM functions are typically implemented based on two alternative schemes, the so-called Broadcast-and-Select (B&S) and Route-and-Select (R&S) ones. On the one hand, the B&S scheme offers cost, power consumption and optical/electronic complexity reductions, as well as low overall system penalties. On the other hand, the R&S practically doubles the number of SSSs to provide superior isolation on the blocking ports and a low insertion loss regardless of the port count [47]. According to [47], the B&S architecture seems the best choice for ROADMs with nodal degree (D) lower or equal than 9, while for D>9, R&S benefits compensate its extra cost. Commercial ROADMs commonly use the B&S scheme to switch traffic. However, for next generation optical networks deploying high-port-count SSSs that will require high isolation between ports, the prevalence of the R&S scheme is foreseen [48].

Bypassing operation of ROADMs is realized by switching any spectral range to any output port. This can be called *spectrum switching granularity*. Nevertheless, when spatial dimension is introduced, this opens some additional options to switch optical channels. For instance, following the criterion of *spectrum granularity* and extending it in order to switch to any spatial channel index of any output port, the so-called *space* and *spectrum switching granularity* is realized [49]. As any spectrum range can be independently switched with spatial conversion, this SDM-ROADM is known in the literature as *Independent Switching* (InS) with *Lane Change* (LC) support SDM-ROADM [49], [50].

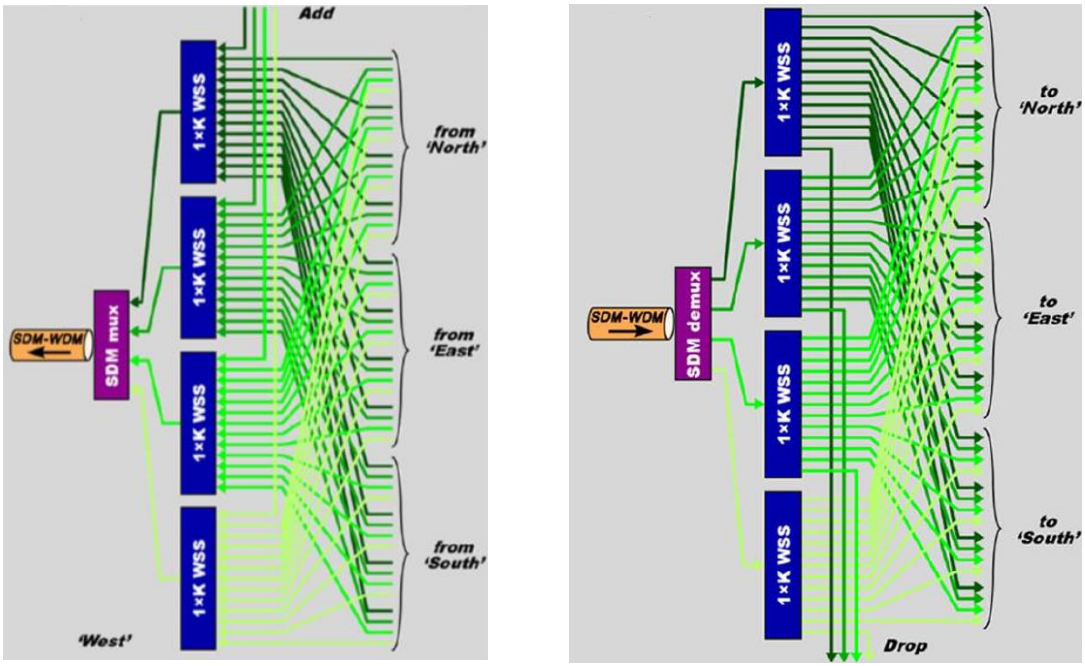

Fig. 2.5. InS with LC support SDM-ROADM for one degree [50]

This SDM-ROADM design, shown in Fig. 2.5 considering R&S scheme, provides a fully flexible interconnection among all ports and available spatial channels but requiring a huge amount of SSSs, two per spatial channel and degree. Therefore, the total number of SSSs per ROADM would be $2 \cdot S \cdot D$. Spatial channels at output/input ports are joined/separated by SDM MUX/DEMUX (e.g., the cores of a MCF by means of Fan-In/Fan-Out [49], [51]) and each spatial channel is connected to one SSS. As these SSSs have one additional port to A/D operation, then the size of each SSS is $1 \times [S \cdot (D-1)+1]$. Consequently, when conventional ROADMs for SMFs turn into SDM-ROADMs the number of required SSS devices and its individual size must be multiplied by S, resulting in an S^2 complexity increase. In order to reduce the system complexity and cost as spatial multiplicity and nodal degree increase, some alternative designs have been proposed:

1) One alternative to simplify node design is to restrict the spatial conversion capability of InS SDM-ROADMs, what is known as InS without LC support nodes. This design consideration has the advantage of reducing the internal SDM-ROADM connections between all ports (and spatial channels) forcing to use a unique spatial channel index (s_i) along the end-to-end lightpaths. Such InS without LC support SDM-ROADM is depicted in Fig. 2.6, where spatial channels at output/input ports are joined/separated by means of SDM MUX/DEMUX and each s_i is connected to $1 \times D$ SSSs. The total number of SSSs per SDM-ROADM is $2 \cdot S \cdot D$ (equal to InS w/ LC support SDM-ROADM) taking into account the R&S scheme as well.
2) Following the requirement of *integration* for SDM technology, switching operation can be done based on *spectrum granularity* but extending across all spatial channels. That is, one spectrum range is switched in all spatial channels at once. This node design is called *Joint*

Switching (JoS) SDM-ROADM [51] and allows reducing the number of SSSs to only two per degree, as shown in Fig. 2.7. In contrast, the number of required ports per SSS is multiplied by S (total spatial channel count per fiber link). That is, for a JoS SDM-ROADM, the conventional SSS of $1\times D$ ports has to scale up to $S \times (1 \times D)$ ports. This new configuration is supported by reprogramming conventional SSSs. For example, a $7 \times (1 \times 2)$ SSS can be configured by means of 1×20 conventional SSSs [51]. Under this design, the number of required SSSs per node is S times lower than those required by InS with/without LC support SDM-ROADMs.

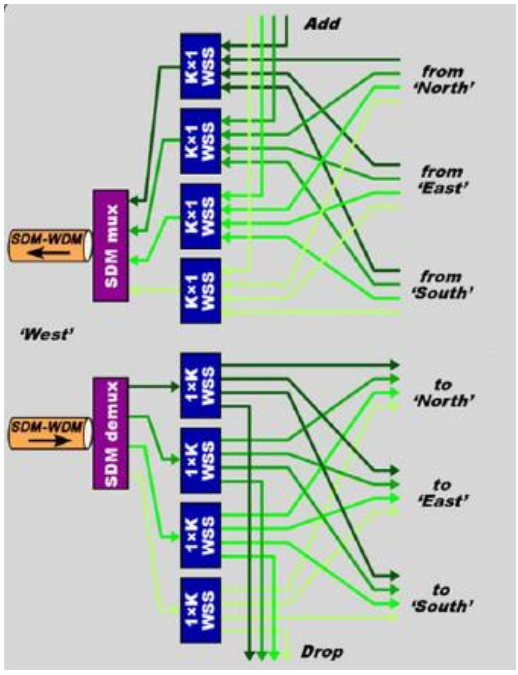

Fig. 2.6. InS without LC support SDM-ROADM for one degree [50]

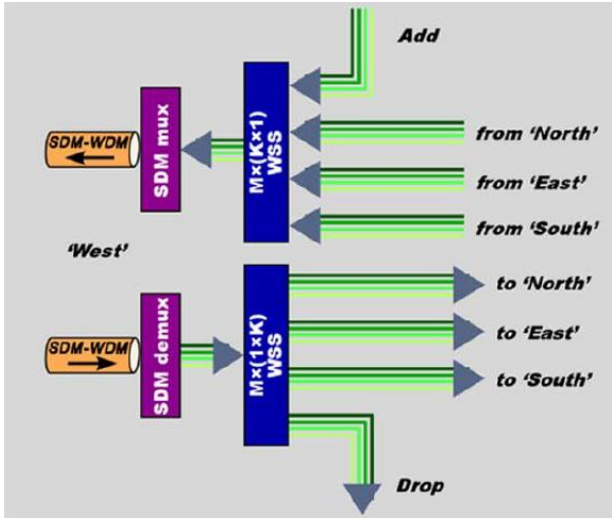

Fig. 2.7. JoS SDM-ROADM for one degree [50]

3) *Fractional Joint Switching* (FJoS) is an intermediate switching solution between InS and JoS. This strategy groups spatial channels into subgroups and JoS is independently applied to

them. The smaller the subgroup size G (number of spatial channels per subgroup), the higher the flexibility in the spatial domain. Unlike InS, where is needed $2 \cdot S$ SSSs per nodal degree, FJoS reduces the number of SSSs to $2 \cdot \lceil S/G \rceil$. For example in Fig. 2.8 with S=4 and G=2, 2 SSSs per degree are required. That is, this node design trades switching flexibility for complexity and cost. The switching between subgroups is also possible and suitable for small subgroup sizes. This leads to two versions of FJoS with LC and without LC, shown in Fig. 2.8.a and Fig. 2.8.b, respectively. As for the number of ports per SSS considering one A/D module, it depends on spatial conversion. This will be equal to $\lceil S/G \rceil \cdot (D-1) + 2$ if spatial conversion is supported, otherwise equal to $G + G \cdot D$. The first FJoS node with LC support, for S=4 and G=2, has been recently demonstrated in [52] in a four-node meshed network.

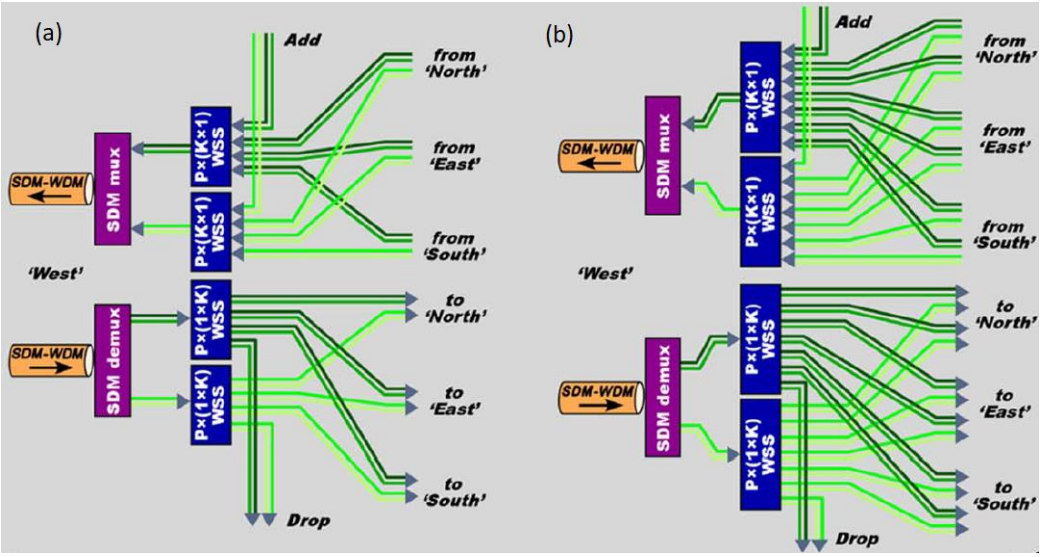

Fig. 2.8. FJoS SDM-ROADM for one degree: (a) without LC support, and (b) with LC support [50]

4) *Architecture on Demand* (AoD) [53], shown in Fig. 2.9, avoids underutilized hardware modules by sharing them on demand via node programmability capabilities. All input/output ports, A/D ports, as well as hardware components, like SSSs, splitters/combiners, amplifiers, mux/demux, etc., are connected to a backplane and interconnected in a customized manner according to the network traffic requirements. However, processing complexity and resilience mechanisms of the backplane are important aspects to be considered. Ref. [54] experimentally demonstrates an SDN-controlled AoD node for SDM networks.

Several works in the literature evaluate the performance and cost of InS (w/o LC support), JoS and FJoS SDM-ROADMs [55]–[61], which have been mainly carried out in the framework of the FP INSPACE European Project [62]. Summing up these works, they conclude that the most economically attractive switching solution is JoS, followed by FJoS and InS in the last place. In contrast, taking into account the network performance measured in terms of Bandwidth Blocking Probability (BBP) or throughput, this order can be inverted. Nevertheless, according to [57] the

network performance strongly depends on the traffic profile observing that in some cases, particularly for large traffic demands, the performance of JoS can meet the one of FJoS or even InS w/o LC. In addition, if lightpaths are reused by traffic demands considering partial or full coincidence of routing paths, then performance of JoS can be improved, as demonstrated in [59]. Cost analysis with other components of SDM-ROADMs like A/D modules, amplifiers and BVTs of network nodes are also addressed in [58], [60]. In these references can be appreciated that the most expensive network equipment in SDM networks are the BVTs. As for AoD, Ref. [41] demonstrates that, for a MCF-enabled network, with this node design the number of SSSs can be reduced by 20-60% with respect to a hard-wired SDM-ROADM, which in practice is an InS with LC support SDM-ROADM. In addition, AoD performance in terms of throughput can be roughly equivalent to InS with LC for this experiments. In any case, as stated before, the resulting SDM-ROADM design with AoD depends on the network scenario and traffic requirements.

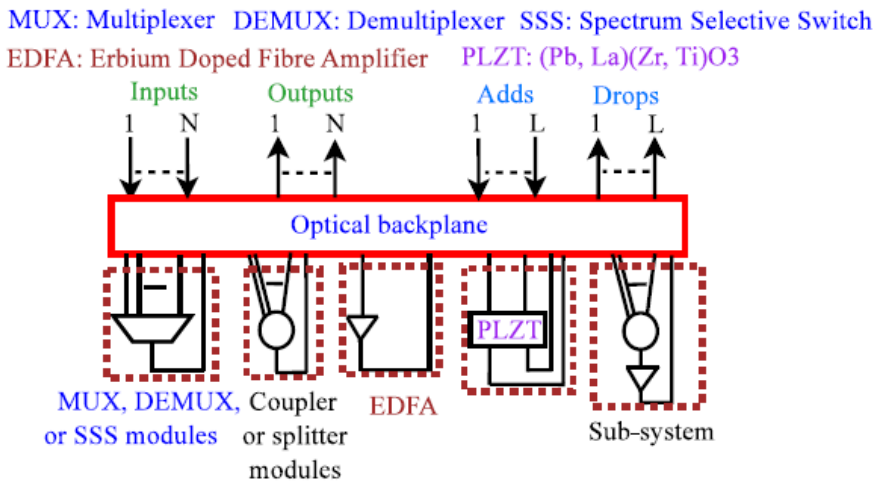

Fig. 2.9. AoD SDM-ROADM [41]

Finally, Table 2.1 summarizes the quantification of the number of SSSs per degree and its size from previous designs considering R&S scheme, some of them presented in [60], [61]. Reference [60] provides general information about SSS metrics for group of spatial channels switched with or without LC support. In fact, all switching strategies, except the one used in AoD, can be generalized as *spatial group switching* [56], [60], [61], e.g., going from G=1 for InS to G=S for JoS. However, we show the SSS information in different rows for clarification purposes. As observed, the required number of SSSs by InS (w/ or w/o LC support) is S times higher than those required by the JoS. Conversely, the port count per SSS (therefore, SSS size) for InS (w/ and w/o LC support) SDM-ROADMs is lower than for JoS ones. That is, JoS SDM-ROAMDs demand a lower number of SSSs in exchange for increasing their size. It is worth noticing that currently available commercial SSSs (with maximum size of 1x35 [63]) could not support JoS. Instead, high-port-count SSSs are necessary, for example, for S=9 and D=4, at least 45 ports would be required. Nevertheless, although these high-port-count SSSs are not commercially available yet,

it is foreseen that cost per port decreases with the SSS size [60]. As for AoD, resultant SSS metrics depends on network scenario and traffic requirements.

Table 2.1: SSSs metrics for different SDM-ROADM designs

SDM-ROADM	Number of SSSs per Degree	SSS port count	SSS size	Required SCh allocation
InS w/o LC support	$2 \cdot S$	$D + 1$	$1 \times D$	Any
InS w/ LC support	$2 \cdot S$	$S \cdot (D-1) + 2$	$1 \times [S \cdot (D-1) + 1]$	Any
JoS	2	$S + S \cdot D$	$S \times (1 \times D)$	Spa-SCh
FJoS w/o LC support	$2 \cdot \lceil S/G \rceil$	$G + G \cdot D$	$G \times (1 \times D)$	Spa-SCh
FJoS w/ LC support	$2 \cdot \lceil S/G \rceil$	$S \cdot (D-1) + 2 \cdot G$	$G \times \left\{1 \times \left[\left\lceil \frac{S}{G} \right\rceil \cdot (D-1) + 1\right]\right\}$	Spa-SCh
AoD	Network- and traffic-dependent	Network- and traffic-dependent	Network- and traffic-dependent	Any

Finally, different SDM transmission medium types restrict the application of one or other switching scheme of SDM-ROADMs. For example, if the parallel SDM paths are coupled together, InS (with or without LC support) or FJoS could not be applied requiring JoS instead in order to jointly process all coupled signals at the receiver end, e.g., by applying MIMO equalization. Conversely, if SDM transmission medium is uncoupled or weakly-coupled, InS (with or without LC support) and FJoS can be applied because MIMO is not mandatory in this kind of SDM fibers. As for AoD, there are no studies available about the AoD implementation for strongly-coupled SDM fibers, but we can expect that the concept of adaptability proposed by AoD can be also applied to switch spectrum ranges across all spatial channels. Finally, one can think in heterogeneous scenarios, i.e., where network links are equipped with different SDM fiber types. For instance, in Ref. [64], a network interoperation with three types of SDM fibers has been demonstrated, where the coupling between cores and modes mandates to apply JoS.

2.3.2 Super-channel allocation required by SDM-ROADMs

Likewise as SDM transmission medium imposes the switching scheme to be implemented in an SDM-ROADM, these switching schemes determine the form of allocating optical channels. Taking into account the limited aggregate bit-rate achieved by Single Carrier (SC) systems and the each time more demanding traffic connections having to be supported by SDM networks, we concentrate on Multi-Carrier (MC) systems where optical channels are accommodated in the form of SChs. In this subsection, we present a brief summary of the main characteristics of different SCh allocations and we associate them with the corresponding switching scheme.

The introduction of the space dimension enables different SCh allocation options, as described in [65]. Indeed, the SCh configuration depends on how its Sb-Chs are arranged across both spectral

and spatial domains. For instance, Sb-Chs of a Spectral Super-Channel (Spe-SCh) are contiguously allocated in the spectral domain over the same spatial channel using MC systems, whereas those of a Spatial Super-Channel (Spa-SCh) are allocated across the spatial domain over an SC. The accommodation of multiple Sb-Chs across both spatial and spectral domains, namely, Spectral-Spatial Super-Channel (S2-SCh) is also feasible in SDM networks. Results reported in [55] show that Spe-SChs may yield better performance (in terms of Bandwidth Blocking Probability, BBP), as they require much less spectral overhead due to GBs. In fact, GBs between Sb-Chs can be eliminated by employing Nyquist-WDM (NWDM) [66], whilst GBs between SChs are always necessary.

Fig. 2.10 illustrates these SCh allocations. An Spa-SCh, as the one shown in Fig. 2.10.a, requires a single Optical Carrier (OC) at frequency f_1, whilst the S2-SCh of Fig. 2.10.b is configured with two OCs at frequencies f_1 and f_2. S2-SCh can be seen as a MC Spa-SCh. According to the definition of JoS operation, it requires that traffic demands be allocated in the form of (SC or MC) Spa-SChs. In fact, the allocation of the same spectrum portion in all (*S*) spatial channels allows jointly switching all optical channels at once. For this purpose, GBs are required to allow SSS filters to properly capture these optical channels. From the channel routing point of view, JoS treats all spatial channels as if they were a single one. Consequently, when a lightpath is established, a spectrum range is reserved in all *S* spatial channels over the end-to-end routing path.

Fig. 2.10.c illustrates an Spe-SCh. As observed, it requires to setup four OCs at frequencies from f_1 to f_4, instead of the one or two OCs required for SC or MC Spa-SCh, respectively. If Nyquist-WDM is employed, GBs between Sb-Chs can be eliminated, requiring only GB/2 at each spectral end of the SCh. That is why Spe-SChs can achieve the best performance. In contrast, a BVT supporting Spa-SChs does not require frequency combs or Arrayed Waveguide Gratings (AWGs) [21], [67], uses shared lasers and joint digital signal processing of spatial sub-channels at the receivers by means of integrated chips [68]. All these aspects potentially reduce the power consumption and cost of the SDM networks.

InS (w/ and w/o LC support) SDM-ROADMs, since they have the finest switching granularity, they do not impose any SCh allocation. In fact, their flexibility allows supporting any of the three SCh types at the same cost. The spatial and spectral resources can be assigned freely to any traffic demand. As seen in Table 2.1, Spa-SChs can be routed by all SDM-ROADM designs, while Spe-SChs are only supported by InS (w/ and w/o LC support) or AoD SDM-ROADMs [41], i.e., for uncoupled or weakly-coupled MCFs.

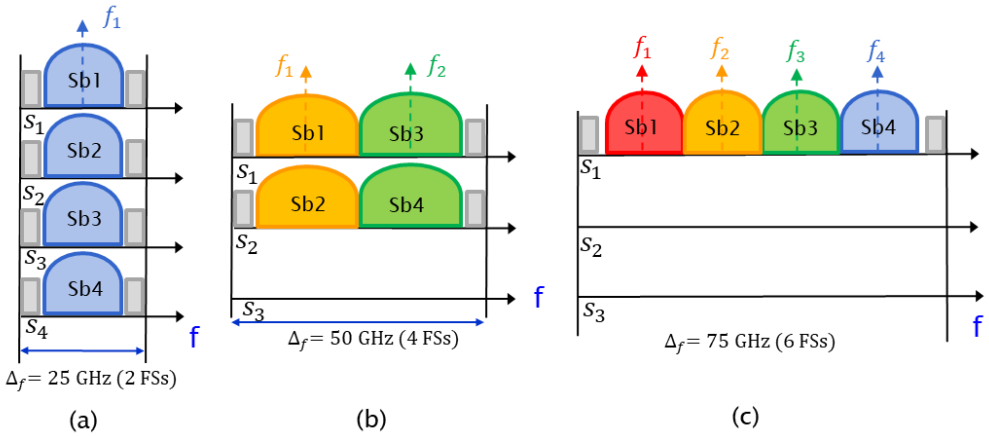

Fig. 2.10. SCh allocation schemes: (a) Spa-SCh, (b) S2-SCh and (c) Spe-SCh

2.4 Resource allocation in Flex-Grid/SDM networks

RA is one of the important problems in optical networks during provisioning tasks since an efficient strategy increase the GoS and, thereby, the revenues of telecom operators. In this section, we present different aspects to be considered during RA process for both network planning and operation scenarios.

The RA problem consists of satisfying connection requests given some input parameters such as network topology, frequency grid granularity, network equipment, Service Level Agreement (SLA), traffic demand, CapEx and OpEx models, power consumption of network equipment, etc. Moreover, RA pursues an objective commonly related with the minimization of the network cost, power consumption or maximization of GoS. In order to evaluate the efficiency of RA process, several network metrics can be used such as Blocking Probability (BP), BBP, spectral utilization, spectral occupation, spectrum fragmentation, connection provisioning time, throughput, etc.

As stated before, at the transport level, connection requests are established in the form of lightpaths with some attributes, which are essentially the physical path (route) plus the spectrum range over which optical signals are transmitted. Initially, the spectrum range was denoted as *wavelength* in traditional WDM networks arising the well-known Route and Wavelength Assignment (RWA) problem [69]–[72]. This can be jointly solved or can be divided into subproblems [73].

As for route assignment subproblem, there are three basic approaches to solve it, namely, fixed, fixed-alternate and adaptive routing [69]. The former one is the most simple and consists of assigning always the same path, for example, the *Dijkstra* Shortest Path (SP). Fixed-alternate maintains a kind of pre-computed routing table with an ordered set of *K*-SPs computed, for example, by means of Yen's algorithm [74]. The latter routing approach is the most flexible

allowing assigning dynamically different routes depending on the network state, e.g., the spectrum occupation, physical layer impairments, etc.

Regarding *wavelength* assignment, in traditional WDM networks, channels of fixed spectral width (e.g., equal to 50 GHz) are assigned to connections. Later on, when the concept of Flex-Grid networks appeared, the term *wavelength* was generalized to as FS where the minimum spectral width is 12.5 GHz, thus giving rise to the Route and Spectrum Assignment (RSA) problem [73], [75]. There are two important constraints to be considered for spectrum assignment. Firstly, *spectrum continuity*, which imposes to assign the same spectrum range along the path for transparent routing. Since Flex-Grid allows assigning a set of FSs, the second constraint, namely, *spectrum contiguity* states that these FSs have to be contiguous in all links of the selected path. Finally, different allocation policies for spectrum assignment sub-problem can be used, e.g., First-Fit (FF), Last-Fit (LF), Best-Fit (BF), Random-Fit (RF), most used, least used, etc.

Fig. 2.11.a and Fig. 2.11.b illustrate the spectrum allocation using 50-GHz fixed frequency grid with mixed line rates versus 12.5-GHz flexible frequency grid, respectively. Let us consider three traffic demands of r_d equal to 200 Gb/s, 40 Gb/s and 10 Gb/s. In case of fixed WDM grid, the 200 Gb/s demand would be served by two OCs (therefore, lightpaths) in blue, not necessarily contiguous, by using *inverse multiplexing* [5]. Meanwhile, other demands only need one OC (in red and green, respectively). As shown, although the optical signals corresponding to each demand occupy different spectrum ranges, the spectrum allocated per lightpath is fixed and equal to 50 GHz. As the 200 Gb/s demand has been split into two lightpaths, we have 4 OCs of 50 GHz (i.e., total occupied spectrum is equal to 200 GHz). As for the Flex-Grid network scenario shown in Fig. 2.11.b, the 200 Gb/s demand does not need to be split, but rather a SCh can be formed with contiguous optical carriers of 100 Gb/s each. As shown, there are significant differences in the spectrum allocated per demand with respect to fixed-grid-based allocation. Instead of fixed-spaced channels, traffic demands occupy different spectrum ranges (minimum 12.5 GHz) as they need considering GBs between adjacent lightpaths. Under flexible grid allocation, the total spectrum occupied for these three demands is 125 GHz. Therefore, in this basic example Flex-Grid reduces the spectrum occupation in about 38% regarding traditional WDM-based networks.

In the context of Flex-Grid networks, the assignment of other tunable parameters, e.g., via Software Defined Network (SDN)-based controller, such as modulation format, code-rate, baud-rate, launch power, etc., and other resources like transponders can be incorporated into the RSA problem [76]–[79] as additional sub-problems, thus giving rise to other route and resource allocation schemes. That is, a multitude of degrees of flexibility is offered by Flex-Grid technology, e.g., assuming flexibility in the spectrum and modulation format, while all other

options are fixed, then Route, Modulation Format, and Spectrum Assignment (RMSA) techniques are applicable.

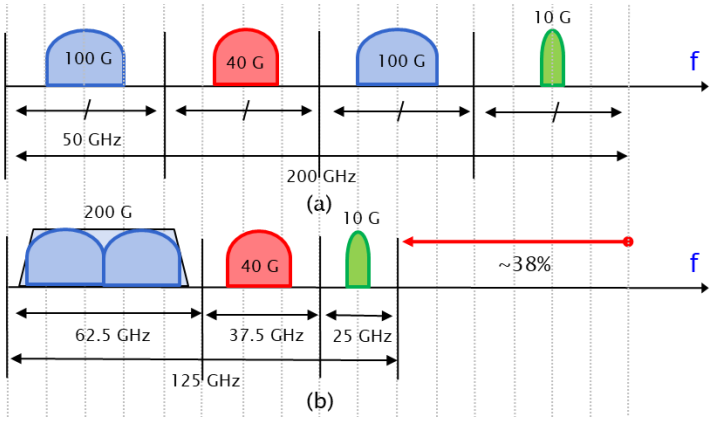

Fig. 2.11. Spectrum accommodation for (a) WDM vs. (b) Flex-Grid networks.

Furthermore, when spatial dimension is considered, i.e., for Flex-Grid/SDM networks, another degree of flexibility can be included in RA process. Note that in a similar way of spectral dimension, spatial one can be fixed or flexible. If JoS operation is applied, although traffic demands can use lower than S spatial channels, the spatial reservation always will be rigid and equal to S. Therefore, spatial assignment can be omitted from RA problem because, implicitly, a spectrum range is reserved across the entire spatial domain. Meanwhile, when spatial granularity decreases, i.e., going from JoS to FJoS and from FJoS to InS, the spatial assignment takes an important role during provisioning tasks. In such cases, adding the spatial assignment sub-problem to the basic RSA problem, RSSA problem arises [36], [38], [80]. For instance, if spatial dimension is enabled by a MCF, then Route, Spectrum and Core Assignment (RSCA) problem is applicable [43], [81], [82]. The interested reader can review the survey [83] about RA schemes in SS-FONs.

Finally, the RA process can be mainly performed in two scenarios, namely, network planning and network operation, which are going to be explained in next subsections.

2.4.1 Network planning scenarios

This scenario known also as *static* or *offline* case, considers all traffic demands are known in advance and the goal is to accommodate traffic demands in the most efficient way. Basically, RA problems for this scenario can be solved by means of two strategies, namely, Integer Linear Programming (ILP)- and/or (meta)heuristic-based algorithms [84].

On the one side, ILP-based algorithms are mathematical formulations of the problem expressed in the form of an objective function plus some constraints, which are linear. They provide optimal solutions pursuing a maximization or minimization objective. The main drawback of this type of solutions is that time complexity can significantly grow with the problem size. In fact, several

works in the literature have demonstrated that RWA and RSA problems are Non-deterministic Polynomial (NP)-hard (i.e., the problem cannot be optimally solved in a deterministic time by means of an algorithm) [73], [75].

On the other side, heuristics are practical methods of finding a valid solution but not necessarily the optimal one. As often they are too greedy, they get trapped in local optimum solutions. Instead, metaheuristics are a kind of stochastic algorithms, i.e., algorithms that provides non-deterministic solutions. Generally, as they take as input several candidate parameters, the combination of them results in different satisfactory solutions. The problem size determines the feasibility of exploring all possible combinations yielding valid solutions. Indeed, for large-problem instances this is practically impossible in a deterministic time. Consequently, suboptimal solutions are returned, e.g., after reaching a certain number of iterations and/or time execution. The advantage of these algorithms is that they can address complex problems with good accuracy and sometimes their solutions can even coincide with the global optimum if they are carefully designed. Although metaheuristics are problem-independent, they have some intrinsic parameters to be fine-tuned in order to adapt the technique to the problem.

There are different types of metaheuristics, e.g., the interested reader can review a good book about network planning and optimization, which summarizes several metaheuristics [84]. The idea consists of exploring the solution space finding each time better solutions. If only one region is explored, myopic solutions are provided and these type of heuristics are known as Local Search (LS). Instead, if this LS procedure is repeated several times in different regions of the solution space, the quality of the solutions can be improved. Examples of LS-based metaheuristics are Iterated LS (ILS), Tabu Search (TS), Simulated Annealing (SA) and Greedy Randomized Adaptive Search Procedure (GRASP). Moreover, SA metaheuristic and others like Ant Colony Optimization (ACO) and evolutionary/genetic algorithms are inspired in natural processes.

Specifically, for Flex-Grid/SDM networks there are several works available in the literature addressing network planning problems by means of ILPs, e.g., see [45], [82], [85]–[87] as well as by means of metaheuristics, e.g., based on SA optimization [56], [61], [85], [88].

2.4.2 Network operation scenarios

During real-time network operation, traffic demands arrive/departure to/from the network in a random fashion, thus motivating other synonym terms such as *dynamic* or *online* RA. For instance, one month Inter-Arrival Time (IAT) with Poisson distribution and one year Holding Time (HT) with negative exponential distribution is assumed in [89]. Demands are one-by-one allocated in a network according they arrive to the network. Since connections with different spectrum requirements are set-up and torn-down the spectrum fragmentation is an "*intrinsic*

issue" of dynamic Flex-Grid networks [65], [90] affecting the overall network performance. Several previous works have addressed this problem in the form of proactive and reactive approaches (e.g., see [91]–[96]). Between these two kinds of approaches, the most critical are the reactive ones, because they may cause service disruption.

In addition, Ref. [65] states that the introduction of the spatial dimension can help the spectrum reassignment and enables another alternative, namely, spatial reassignment, for the defragmentation process. In such situations, the spatial dimension could alleviate the need for advanced laser tuning and DSP at the coherent detectors. Ref. [65] also describes different cases of flexible optical networking. In some of them, the defragmentation process can be favored by the introduction of spatial dimension, but fragmentation continues being an important issue to be addressed even if fragmentation-aware RA strategies are considered, as described in [82], [97]. Meanwhile, in case of JoS-enabled Flex-Grid/SDM networks (as it is equivalent to Flex-Grid over single spatial channel) the fragmentation issue is the well-known case study of the literature related to multi-rate and multi-modulation-formats of the Flex-Grid networks.

Finally, similar to network planning scenario, there are several works available in the literature addressing RA for Flex-Grid/SDM during network operation, e.g., see [39], [43], [57], [59], [81], [98].

Chapter 3

3 Spatially fixed Flex-Grid/SDM optical networks

In the same way that a rigid spectral grid is assigned to channels in traditional WDM networks, the *spatially fixed* term refers to allocation of a rigid number of spatial channels to every lightpath. Indeed, this would be equivalent to reserve S or S/G spatial channels over a specific spectrum range per lightpath when JoS or FJoS are used, respectively. As seen, the most restrictive is JoS, which can be considered as the lower bound of spatially fixed Flex-Grid/SDM networks performance and the cheapest one solution regarding the bypass part of SDM-ROADMs [55]. Throughout this chapter we are specifically referring to the JoS case study, i.e., when a rigid number equal to S spatial channels are reserved per lightpath. This means that, the straightforward allocation policy to be applied is Spa-SChs introduced in subsection 2.3.2, where each spatial channel allocates one fraction of the required bandwidth.

This chapter studies spatially fixed Flex-Grid/SDM networks in two main sections considering both MF and MCF solutions. The first main section 3.1 is focused on the operation of such networks in five subsections. Subsection 3.1.1 addresses the problem of maximum transmission distance, hereinafter referred to as Transmission Reach (TR), for SDM fibers affected by physical impairments, where one of the most relevant is ICXT present in MCFs. The second subsection 3.1.2 studies the characteristics of Spa-SChs and analyzes the impact of GB width on the performance of spatially fixed Flex-Grid/SDM networks. Subsection 3.1.3 proposes a cost-effective Spa-SCh configuration called Partial Space Assignment (PSA) for either fixed or flexible spatial dimension. At first, TR estimations of subsection 3.1.1 are used to compare the PSA configuration against a rigorous configuration called Full Space Assignment (FSA). Since the spatial rigidity causes spectral wastage (the spectral-spatial resources left unused after the allocation of demands) and ICXT increases as core count increases[2], one question that arises is: *Does spatial multiplicity increment yield the same proportional throughput gain in MF and MCF SDM solutions?*. This question is answered in the fourth subsection 3.1.4. One solution to counteract the spectrum wastage issue of spatially fixed Flex-Grid/SDM networks is to apply end-to-end spatial traffic grooming, a solution equivalent to the one called *full-match resource reuse* in [59]. However, this solution strongly depends on Spa-SCh configuration. Hence, a dynamic

[2] For a same fiber layout (e.g., equal cladding and core diameter). ICXT can be lower for higher core count by increasing the cladding diameter or using heterogeneous MCF design.

end-to-end spatial traffic grooming strategy is proposed and evaluated in the fifth subsection 3.1.5 under several traffic conditions.

On the other hand, the performance of MCF-enabled optical core networks is affected by ICXT. In order to counteract this negative effect, MIMO processing is proposed to be applied to spatially fixed Flex-Grid/MCF networks in a network planning scenario in the second main section 3.2 of this chapter. A careful MIMO application scheme has to be designed in order to not increase a lot the network cost and computational complexity. According to this purpose, ILP as well as SA-based metaheuristic solutions are proposed.

Finally, last section 3.3 provides the main conclusions of this chapter.

3.1 Network operation scenario

This subsection studies the operation of spatially fixed Flex-Grid/SDM networks, i.e., in dynamic scenarios where traffic demands arrive to the network one after another. It is worth mentioning that some concepts in this subsection can be applied either to planning or operation scenarios, e.g., TR estimations and PSA strategy, presented in subsections 3.1.1 and 3.1.3.2, respectively. Moreover, they can be used in RA strategies for spatially fixed and spatially flexible Flex-Grid/SDM optical networks. However, to ease the organization of this thesis they appear for the first time in this subsection.

3.1.1 TR estimations for Flex-Grid/SDM networks

RA strategies require knowing the maximum TR along which an optical communication is possible without regeneration. However, this is a difficult task, since TR is dependent on many different variables like the type of fiber, the amplification scheme, the dispersion map, the nonlinear effects compensation capability, the modulation format, the channel spacing, etc..
This subsection concentrates on the TR estimations for both MF and MCF SDM solutions. In general for both, the overall TR is considered to be the minimum between the one imposed either by intra- or inter-core impairments (which is also assumed in [99]). In a MF solution, as the cores are isolated the resulting TR will be only imposed by intra-core impairments.
As for the TR limitation imposed by intra-core impairments, the Gaussian noise (GN)-model has been presented in [100], and its reliability for nonlinear fiber propagation has been proven in most cases of interest. An enhanced version (EGN-model) has been also developed in [101] to provide even better accuracy, being the previous one an upper bound of the Non-Linear Interference (NLI) calculation, which leads to a slightly pessimistic reach estimation. More specifically, the GN-model considers ASE noise and NLI as independent and additive Gaussian-like noises at least for low-to-moderate nonlinearity. Moreover, it determines the optimum launch power per channel

maximizing the Optical Signal-to-Noise Ratio (OSNR), therefore, the TR for several modulation formats. Note that low optical power levels in transport networks decrease nonlinear effects. The linear impairments, such as chromatic and polarization dispersion, can be electronically compensated by means of DSP capabilities of coherent detectors, so that they are not considered as TR limiting factors. Another particularity of the GN-model is that, given a specific modulation format and SE, NLI is independent of the number of channels.

In the studies carried out throughout this PhD thesis, the same scenario as "Link 1" in [100] is assumed, whose details are listed as follows:

- 85-km spans of standard SMFs.
- Erbium-doped fiber amplifier (EDFA) with noise factor NF=5 dB.
- Polarization-multiplexed (PM) quadrature amplitude modulation (PM-QAM).
- Ideal Nyquist WDM (i.e., channel spacing equal to the baud-rate).
- Full DSP-based chromatic dispersion compensation.
- No fiber nonlinearities compensation.
- No Polarization-Mode Dispersion.
- State-of-the-art soft FEC with 20% overhead at pre-FEC BER of 2.7× 10−2.
- 3-dB Signal-to-Noise Ratio (SNR) margin from ideal performance and 1.5-dB penalty of soft FEC with respect to infinite-length codes ideal performance.

The resulting TR estimations for intra-core impairments (i.e., the one imposed by OSNR in GN-model) for several modulation formats are provided in Table 3.2. This is a pessimistic estimation for several reasons. Firstly, as mentioned previously, the GN-model is intrinsically pessimistic. Secondly, the channel spacing is set to its theoretical minimum, while in our simulations GBs are included. Thirdly, no fiber nonlinearities compensation is assumed. Lastly, no Raman amplification is employed.

Regarding the TR limitation imposed by inter-core impairments (i.e., ICXT), the maximum in-band crosstalk tolerated by each modulation format for a 1-dB OSNR penalty is considered [102] with a 4-dB penalty margin, as most operators do [85], [103]. In principle, Spa-SChs span over the entire spatial domain when JoS is realized, so that the maximum XT interference appears. Since estimations based on average ICXT may be way too optimistic, we have taken into account the worst ICXT introduced by the fiber along propagation. Under this assumption, Spa-SChs can use any core index (no core assignment restriction is necessary). Table 3.1 shows the measured worst aggregate ICXT for five weakly-coupled MCFs reported in the literature and considered throughout this PhD thesis. Note that the 30-core MCF prototype has lower ICXT than 19-core and 22-core MCF prototypes because it is a heterogeneous design. One important aspect to be emphasized in the case of weakly-coupled MCFs is that ICXT can be treated as independent of NLI. In fact, some models (e.g., see [104], [105]) consider ICXT effect as an additional and

independent Gaussian-like noise source. Therefore, they include ICXT as an additive Gaussian noise in the calculations of OSNR.

Table 3.2 shows the TR limitation imposed by OSNR (using the GN-model), ICXT, as well as the overall TR for different MCFs and modulation formats. Looking at the overall TR values, we can appreciate that ICXT is not the limiting factor in 7- and 12-core MCFs, but it is in 19-, 22- and 30-core MCFs.

Table 3.1: Measured worst aggregated ICXT in dB/km

7 cores [27]	**12 cores** [28]	**19 cores** [29]	**22 cores** [30]	**30 cores** [31]
-84.7	-61.9	-54.8	-56.2	-60

Table 3.2: Transmission reach in km

MCF	Limited by	64-QAM	16-QAM	QPSK	BPSK
7-core	OSNR	600	2,000	9,000	>20,000
	ICXT	148,098	589,589	2,347,195	4,683,271
	Overall	600	2,000	9,000	>20,000
12-core	OSNR	600	2,000	9,000	>20,000
	ICXT	769	3,062	12,190	24,322
	Overall	600	2,000	9,000	>20,000
19-core	OSNR	600	2,000	9,000	>20,000
	ICXT	150	599	2,383	4,755
	Overall	150	599	2,383	4,755
22-core	OSNR	600	2,000	9,000	>20,000
	ICXT	209	832	3,311	6,607
	Overall	209	832	3,311	6,607
30-core	OSNR	600	2,000	9,000	>20,000
	ICXT	501	1,995	7,943	15,849
	Overall	501	1,995	7,943	15,849

3.1.2 Impact of spatial super-channel guard-bands

This subsection assesses the impact of GBs of Spa-SChs on the performance of spatially fixed Flex-Grid/SDM networks. For this purpose, firstly, the main characteristics of Spa-SChs are discussed. Next, simulation results are presented with different reference networks and GB widths.

3.1.2.1 Characteristics of spatial super-channels

An Spa-SCh, introduced in subsection 2.3.2, can be formed by a shared-laser source (which implies one unique central frequency for all Sb-Chs) and a certain number of Dual-Polarized In-phase&Quadrature Modulators (DP I/Q Mods). The maximum baud-rate of the signals generated by Digital-to-Analog Converters (DACs) will determine whether the Spa-SCh is based on a SC

or MCs (which can also be seen as an S2-SCh). Indeed, if the requested bit-rate per spatial channel exceeds the $baud\_rate \times n$ product, where n is the number of bits per symbol of the modulation format, more than one OC, namely, n_{OC} OCs will be required. Note that at the receiver, opposite devices to the transmitter such as DP Coherent Detectors and Analog-to-Digital converters (ADCs) are placed.

Fig. 3.1 shows two integrated SCh BVTs with SC (Fig. 3.1.a) and MC (Fig. 3.1.b), respectively. One DP I/Q Mod plus one DP Coherent Detector form a Transceiver (TRx), where their DACs and ADCs are associated with DSP engines [106], [107]. Each DP I/Q Mod modulates a fraction of the original demand that comes from DACs generating a Sb-Ch. Besides, GBs must be added to each Sb-Ch (denoted only as "Sb" in Fig. 3.1 for simplicity) or group of Sb-Chs per spatial channel to allow SSS filters to properly capture the incoming optical signals. Each OC at frequency f_i is generated by one laser source, shared by several I/Q Mods. GBs between Sb-Chs of the same SCh can be avoided if ideal NWDM is assumed. Note in Fig. 3.1.b that an integrated S2-SCh BVT can be formed by n_{OC} Spa-SCh BVTs where their corresponding Sb-Chs are multiplexed by means a combiner.

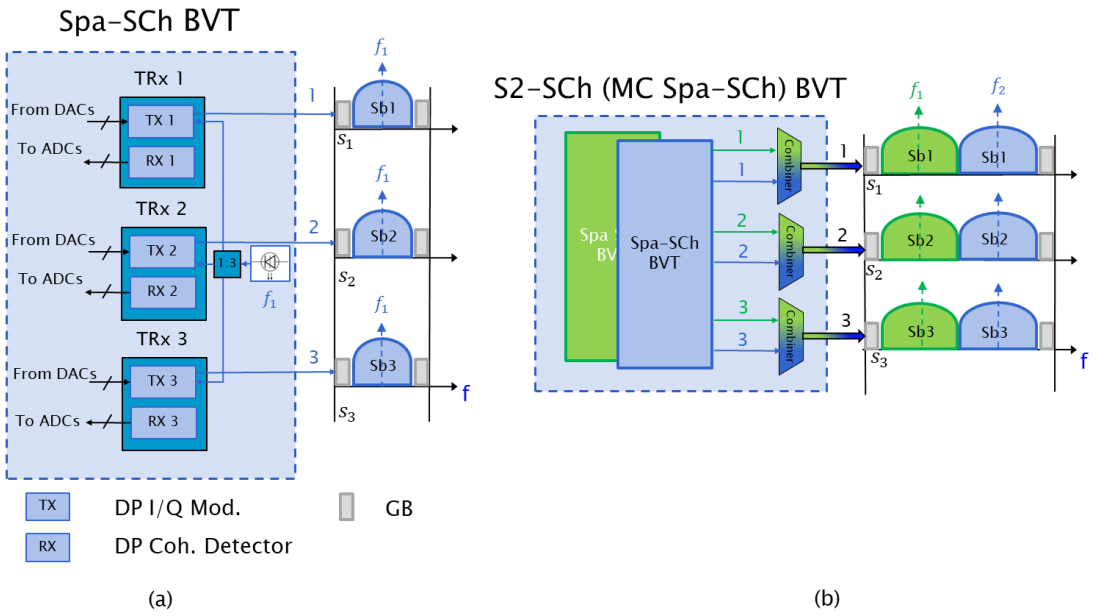

Fig. 3.1. Simplified integrated Spa-SCh BVT diagram with: (a) SC and (b) MC

As introduced before, this chapter considers that spatial dimension is rigid from the RA point of view. Specifically, JoS reserves a spectrum range across all S spatial channels per lightpath. Therefore, one can assume a prorated transmission by equally sharing an original requested bit-rate between S spatial channels, where each Sb-Ch supports r_d/S b/s. Specifically, we can compute the minimum number of FSs (n_{fs}) required to be assigned per spatial channel by using equation (3.1), where SE is in b/s.Hz and W in GHz, e.g., 12.5 GHz, as suggested by the ITU-T

for Flex-Grid in [12]. Note that by equally splitting r_d over all available spatial channels, we are indeed squeezing the spectral requirements of the Spa-SCh to the minimum ones.

$$n_{fs} = \left\lceil \frac{r_d/(S \cdot SE) + GB}{W} \right\rceil \tag{3.1}$$

By keeping fixed all parameters in equation (3.1) except the GB value, we can assess the GB impact on spectral occupation and, therefore, on network performance. The imposed GBs increase the necessary number of FSs, leading to potential underutilization of the spectrum. For example, in Fig. 3.2 we consider a 400 Gb/s connection, employing DP-64QAM modulation format with SE at the Nyquist limit (12 bits/s·Hz), S=12 and W=12.5 GHz. If a GB=10 GHz is employed (Fig. 3.2.a), two FSs are employed (Δ_f=25 GHz) with most of the spectrum being unutilized. However, if lower GBs are considered, like in Fig. 3.2.b, where GB=5 GHz, only one FSs is employed (Δ_f=12.5 GHz). Thus, the value of the imposed GBs plays a critical role in the resource utilization of Spa-SChs.

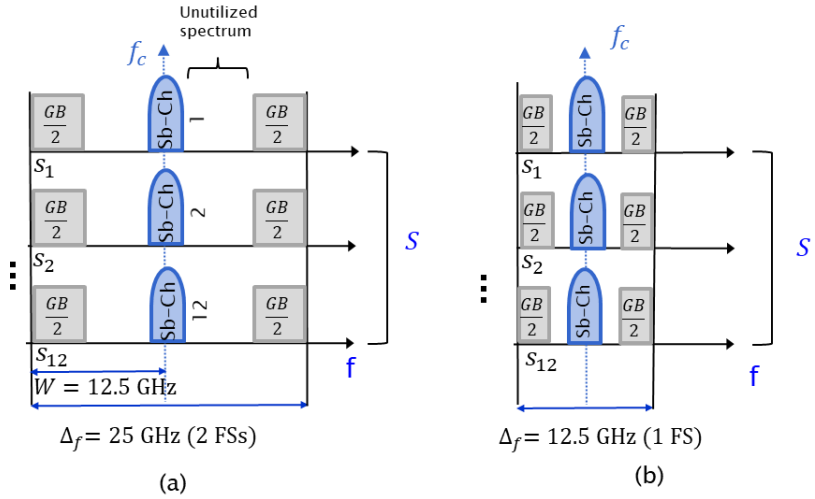

Fig. 3.2. Spa-SCh allocation with different GB: (a) GB=10GHz and (b) GB=5GHz

3.1.2.2 Simulation results

As mentioned above, a drawback of Spa-SChs is the spectral wastage caused by GBs having to surround each sub-channel. In this subsection, we aim to assess the impact of different GB values specifically on the performance of Flex-Grid/MCF networks, measured in terms of the experienced BBP.

To this end, we consider two network topologies: the Deutsche Telekom national backbone network (DT12) and a long-haul US backbone network (US26), shown in Appendix A together with their main characteristics. Each network link is deployed with the MCF prototype of 22 cores presented in Table 3.1 with the corresponding TR values shown in Table 3.2. Moreover, each MCF core has 320 FSs of 12.5 GHz width available along the 4 THz C-Band. We assume demand requests arrive at the network one after another following a Poisson process, with a negative

exponentially distributed Inter-Arrival Time (IAT). Each request asks for a bidirectional lightpath between randomly chosen source and destination nodes (uniform traffic distribution in the network) with bit-rate equal to r_d during a certain Holding Time (HT), which also follows a negative exponential distribution. To decide on the specific r_d value, we assume a long-term traffic profile (TP) with predominance of ultra-high bit-rate super-channel requirements. To this end, we assume that r_d can take any of the following bit-rates with equal probability, TP = {400, 600, 800, 1000, 1200, 1400} Gb/s, resulting in an average bit-rate per demand of 900 Gb/s. To simulate different offered load (L) conditions (i.e., L = HT/IAT), we fix the mean IAT value, and modify the mean HT value of the super-channels accordingly. To get statistically relevant results, we offer $2x10^5$ demand requests per execution.

For each traffic demand we compute K=3 candidate SPs between its s_d and t_d nodes by means of Yen's algorithm [74], taking their physical length (in km) as a metric. This value provides good enough network performance and low computational complexity. Even though the consideration of a larger number of (longer) candidate paths could further avoid the blocking of demand d, an excessive amount of resources might be required (higher number of hops traversed, utilization of a modulation format with low SE), causing the blocking of multiple demand requests in the future. Over each candidate path, the required spectral resources per Spa-SCh, computed by means of equation (3.1), are attempted to be allocated on FF basis.

Furthermore, we consider SC Spa-SChs with up to 32 GBaud (typical industry standard value [100]) DP-BPSK, DP-QPSK, DP-16QAM, DP-64QAM signals. The Most Spectrally Efficient (MSE) modulation format is selected . As for GB widths, we start considering a very commonly assumed GB width of 12.5 GHz [51], [55], decreasing it until the ideal 0 GHz value with 2.5 GHz granularity. This should give us an insight into intermediate GB width values, adoptable by current and/or short-term SSS filter devices, while yielding increased network performance.

Fig. 3.3.a and Fig. 3.3.b show BBP in function of the offered load L for both reference networks, namely, DT12 and US26 networks, respectively. We can see that for a specific offered load, BBP performance depends on the combination of two factors, namely, the network size and GB.

In the case of DT12 network depicted in Fig. 3.3.a, for a target BBP = 1%, every 2.5 GHz GB width reduction generally translates into significant improvements in the admissible offered load (up to 44% increase), except for the transition from 2.5 to 0 GHz, for which the same BBP performance is observed. This can be explained as follows. Referring to equation (3.1), it may occur that even reducing the GB width, n_{fs} remains identical, since the allocated spectrum has a strong dependence on the FS granularity (12.5 GHz in this work). In some particular cases, this may happen for any of the bit-rates in the traffic profile and employing any modulation format. As an example, let us consider a 1400 Gb/s demand to be served with any of the following

modulation formats: DP-QPSK, DP-16QAM, and DP-64QAM in a 22-core MCF network. According to equation (3.1) for both 2.5 GHz and 0 GHz the number of FSs (n_{fs}) allocated are always 2, 1 and 1, respectively. This does not occur in the case of the US26 network (Fig. 3.3.b). As it can be seen, improvements in terms of extra load that can be offered for the same BBP = 1% target can reach up to 20% per 2.5 GHz GB width reduction step.

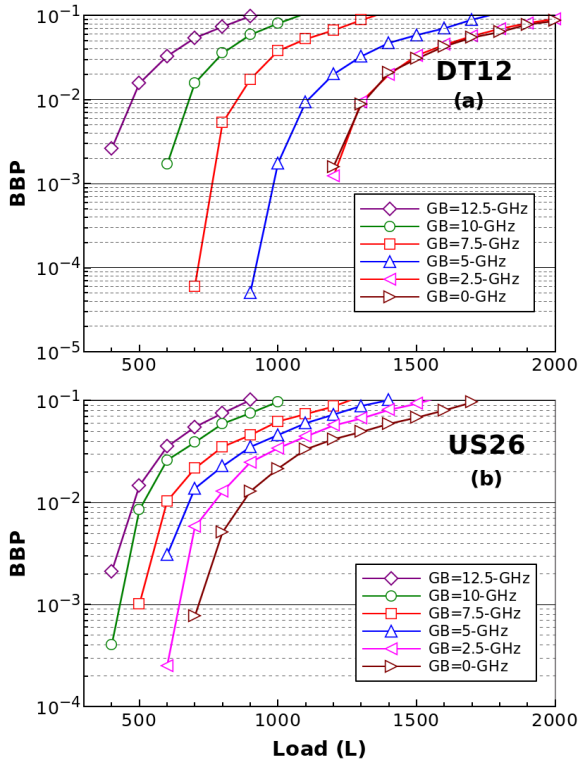

Fig. 3.3. BBP metric vs. offered network load in the DT12 (a) and US26 (b) network assuming 22-core MCFs per link, for different GB widths.

As an outcome of this subsection results, we select an adequate GB width value based on two considerations: the BBP performance benefits and the technological constraints. In this sense, among the different GBs analyzed, BBP benefits obtained with a GB equal to 7.5 GHz are significant. Indeed, we have verified that, for a target BBP = 1%, reducing GB from 12.5 to 7.5 GHz allows increasing the offered load by 77% and 25% in the DT12 and US26 networks, respectively (Fig. 3.3). Moreover, a 7.5 GHz GB is technologically feasible given the fine resolution of the state-of-the art of SSS filters [108]. Therefore, a GB width of 7.5 GHz is assumed in all results presented hereinafter.

3.1.3 Cost-effective spatial super-channel configuration

Given a requested demand bit-rate r_d to be accommodated over a spatially fixed Flex-Grid/SDM network one question that arises: *How to configure the corresponding Spa-SChs?*. The configuration of Spa-SCh refers to selection of the number of spectral and spatial resources,

namely, n_{fs} and n_s, respectively. One strategy is to use the spectral-spatial resources per Spa-SCh according to equation (3.1), which can be called Full Space Assignment (FSA). This subsection aims to address in more detail this strategy and present another called Partial Space Assignment (PSA) in order to answer the aforementioned question. This is a crucial study because Flex-Grid technology allows assigning different spectrum ranges thanks to baud-rate flexibility. It is worth mentioning that other previous works directly assume demand requirements in terms of number of Sb-Chs and/or with fixed baud-rates (e.g., see [55], [59], [61], [99]) where the determination of Spa-Ch configuration can be trivial.

To this end, let us present a general scheme for Route, Modulation Format and Spectrum Assignment (RMSA) heuristic, as shown in Table 3.3. Recall that JoS forces to reserve spectral resources (i.e., n_{fs} FSs) across all spatial channels, therefore, RA problem is equivalent to Flex-Grid over a single spatial channel. In more detail, when a demand request d arrives at the network, the K feasible candidate SPs between its s_d and t_d nodes are computed, taking their physical length (in km) as a metric (line 3). Next, for each of the computed candidate paths we select the MSE modulation format with a TR equal or higher than its physical length, based on the TR estimations reported in subsection 3.1.1 (line 6). Then, we compute the minimum number of contiguous FSs (n_{fs}) per spatial channel necessary to allocate the Spa-SCh over the currently evaluated candidate path between its s_d and t_d nodes by means of equation (3.1). The next step performed by the heuristic is to find if n_{fs} FSs (including GBs) are available in the first spatial channel along the evaluated candidate path, ensuring the spectrum continuity (i.e., no spectrum conversion capability is assumed in the network) and contiguity constraints (line 8). The first available FSs found are chosen, that is, a FF spectrum assignment is applied. If no available FS of n_{fs} FSs is found along the evaluated candidate path, the heuristic moves to evaluate the following candidate path, performing the same steps again (i.e., modulation format selection, n_{fs} computation and spectrum assignment). If no FSs are found on any of the K candidate physical paths, the incoming demand is considered as blocked (line 18).

Assuming that a successful spectrum assignment along any of the K candidate physical paths, this means that the Spa-SCh can be established. Therefore, the *Spa-SCh configuration procedure* can be initiated. The following two subsections present two strategies to configure Spa-SChs employing JoS technique, namely, FSA and PSA. Both approaches contemplate three degrees of flexibility: baud-rate, modulation format and sub-channel multiplicity. Besides, they can be applied to either MF or MCF solutions and with any switching strategy at SDM-ROADMs.

Table 3.3: RMSA heuristic for Spa-SCh configuration

1:	**Input:**
	G=(|N|,|E|) //Physical Network, N: Set of nodes, E: Set of links.
	d //Incoming demand request to be served
2:	**Begin:**
3:	*P* ←Compute *K* candidate SPs between s_d and t_d of d
4:	X ←false//binary flag: "0" if d is blocked, "1" if it is accepted
5:	**For** each p in *P* **do**
6:	Find the MSE modulation format with TR ≥ physical length of p [km]
7:	Compute minimum n_{fs} ←Number of FSs to serve r_d using *S* spatial channels, by means of eq. (3.1)
8:	Find available n_{fs} FSs continuous and contiguous along the path to allocate the Spa-SCh
9:	**If** n_{fs} FSs have been found **then**
10:	Initiate the *Spa-SCh configuration procedure*
11:	Allocate the spectral resources
12:	Configure BVTs as decided by the Spa-SCh configuration strategy used
13:	*X* ←*true,* considering *d* as served
14:	Break
15:	**end if**
16:	**end for**
17:	**If** *X* is false **then**
18:	Consider *d* as blocked
19:	**end if**
20:	**End.**

3.1.3.1 Full Space Assignment (FSA) strategy

As presented in subsection 3.1.2.1, one can be assumed that a requested bit-rate is split into S spatial channels, which corresponds with the reservation of a spectrum range across the entire spatial dimension when JoS is applied. This strategy is a rigid configuration that we call FSA and targets the minimization of the allocated bandwidth, i.e., n_{fs} FSs assigned per Spa-SCh.

Each spatial channel supports a bit-rate r_d/S over a free spectrum range found. Therefore, S transceivers (S DP I/Q Mods + S Coherent Detectors) are required to establish the Spa-SCh operating at gross baud-rate $R_s = r_d/(S \cdot n)$. Although FSA targets the minimization of the bandwidth (Δ_f) required to allocate the Spa-SCh by using the entire spatial domain, it may happen that a significant portion of spectrum still remains wasted. This can occur when the Sb-Ch bandwidth does not tightly fit into an integer number of FSs. To put this in numbers, let us assume in Fig. 3.4.a that 22-core MCFs (from s_1 to s_{22} in Fig. 3.4) have been deployed in the network, and that we want to serve a 1 Tb/s incoming demand request by means of a Spa-SCh configured using the FSA strategy. Moreover, we assume that the length of the physical path allows us to modulate the Sb-Chs using DP-64QAM. If we assume 10 GHz GBs (5 GHz per side), which is a

typical GB width assumed in the related literature [5], we need 2 FSs ($\Delta_f = 25$ GHz), but the spectrum occupied by the Sb-Chs (Δ_{Sb}) reduces to merely 3.8 GHz [1000 Gb/s ÷ (22 cores · 12 b/s/Hz)]. That is, there exists an 11.2 GHz of spectrum gap per core (unutilized spectrum) left by FSA.

3.1.3.2 Partial Space Assignment (PSA) strategy

Upon situations such as those mentioned above in the FSA strategy, it would be much more efficient to adjust the number of assigned spatial channels to $n_s \in \mathbb{Z}^+ : 1 \leq n_s \leq S$, thus increasing the spectrum utilization, while reducing the number of transceivers to be used per Spa-SCh. In this case, the same n_{fs} FSs computed by means of equation (3.1) are allocated in n_s spatial channels instead of allocating in all S spatial channels (as FSA does). That is, lightpaths would reserve S spatial channels, but the real spatial occupation would be what n_s determines. This is the reason why JoS technique continues being applied releasing spatial and spectral resources, yet providing the same network GoS as FSA.

In order to compute this optimal number n_s of spatial channels over which optical signals are transmitted, we aim to fill the abovementioned spectrum gaps left by FSA in each spatial channel. To this end, we find the maximum Sb-Ch spectral width (Δ_{Sb}) by subtracting the GB width from Δ_f (max $\Delta_{Sb} = n_{fs} \cdot \Delta_{fs} - GB$). Next, the programmable BVTs are configured to operate at $R_B = \max \Delta_{Sb}$ if $R_B \leq R_B^{max}$ (i.e., their maximum baud-rate is not exceeded). Otherwise, they are configured to operate at $R_B = R_B^{max}$. In this way, the total number of spatial channels used to transmit the Spa-SCh with PSA is $n_s = \lceil r_d/(R_B \cdot n) \rceil$. Note that the aggregate bit-rate ($R_B \cdot n \cdot n_s$) with PSA can become slightly higher than r_d as a result of the ceiling operation. However, the final operational baud-rate could be readjusted later to $R_B = r_d/(n \cdot n_s)$.

The benefits achievable by using PSA are illustrated in Fig. 3.4.b, where the same assumptions previously made for exemplifying the performance of FSA are considered. In contrast to FSA, with PSA we have that max Δ_{Sb} can be 15 GHz ($2 \cdot 12.5 - 10$). Then, assuming a maximum flexible baud-rate of the transceivers equal to 32 GBaud (R_B^{max} = 32 GBaud), n_s can be decreased down to 6 ($\lceil 1000/(15 \cdot 12) \rceil$), considering that DP-64QAM is employed as in the previous example. So, each core transmits 180 Gb/s ($15 \cdot 12$) and the aggregate bit-rate is 1080 Gb/s ($15 \cdot 12 \cdot 6$). Note that the allocated spectrum continues being the same as in the FSA strategy (i.e., 2 FSs), ensuring identical network BBP. Nevertheless, as 6 spatial channels are supporting the Spa-SCh, only 6 transceivers are required. In conclusion, adjusting the number of spatial channels simultaneously used improves the spectral occupancy (avoiding spectrum wastage) and potentially reduces the number of transceivers to be equipped per node, which will be quantified in next subsection 3.1.3.3.

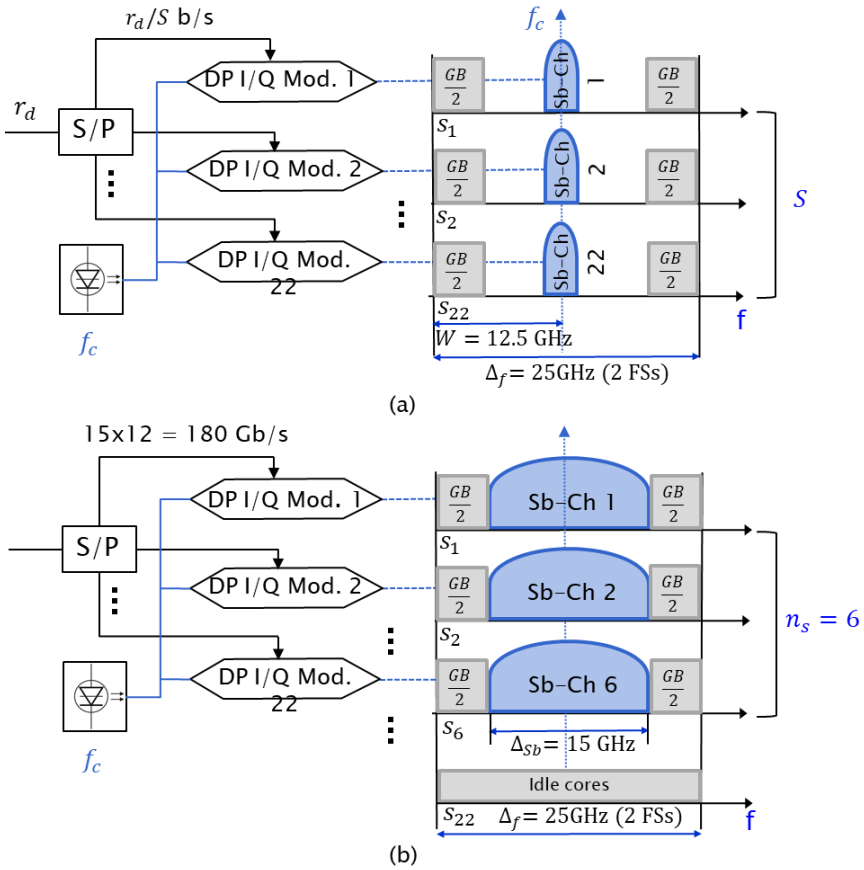

Fig. 3.4. Spa-SCh allocation using FSA (a) and PSA (b) strategies. 22-core MCFs are considered. There, a Spa-SCh has to be allocated to support a 1 Tb/s demand. Optical modulators with maximum flexible baud-rate of 32 GBaud employing DP-64QAM are assumed. GBs are set to 10 GHz.

3.1.3.3 Comparison of PSA and FSA strategies

As explained in previous subsections, FSA and PSA strategies yield identical BBP performance because the spectrum range assigned per Spa-SCh is the same for both strategies. In this subsection, we aim to evaluate network complexity reduction that could be achieved by employing the PSA strategy through the minimization of the required number of spatial channels (therefore, transceivers). To this end, we take into consideration the same assumptions mentioned in previous subsection 3.1.2.2 and setting the GB to 7.5 GHz, as recommended at the end of that same subsection.

In a dynamic network scenario as the one assumed in the present subsection, every time an incoming demand d is accepted, n_s transceivers (TRx) should be assigned to the programmable BVTs, so as to properly generate the Spa-SCh. These transceivers will then be released once the demand is torn down (i.e., when its HT expires). In order to illustrate the number of transceivers that would be required in the network, we get samples of the number of active transceivers in the network (m_{TRx}) every time a Spa-SCh has been allocated. We do this in both DT12 and US26 networks with 22-core MCFs per link and under an offered load yielding a BBP of 1% (i.e., L=850

and L=600 for DT12 and US26 networks, respectively, as shown in Fig. 3.3 for GB = 7.5 GHz curve), aiming to evaluate a reasonable network scenario.

Fig. 3.5 and Fig. 3.6 show m_{TRx} histograms using both FSA (in blue) and PSA (in purple) strategies in the DT12 and US26 networks. They depict the percentage of samples (occurrences) where the measured m_{TRx} has fallen into each of the predefined X axis intervals. Recall that we offer $2x10^5$ demand requests per simulation execution. Although some of these requests will be blocked eventually, the low BBP in the evaluated network scenario ensures that more than $1.98x10^5$ samples are used to generate these histograms, as larger connections (in terms of bit-rate) are more prone to blocking than smaller ones.

Looking at the obtained results, they describe a Gaussian-like probability distribution along the evaluated m_{TRx} intervals, although for PSA it is clearly shifted to the left, showing a remarkable reduction of the active transceivers. Indeed, in the DT12 network (Fig. 3.5), whereas with FSA the average m_{TRx} value is 36376, with PSA it is reduced to 20317 (i.e., 44% reduction). Another very interesting outcome is that with PSA no occurrence falls into those m_{TRx} intervals larger than 23500, which could be taken as the peak number of active transceivers required in the network. Conversely, with FSA this peak value shifts until 40900. This also represents a reduction around 44%. In the US26 network (Fig. 3.6), the average m_{TRx} value reduction achieved by PSA is around 33% (26230 vs. 17665). In terms of peak active transceivers, a reduction around 33% is also obtained (30500 vs. 20300).

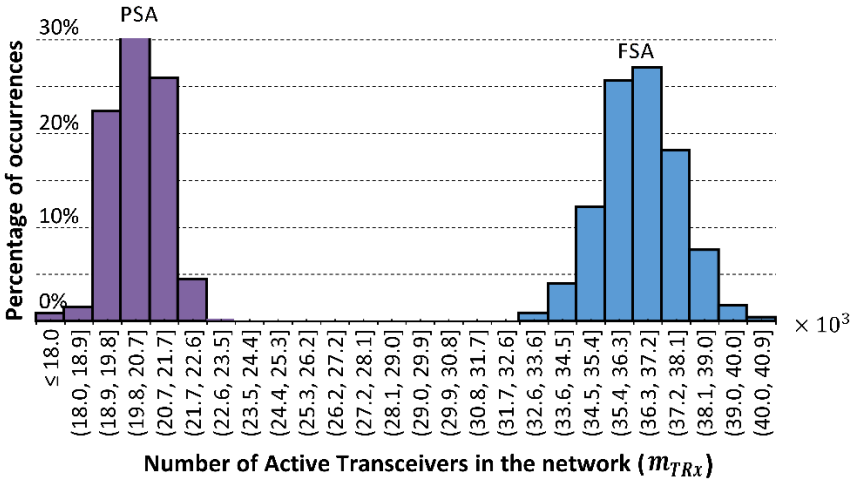

Fig. 3.5. m_{TRx} histogram in the DT12 network with 22-core MCFs using FSA (in blue) and PSA (in purple) strategies. An offered load yielding a 1% BBP has been considered.

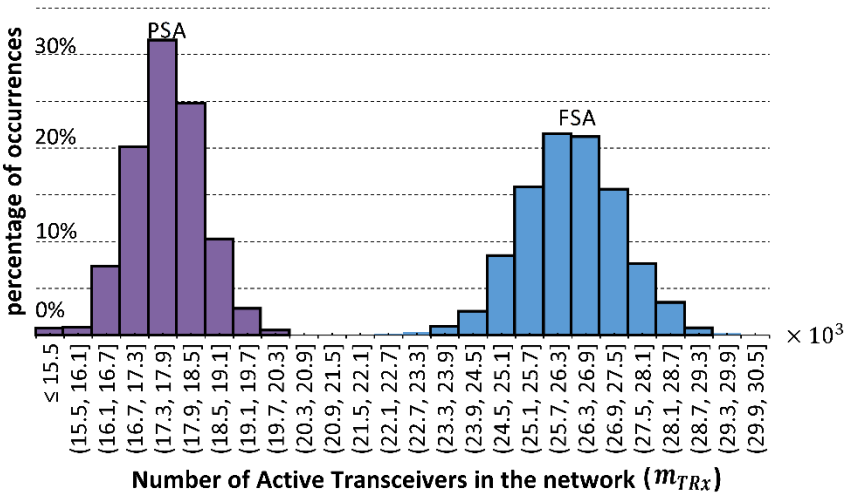

Fig. 3.6. m_{TRx} histogram in the US26 network with 22-core MCFs using FSA (in blue) and PSA (in purple) strategies. An offered load yielding a 1% BBP has been considered.

To ensure that no demand request blocking happens by transceiver unavailability, the aforementioned peak active transceivers requirement should at least be equipped network-wide. In order to evaluate this behavior also at the node level, we have measured the average peak number of active transceivers per node along the whole simulation, getting again samples after each Spa-SCh allocation. We have observed that the average number of transceivers to be equipped per node using PSA is 2229 and 1084 in the DT12 and US26 networks, respectively. These requirements can be contrasted with those obtained by using FSA, which are 3913 and 1577 in both networks, respectively. Hence, the proposed PSA strategy can potentially yield substantial cost savings derived from the lower requirements in terms of optical transceivers to be equipped at network nodes. Of course, as future work, an accurate offline Flex-Grid/MCF network planning contemplating PSA vs. FSA would also be welcome to give further insight in this regard.

Note that, in spite of the longer distances in the US26 continental backbone network, it requires a lower number of transceivers per node than the national DT12 backbone network. This means that the longer distances have required to modulate the signals with less efficient modulation formats, causing to allocate wider spectrum widths (consequently higher baud-rates) but transmitting in a lower number of cores (n_s). However, the operational baud-rate of the transceivers in the US26 network will be higher. To shed light on this concern, Fig. 3.7.a and Fig. 3.7.b show the transceiver operational baud-rate histograms in the DT12 and US26 networks, respectively. Again, an offered load leading to 1% BBP has been considered. We can observe that, for PSA in the DT12 network, the percentages of occurrences are almost equally concentrated in two intervals (4,5] and (17,18] GBaud, whilst in the US26 there is a high percentage (73%) of the operational baud-rates corresponding to the (17,18] GBaud interval plus a small one (2.2%) of baud-rates to the (29,30] and (31,32] GBaud intervals. To be more concise,

the mean baud-rate is 10.95 GBaud and 14.69 GBaud in the DT12 and US26 networks, respectively, which are intrinsically higher than in FSA taking into account that PSA tries to maximize the spectrum occupied per spectrum allocated. For example, when the demands require allocating 1, 2 or 3 FSs with a 7.5 GHz GB, the maximum operational baud-rates are: 5, 17.5 or 30 GBaud, respectively. Note that, the low percentage of occurrences that require the highest baud-rates, 30 and 32 GBaud, in US26 could be discarded due to its high cost of generation/detection, presumably with the BBP metric being not greatly affected. Regarding the FSA strategy, we can observe that the operational baud-rates are more granular than with PSA, because they have more flexibility, as FSA always employs all S spatial channels without considering the maximization of the spectrum occupation. The lower baud-rate requirements of FSA may look like an advantage; however, it should be seen in terms of transceiver's bandwidth utilization. In our case, the nodes are equipped with 32 GBaud transceivers, which are underused in the case of FSA. Such high bandwidth transceivers are a must in view of an eventual traffic demand increase.

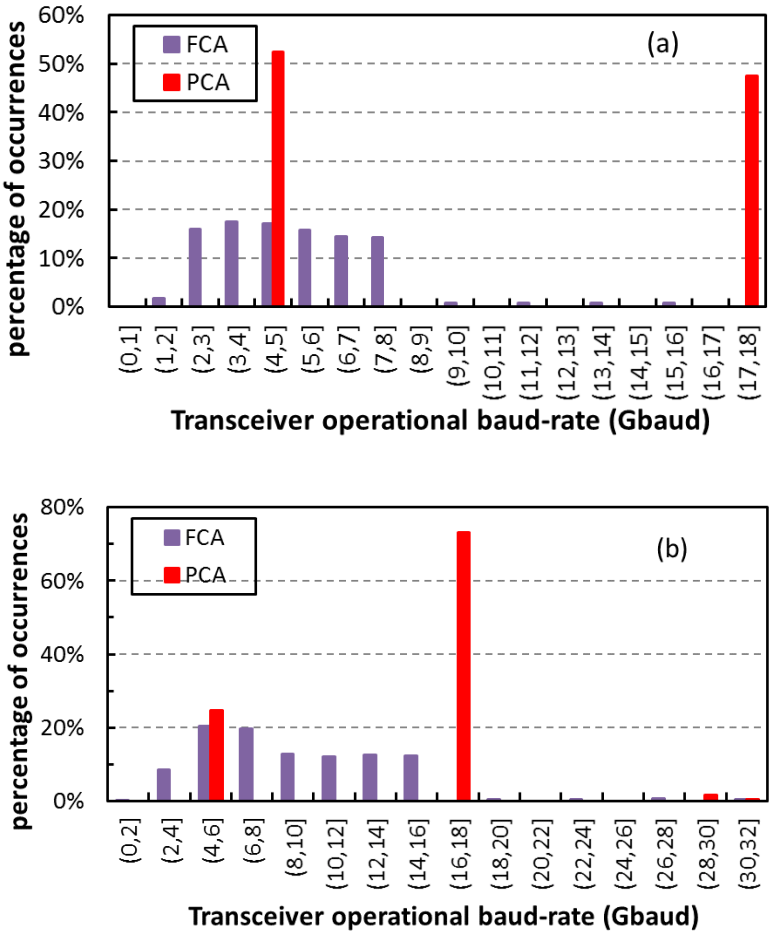

Fig. 3.7. Transceiver operational baud-rate histogram in the DT12 (a) and US26 (b) network. An offered load leading to BBP around 1% has been considered.

3.1.3.4 ICXT Impact Analysis

In this subsection, we investigate ICXT impact on the network performance by considering an equivalent Flex-Grid/MF network as benchmark scenario. For a given transmission distance, ICXT may impose the necessity of less efficient modulation formats in a MCF-enabled network compared to an equivalent MF alternative (as no coupling exists between bundles of single-core fibers). In more detail, ICXT can lead to one of the following three situations when allocating a Spa-SCh to carry an incoming demand request:

i) The number of cores per Spa-SCh (n_s) to carry the entire r_d is increased (compared to the MF equivalent scenario), as a lower bit-rate is transmitted per core. However, the number of required FS (n_{fs}) stays unaffected.

ii) n_{fs} is increased. However, as the Spa-SCh has allocated a wider bandwidth, a higher bit-rate may be transmitted per core and, thus, n_s can be lowered.

iii) n_{fs} is increased. This time the reduction of the *SE* also leads to an n_s increase (more cores are required for the Spa-SCh).

To exemplify these situations, let us assume that a 1 Tb/s demand should be carried by means of a Spa-SCh, either over a MCF- or an equivalent MF-enabled network. The first situation (i) would occur if the end-to-end path length is equal to 1000 km. In this case, the most efficient modulation format in a MF scenario is DP-16QAM. Therefore, we have that $n_{fs} = 2$ and $n_s = 8$ if the PSA strategy is employed. In contrast, in a 22-core MCF network, the most efficient modulation format lowers to DP-QPSK. So, we still have n_{fs} = 2, but n_s raises up to 15. As for the second situation (ii), it would occur if the end-to-end path length would shorten to 400 km. The most efficient modulation format in a MF scenario is DP-64QAM. Therefore, $n_{fs} = 1$ and $n_s = 17$. In 22-core MCF scenario, the most efficient modulation format lowers to DP-16QAM. Thus, $n_{fs} = 2$ and $n_s = 8$ (we have a bandwidth increment and the number of cores used is reduced). Finally, the third situation (iii) would occur if the end-to-end path would lengthen to 3500 km. The most efficient modulation format in a MF scenario is DP-QPSK, so that $n_{fs} = 2$ and $n_s = 15$. However, in a 22-core MCF scenario, the most efficient modulation format lowers to DP-BPSK, resulting in $n_{fs} = 3$ and $n_s = 17$ (i.e., an increment of both bandwidth and the number of cores used). Assuming that JoS is employed at intermediate nodes, situations ii) and iii) lead to higher BBP in the MCF-enabled network compared to the equivalent MF case, as a wider spectrum range is necessary to allocate the same super-channel. To quantify such negative effects of ICXT, Fig. 3.8 depicts the network BBP vs. offered load in our Flex-Grid/MCF network scenarios describing the DT12 and US26 network topologies, together with that of an equivalent MF scenario with a bundle of 22 independent single-mode fibers per link. The proposed PSA strategy is employed in all cases. Moreover, as argued at the end of subsection 3.1.2.2, a GB equal to 7.5 GHz has been

assumed. As can be observed in the figure, the MF clearly outperforms the MCF-enabled one. For example, for a target BBP=1%, around 14% and 17% offered load reduction is evidenced in the MCF-enabled scenario versus the equivalent MF in the DT12 and US26 networks, respectively.

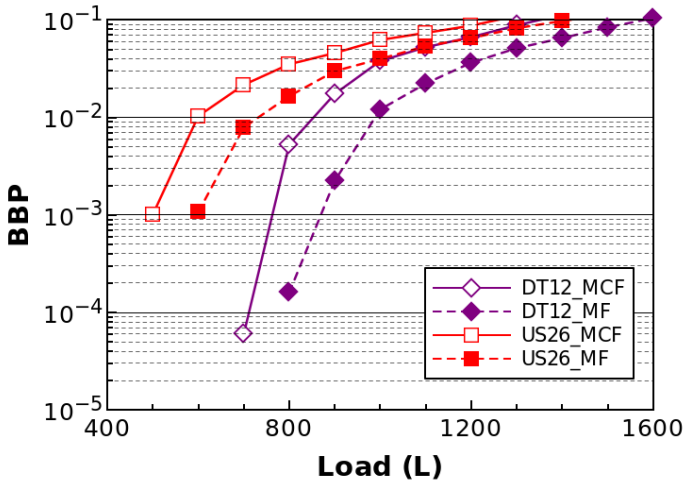

Fig. 3.8. BBP vs. offered load in DT12 and US26 network topologies with MCF- and MF-enabled links. 22-core MCFs or bundles of 22 fibers per link are assumed in each case. GB=7.5 GHz.

To complement this analysis, Fig. 3.9 shows the distribution of the usage of the modulation formats in MCF scenarios compared to MF ones. To obtain these results, we have focused on an offered load leading to 1% BBP. As we can see, ICXT has a more remarkable effect in the US26 continental backbone network, being necessary to employ more robust modulation formats, even DP-BSPK in some cases. In MCF-enabled scenarios, the most utilized modulation format is DP-QPSK, whilst for those equivalent MF solutions the most utilized one is DP-16QAM. As for the case of the DT12 national backbone network, the shorter distances allow using higher order modulation formats. In the MCF-enabled scenario the modulation format used with the lowest efficiency is DP-QPSK, whilst in the equivalent MF scenario it is only necessary to lower it down to DP-16QAM. In addition, whereas in MCF-enabled scenarios the most utilized modulation format is DP-16QAM, for MF ones the most utilized one is DP-64QAM.

To end this subsection, we also compare the requirements of both MCF- and equivalent MF-enabled solutions in terms of active transceivers in the network (m_{TRx}). An increased number of active transceivers may be expected in the MF scenario, resulting from situation ii) analyzed before, as well as from the fact that the MF solution can accommodate more demands (an increased offered load can be supported for the same target BBP, e.g., 1%, as seen in Fig. 3.8). On the other hand, situation iii) has the opposite effect; however, this is less likely to occur.

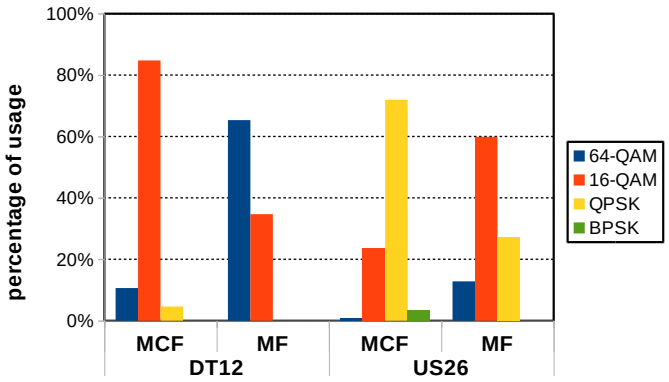

Fig. 3.9. Distribution of the usage of modulation formats in each network, DT12 and US26, for MCF-enabled and equivalent MF scenarios. An offered load leading to 1% BBP is assumed.

Fig. 3.10 illustrates the m_{TRx} CDFs for MCF- and equivalent MF-enabled scenarios in the DT12 and US26 backbone networks, always employing the proposed PSA strategy. Again, an offered load leading to 1% BBP is assumed. As observed, our expectations are accomplished in both networks, being the m_{TRx} differences between MCF and MF scenarios more remarkable in the DT12 network (12% and 9% increment in the peak number of active transceivers for MF vs. MCF, for DT12 and US26 networks, respectively). It shall be mentioned, though, that the estimated mean operational baud-rate of the transceivers in the MF scenarios is lower than in the MCF-enabled ones, i.e., 8.66 vs. 10.95 GBaud (26% increment), and 12.15 vs. 14.69 GBaud (20% increment), in DT12 and US26, respectively.

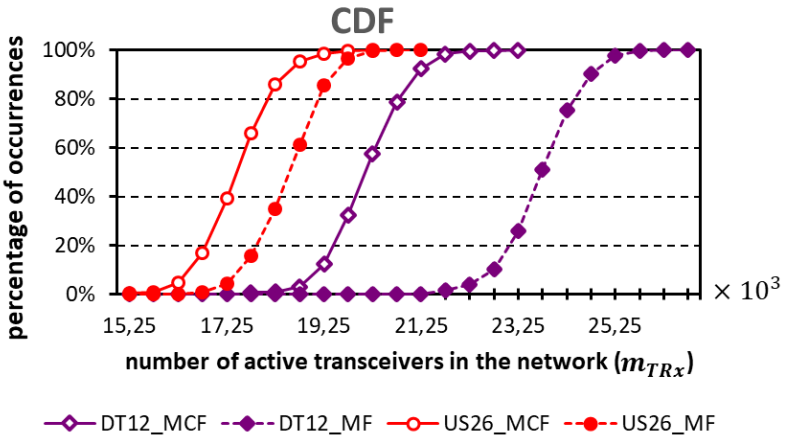

Fig. 3.10. m_{TRx} CDFs in DT12 and US26 networks for MCF- and the equivalent MF-enabled solution.

3.1.4 Network throughput vs. spatial multiplicity analysis

As already introduced before, spectral wastage of spatially fixed Flex-Grid/SDM networks and the increment of ICXT as core count increases can negatively affect the network GoS. In order to quantify the throughput gain as a function of spatial multiplicity, in this subsection, we evaluate the scalability of spatially fixed Flex-Grid/SDM networks by considering the first SDM region to be explored [109], namely, scaling spatial multiplicity S from 7 to 30 spatial channels. We

contemplate MF solutions as well as several MCF prototypes available in the literature. In more detail, subsection 3.1.4.1 describes the SCh allocation in spatially fixed Flex-Grid/SDM networks and presents a heuristic for RA with end-to-end spatial traffic grooming. Meanwhile, subsection 3.1.4.2 presents throughput scalability results of spatially fixed Flex-Grid/SDM networks.

3.1.4.1 SCh allocation in spatially fixed Flex-Grid/SDM networks

As explained in subsection 3.1.3.2, although JoS is realized across all spatial channels (S), the optimal allocation of one traffic demand may only require some of them (n_s), depending on the demand bit-rate r_d. Another particularity of JoS is that RA problem is equivalent to Flex-Grid over a single spatial channel. The goal is to assign enough n_s in order to minimize the n_{fs} allocated to each spatial channel, thus maximizing, therefore, the GoS of the network. n_s can take any value in the interval $1 \leq n_s \leq S$. The largest demands (in terms of bit-rate) could require allocating even S, while the smaller ones could require just one spatial channel in order to obtain the lowest n_{fs} value. The minimum n_{fs} is ensured when r_d is split over the entire S according to equation (3.1). Note that we can rewrite this equation by introducing n_s value (obtained by executing PSA procedure) instead of S, as follows:

$$n_{fs} = \left\lceil \frac{r_d/(n_s \cdot SE) + GB}{W} \right\rceil \tag{3.2}$$

From the situation described above, one question that arises: *What can we do with spectral-spatial resources not used by one lightpath?*. For example, in the previous example in Fig. 3.4.a 2 FSs were assigned in 6 (out of 22) spatial channels for a 1 Tb/s demand. Therefore, the unallocated spatial channels ($n'_s = S - n_s$) were 16. If we employ directly the JoS technique, we are wasting 2 FSs x 16 = 32 FSs. An alternative to increase the spectrum usage would be to reuse the active lightpaths in such a way that the free spectrum ranges of the unused spatial channels can be assigned to other demands that share the same source (s_d) and destination (t_d) nodes. This can be called end-to-end spatial traffic grooming (e2e-grooming), similarly as the technique called *full-match resource reuse* in [59], without modifying the ROADM architecture for JoS and only requiring flexibility in the s_d and t_d nodes to aggregate/disaggregate traffic to the active lightpaths. One lightpath (lp) can be reused as many times as needed until filling all spatial channels, all of them switched together using JoS. To illustrate e2e-grooming, let us consider another example shown in Fig. 3.11. In this case, we have a network with 7 available spatial channels per link and four traffic demands to be accommodated. Three demands d_1, d_3 and d_4 are co-routed because they share s_d and t_d nodes. Therefore, if the available and required spatial resources allow it, they can share the same lightpath established for demand d_1 ($lp1$). Note that, all signals that share $lp1$ are modulated over the same OC at central frequency f_i. Meanwhile, the fourth demand d_2 has to establish a new lightpath $lp2$ because it has different s_d and t_d nodes.

In this example, two demands reuse $lp1$, hence reducing the spatial wastage from 4 to 0 (7/7 spatial channels are occupied). Meanwhile, the spectrum wastage is reduced from 8 FSs to 4FSs (because $lp1$ is shared by different demands in terms of the number of required FSs).

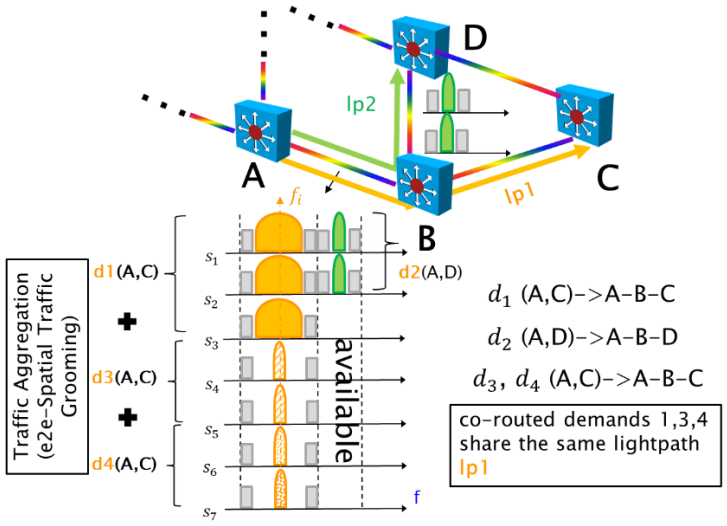

Fig. 3.11. Spatial super-channel allocation with e2e-grooming.

A greedy heuristic to solve the Route, Modulation Format, Space, and Spectrum Assignment (RMSSA) with e2e-grooming in spatially fixed Flex-Grid/SDM networks is shown in Table 3.4 and Table 3.5. When a new demand d_i arrives at the network, we firstly test if e2e-grooming operation is feasible (see the algorithm shown in Table 3.5). For this purpose, we find out in the set of active lighpaths (Lp) the ones that share the same source and destination nodes as d_i ($Lp_{s,t} \subseteq Lp$) and check if any of them has enough spectral and spatial resources available to be assigned to d_i (Table 3.5, line 9); otherwise, a new lightpath lp has to be established. To this end, K-SPs are used as feasible candidate paths. For each candidate path (p), the MSE modulation format, with a TR equal or higher than the physical path length, is selected (Table 3.4, line 8). Then, the optimal amount of required spatial and spectral resources (n_s, n_{fs}) are determined by using PSA strategy (Table 3.4, lines from 10 to 16). Finally, if there exist n_{fs} free FSs in the available spectrum (F: set of FSs) of the first spatial channel along p, demand d_i is allocated. Otherwise, the subsequent candidate paths are analyzed. If no candidate path can allocate d_i, it is finally blocked (Table 3.4, line 27).

The time complexity of the RMSSA heuristic described above can be analyzed as follows. In the worst-case, the allocation of a lightpath includes searching free spectral-spatial resources over all established lightpaths (for e2e-grooming operation) and overall K-SPs. Specifically, for the e2e-grooming operation (Table 3.5), its time complexity is the sum of finding, over $|Lp|$ established lightpaths, those ones whose source (s) and destination (t) nodes are equal to the ones of d_i plus the time complexity of sorting $Lp_{s,t}$ in ascending order (to do this, the well-known Timsort

procedure is used, therefore, the time complexity of this procedure is $|Lp_{s,t}| \cdot log|Lp_{s,t}|$) and plus the time complexity of selecting the MSE modulation format (from $|M|$ possible ones) together with the computation of the optimal spectral-spatial resources per SCh (by using PSA strategy, $\mathcal{O}(S)$) for each $lp \in Lp_{s,t}$. Then, the overall time complexity of the e2e-grooming operation is equal to $\mathcal{O}(|Lp| + |Lp_{s,t}| \cdot log|Lp_{s,t}| + |Lp_{s,t}|(|M| + S))$. As for the time complexity of searching for free spectral-spatial resources over *K*-SPs (Table 3.4), firstly, the *K*-SPs are computed by using the Yen's algorithm [74], i.e., the time complexity of this step is equal to $\mathcal{O}(K|N|(|E| + |N| \cdot log|N|))$, where $|N|$ and $|E|$ account for the number of nodes and links in the network, respectively. To this time complexity has to be added the one of selecting the modulation format together with the one of the PSA strategy, plus the time complexity of searching for free spectral resources in F over up to $|E|$ links for each $p \in P$, i.e., $\mathcal{O}(|P|(|M| + S + |F||E|))$. Note that, for a new lightpath, the spectral assignment needs searching only in the F of the first spatial channel per link. Finally, the overall time complexity per arrival connection of this RMSSA heuristic is $\mathcal{O}(|Lp| + |Lp_{s,t}|(log|Lp_{s,t}| + |M| + S) + K|N|(|E| + |N| \cdot log|N|) + |P|(|M| + S + |F||E|))$. In the best case, the computational complexity would only include the search of free spectral-spatial resources over the already established lightpaths (i.e., successful e2e-grooming operation).

Table 3.4: RMSSA heuristic for spatially fixed Flex-Grid/SDM networks

1: **Input:**
G=(|N|,|E|) // Physical Network
GB // Assumed guard-band per Sb-Ch
d_i // Demand arriving at the network
Lp // Set of active Lightpaths
F // Set of FSs per spatial channel
S // Total number of spatial channels of MF or MCF
M // Set of modulation formats
2: **Begin:**
3: $Y_i \leftarrow e2e\_Grooming(Lp, d_i, S)$ //binary flag for grooming
4: **If** Y_i is false **then**
5: P ←Compute *K* candidate SPs between s_d and t_d in *G*
6: X_i ←false // binary flag:"0" d_i is blocked,"1" d_i is accepted
7: **For** each p in P **do**
8: Find the MSE modulation $m \in M$ format with $TR \geq$ Physical length of p [km]
9: $n_s = S$ //initial value: all S spatial channels
10: Compute minimum $n_{fs} \leftarrow \lceil (r_d/(n_s \cdot SE) + GB)/W \rceil$
11: **do**
12: Compute $n_{fs\_new} \leftarrow \lceil (r_d/((n_s - 1) \cdot SE) + GB)/W \rceil$
13: **If** $n_{fs\_new} = n_{fs}$ **then**
14: $n_s \leftarrow n_s - 1$

15: **else** break
16: **while** ($n_{fs\_new} = n_{fs}$)
17: **If** continuous and contiguous n_{fs} FSs are free in F of 1st spatial channel along p **then**
18: Allocate the spectral resources
19: Establish new lightpath lp_i
20: $n_s(lp_i) \leftarrow n_s$
21: $L_p \leftarrow L_p \cup \{lp_i\}$
22: $X_i \leftarrow true$, considering d_i as served
23: break
24: **end if**
25: **end for**
26: **If** X_i is false **then**
27: Consider d_i as blocked
28: **end if**
29: **end if**
30: **End.**

Table 3.5: e2e-grooming algorithm for JoS-enabled Flex-Grid/SDM networks

1: **Input:**
Lp // Set of active Lightpaths
d_i // Demand arriving at the network
S // Total number of spatial channels in MF or MCF
2: **Begin:**
3: Find $Lp_{s,t} \subseteq Lp$ with s and t equal to the ones of d_i
4: $Lp_{s,t} \leftarrow$Sort $Lp_{s,t}$ by length in ascending order
5: $Y_i \leftarrow$false // binary flag to determine if d_i share one lp
6: **For** each lp in $Lp_{s,t}$ **do**
7: $n'_s \leftarrow S - n_s(lp)$ // Free spatial channels in lightpath lp
8: Compute $n_{fs}, n_s \leftarrow$idem as steps from 8 to 16 in Table 3.4
9: **If** $n_{fs} \leq n_{fs}$ (lp) and $n_s \leq n'_s$ **then**
10: allocate the d_i in the current lighpath lp
11: $n_s(lp) \leftarrow n_s(lp) + n_s$ // Update n_s of lightpath lp
12: $Y_i \leftarrow true$, considering d_i as served
13: break
14: **end if**
15: **end for**
16: return Y_i
17: **End.**

3.1.4.2 Simulation results

This subsection aims to assess the throughput scalability of spatially fixed Flex-Grid/SDM optical networks. To this end, we scale up the spatial multiplicity S from 7 to 30 spatial channels and for

each point we measure the average carried traffic –hereinafter referred to as network throughput (in Pb/s)– for a BBP≈1%. We compute this network throughput as the average of the instantaneous carried traffic samples after each lightpath establishment/release. As introduced, this chapter is concentrated on the applicability of JoS switching strategy, where S spatial channels are reserved per lightpath. Therefore, the results are referring to the ones of JoS-enabled Flex-Grid/SDM networks with or without e2e-grooming. For this purpose, we follow the RA procedure presented in previous subsection 3.1.4.1, where for each traffic demand we compute K=3 candidate SPs between its s_d and t_d nodes.

In more detail, in order to estimate the throughput scalability of Flex-Grid/SDM networks, we consider reference networks DT12 and US26, whose topologies and main characteristics are shown in Appendix A. In each network link, we scale up the spatial multiplicity S from 7 to 30. We consider MF- as well as MCF-based solutions. For MF ones, 1-spatial channel granularity is considered, while for MCF ones the five best single-mode MCF prototypes found in the literature [27]–[31] are taken into account, i.e., $S \in \{7, 12, 19, 22, 30\}$. The worst aggregate ICXT measurements for the considered MCFs and their TRs are the one shown before in Table 3.2. Each fiber/core has 320 available FSs of 12.5 GHz width. We also consider that the GB between SChs is equal to 7.5 GHz.

Traffic demands arrive at the network following a Poisson process with negative exponentially distributed IAT. Each request asks for a bidirectional lightpath between uniformly distributed source and destination nodes with bit-rate equal to r_d during a certain HT, which also follows a negative exponential distribution. We consider two TPs: TP1 = {100, 400, 1000} Gb/s with probabilities {0.4, 0.3, 0.3}, so that the mean bit-rate is 460 Gb/s; and TP2 = {400, 1000, 2000} Gb/s with the same previous probabilities, resulting in a mean bit-rate equal to 1.06 Tb/s. Different offered loads (HT/IAT) are simulated until we obtain a BBP close to 1% for each spatial multiplicity value. To get statistically relevant results, we offer $5x10^5$ bidirectional connection requests per execution. Note that, there exists an initial transient period due to the Poisson process of arrivals before getting the steady state of 1% target BBP. To isolate this transient period from the statistic, we must either (i) use a relevant time of observation compared with the transient (i.e., use a statistical sample with significant size) or (ii) identify all connections occurred during the transient and directly discard them from the statistic. We use (i), but first we have verified with (ii) that the *Avg. Carried Traffic* metric remains unaffected.

Fig. 3.12 shows the network throughput for different S values in the DT12 and US26 networks, under both TP1 and TP2. Focusing on the MF solution, increasing S does not always imply a reduction of the allocated spectrum, due to the spectral grid constraint. Besides, JoS penalizes

spectrum occupation, as unused spatial channels cannot be allocated to other demands. These two factors cause the step-like shape seen in Fig. 3.12.

In the DT12 network, the results presented in Fig. 3.12.a and Fig. 3.12.b disclose that the spatial multiplicity is poorly exploited without e2e-grooming (NonGr plots). As observed, for a 4.3× spatial multiplicity factor (i.e., from S=7 to S=30), network throughput scales only up to 1.5× and 2× for TP1 and TP2, respectively. However, when e2e-grooming is considered (Gr plots), network throughput increases considerably, around 3.5× and 3.3× for TP1 and TP2, respectively. As for the US26 network (Fig. 3.12.c and Fig. 3.12.d), which has longer network diameter, smaller differences between these scenarios with or without e2e-grooming are observed. The fact is that connections over long distance paths require employing less efficient modulation formats. Then, the transmitted bit-rate per spatial channel is lower and, consequently, higher n_s values are needed, which reduces the possibilities of reusing lightpaths. This effect is even more evident with larger demands. For example, under TP2 (Fig. 3.12.d), the results with e2e-grooming are practically equal (or very close) to those without it, whilst differences are more significant under TP1 (Fig. 3.12.c), particularly as the spatial multiplicity increases (e.g., from S=15 onwards). Moreover, for 4.3x spatial multiplicity factor, network throughput with e2e-grooming scales up to a factor very similar as in the DT12 network, namely, about 3.1× and 3.5× under TP1 and TP2, respectively. As highlighted before, the performance of spatially fixed Flex-Grid/SDM networks is sensitive to the network size and TP. For example, in the DT12 network, Fig. 3.12.a and Fig. 3.12.b, the e2e-grooming effect is evidenced earlier under TP1 (from S=8 onward) than under TP2 (from S=15 onward). In contrast, in the US26 network, the e2e-grooming effect is evidenced from S=14 onward under TP1, while almost inappreciable under TP2. The higher the network size (less efficient modulation formats have to be explored) or the bigger the r_d value, the larger the allocated n_s leaving less spatial resources for e2e-grooming.

Regarding MCFs, as expected, the larger the network size, the higher the ICXT impact. ICXT forces to employ more robust modulation formats along a physical path, and may increase both spectral and spatial allocated resources. In both DT12 and US26 networks, 7-core, 12-core and 30-core MCFs evidence the same or very close performance as the MF equivalent solutions, since their extremely low ICXT does not become the TR limiting factor, being SNR instead, as in the equivalent MF solutions. However, the 19- and 22-core MCFs exhibit substantial differences against the equivalent MF solutions. Since the 19-core MCF shows the highest ICXT level, network performance degradation is relevant. Indeed, these differences in terms of network throughput are up to 50% (in the worst cases) for both DT12 and US26 network. Regarding the e2e-grooming utilization, significant benefits are obtained especially in the DT12 network (Fig. 3.12.a and Fig. 3.12.b), whilst in the US26 network (Fig. 3.12.c and Fig. 3.12.d) ICXT (for 19-core and 22-core MCFs) may prevent any lightpath reuse. Finally, the network throughput for

MCF scales up to practically the same factor as the MF solution (0% penalty versus MF solution, except for penalties evidenced in the 19- and 22-core MCFs) in both DT12 and US26 networks, which indicates the feasibility of MCF deployments in the assessed spatial multiplicity interval.

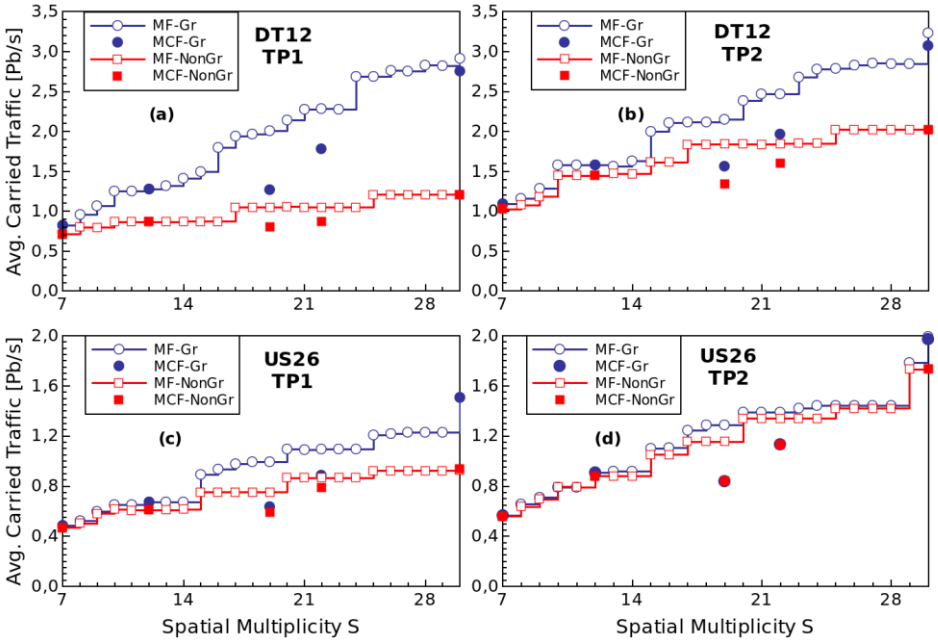

Fig. 3.12. Network Throughput (in Pb/s) versus S in JoS-enabled Flex-Grid/SDM networks for: (a) DT12 under TP1, (b) DT12 under TP2, (c) US26 under TP1, (d) US26 under TP2.

3.1.5 Dynamic end-to-end spatial traffic grooming

In the previous subsection, it was presented e2e-grooming spatial grooming for spatially fixed Flex-Grid/SDM networks, as a mechanism to leverage the spectral-spatial resources left unused after the allocation of demands. However, it was also demonstrated that large Spa-SChs in terms of n_s spatial channels could hinder e2e-grooming operation, thus making it useless. In this subsection, we study an alternative to counteract this issue by exploring the fittest SCh configuration during the e2e-grooming operation. We name this strategy as d*ynamic* e2e-grooming and we evaluate its benefits under several traffic conditions. To this end, we firstly present the methodology and greedy heuristic for *dynamic* e2e-grooming and, finally, the simulation results.

3.1.5.1 Methodology for *dynamic* e2e-grooming

Thanks to the spectrum flexibility given by Flex-Grid, for the same demand d, different SCh configurations are valid to allocate it. Specifically, given a fiber with S spatial channels different (n_s, n_{fs}) tuples are possible to serve d, being n_s the required number of spatial channels and n_{fs} the required number of FSs per spatial channel. For instance, for a demand with bit-rate r_d = 400 Gb/s using DP-QPSK modulation format with SE at the Nyquist limit (4 b/s·Hz), S=9, W = 12.5

GHz and 7.5 GHz GB, SCh candidates (Ω), expressed as a set of (n_s, n_{fs}) tuples are: Ω = {(1,9), (2,5), (3,4), (4,3), (6,2)} (see Fig. 3.13), computed by means of equation (3.2) from n_s=1 to n_s=S. i-th tuples (n_s, n_{fs}) that do not yield lower n_{fs} than their (i-1)-th are trivially discarded at the very beginning. As appreciated, the higher the number of spatial channels n_s, the lower the number of FSs n_{fs}.

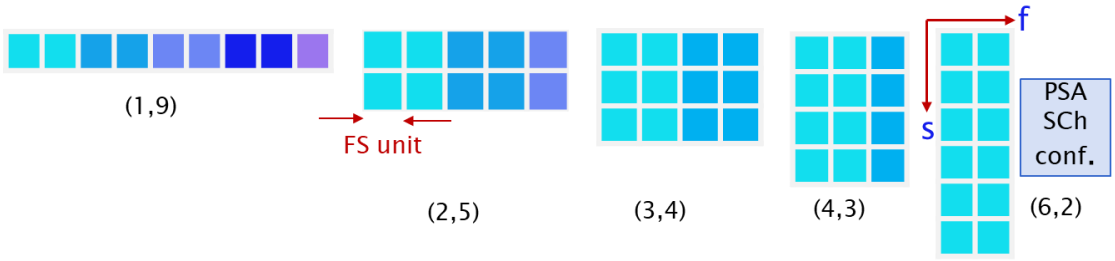

Fig. 3.13. Candidate SCh configurations for r_d = 400 Gb/s using DP-QPSK modulation format with SE at the Nyquist limit (4 b/s·Hz), S=9, W=12.5 GHz and GB=7.5 GHz.

As presented in subsection 3.1.3.2, the typical goal in JoS-enabled Flex-Grid/SDM networks is to allocate the finest spectrum portion across n_s spatial channels in order to maximize the network GoS . Therefore, among the SCh candidates in the previous Ω example, the last tuple (6,2) would be the most suitable one, which, in fact, is obtained following the PSA procedure, presented in the same subsection 3.1.3.2. If this PSA SCh configuration is followed to allocate new lightpaths as well as during 2e2-grooming, it can occur that some lightpaths are not reused by co-routed demands because the free spectral-spatial resources are not able to accommodate other demands, as already demonstrated in the previous subsection 3.1.4. This procedure can be called as *predefined* e2e-grooming.

As alternative approach, we can suggest testing other unexplored SCh configurations (i.e., other tuples in Ω) only during the e2e-grooming operation. Note that in that case the selected SCh configuration for grooming could include configuring a MC Spa-SCh or even a Spe-SCh depending on the transmission baud-rate. If one lightpath has free spectral-spatial resources to groom another demand, we could start testing from the least demanding SCh configuration (in terms of n_s) to the most demanding one. This procedure can be called as *dynamic* e2e-grooming. For example, Fig. 3.14 shows a Spa-SCh allocation for the 400 Gb/s demand (d_1), previously introduced. After allocating d_1 there would be 3x2 free spectral-spatial resources that might be used to allocate a co-routed demand, e.g., d_2 of 100 Gb/s with DP-QPSK. The SCh candidates (Ω) of d_2 are: (1,3), (2,2) and (5,1). The *predefined* e2e-grooming would select the (5,1) tuple, which does not suitably fit into the free spectral-spatial resources. Nevertheless, following our *dynamic* e2e-grooming proposal, the first candidate tuple (1,3) is discarded because it requires higher spectral resources, whereas the second one (2,2) fits properly and even 1x2 spectral-spatial resources are still available to groom other demand in s_9.

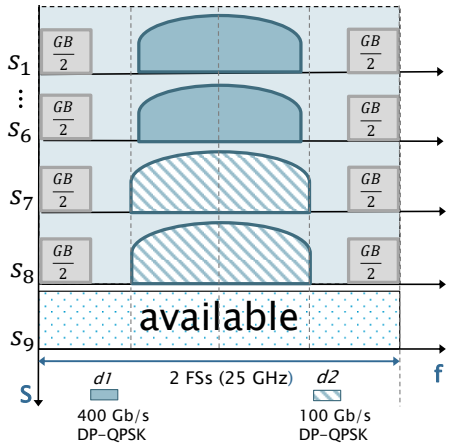

Fig. 3.14. *Dynamic* e2e-grooming for two co-routed demands

3.1.5.1.1 RMSSA heuristic

In this subsection, we elaborate on the RMSSA greedy heuristic for JoS-enabled Flex-Grid/SDM networks with *dynamic* e2e-grooming. In general (see algorithm in Fig. 3.15), when a new demand d arrives at the network, it should be firstly checked if the e2e-grooming operation is feasible. To this end, all lightpaths sharing the same s and t nodes as d are found. Then, for each of these lightpaths the MSE modulation format is selected according to its physical length, in order to compute Ω. The available spectral-spatial resources per lightpath are contrasted with those required by each SCh candidate ∈ Ω. If one SCh candidate suitably fits into the available resources, d is considered as served; otherwise, a new lightpath has to be established. For this purpose, the K=3 SPs are used as candidate physical paths. Starting with the shortest one, the following procedure is executed: 1) Select the MSE modulation format with an optical reach equal or higher than the physical path length; 2) Compute the (n_s,n_{fs}) tuple by using the PSA strategy, i.e., the SCh configuration minimizing n_{fs}; 3) Find if continuous and contiguous n_{fs} FSs are available in the spectrum of the first spatial channel along the candidate path. If so, directly reserve them across n_s spatial channels and consider d as served. Otherwise, subsequent candidate paths are analysed. If no candidate path can allocate d, it is finally considered as blocked.

3.1.5.2 Simulation results

To evaluate the proposed *dynamic* e2e-grooming, we consider the DT12 reference network. Each fiber link consists of 22 spatial channels (bundle of standard SMFs), each one with 320 FSs of 12.5 GHz (4 THz C-band). The TR estimation per Spa-SCh is computed by following the procedure detailed in subsection 3.1.1 for standard SMF with up to 32 GBaud DP-BPSK, DP-QPSK, DP-16QAM, DP-64QAM signals.

A dynamic scenario where demands arrive at the network following a negative exponentially distributed IAT is assumed. Each request asks for a bidirectional lightpath between uniformly

distributed s and t nodes with bit-rate r_d during a certain HT, also following a negative exponential distribution. The r_d value follows several TPs with different mean (μ) and standard deviation (σ) bit-rate. Different offered L values are obtained by fixing the IAT and varying the HT accordingly (L=HT/IAT). To get statistically relevant results, we offer $5x10^5$ bidirectional requests per execution.

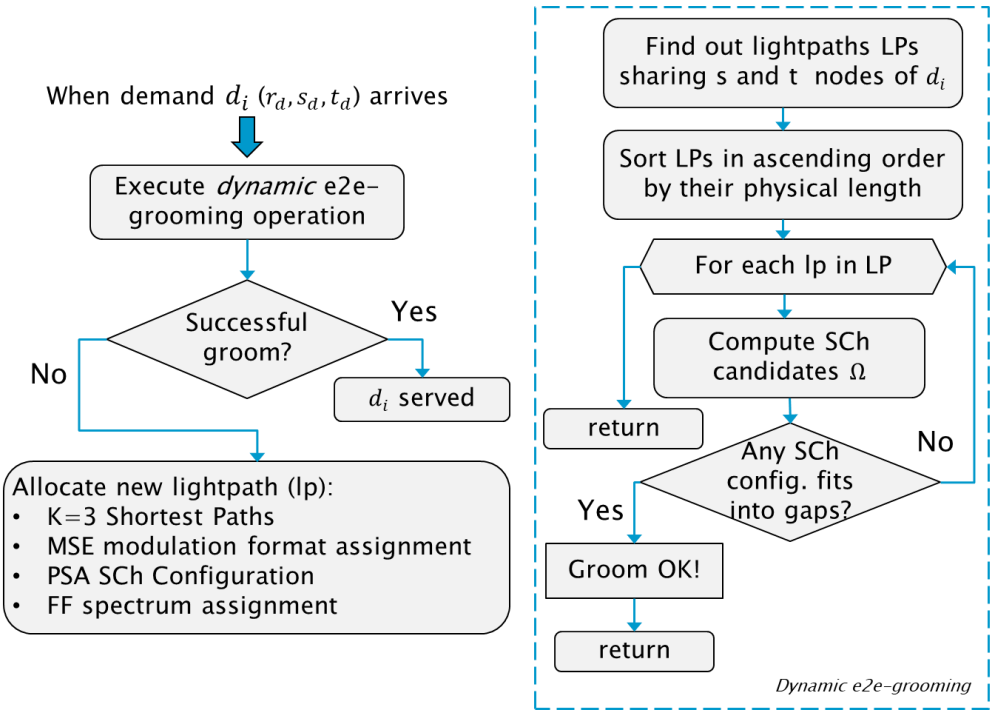

Fig. 3.15. RSSA algorithm for JoS-enabled Flex-Grid/SDM networks with *dynamic* end-to-end spatial traffic grooming

Fig. 3.16.a-f show the BBP vs. L (in Pb/s) for 6 TPs (μ, σ) from TP1 to TP6, respectively. Three curves are shown per graph disclosing results without e2e-grooming (No-Grooming, plots in purple), with *predefined* e2e-grooming (Predef-Grooming, plots in blue) and with *dynamic* e2e-grooming (Dyna-Grooming, plots in red). In the first set of simulations –Fig. 3.16.a-c on top– the μ value per connection is the same, while the σ one is increased, namely, TP1 (2.0,0.0), TP2 (2.0,0.8) and TP3 (2.0,1.6), where μ and σ values are in Tb/s. Conversely, in the second set of simulations –Fig. 3.16.d-f at the bottom– the σ value is the same, while the μ one is increased, namely, TP4 (0.5,0.4), TP5 (1.0,0.4) and TP6 (2.0,0.4).

Looking at the results, for a fixed μ=2, the higher the σ, the higher the benefits (in terms of L) of *dynamic* versus *predefined* e2e-grooming. Specifically, for an homogeneous TP1 (i.e., σ=0) the benefits of *dynamic* e2e-grooming are inappreciable. However, for heterogeneous TPs (i.e., σ>0) these benefits are up to 6% and 10% for σ=0.8 –TP2– and σ=1.6 –TP3–, respectively, for a 1% target BBP. Meanwhile, for a 10% BBP these benefits raise up to 7% and 15% for both cases of σ=0.8 and σ=1.6, respectively.

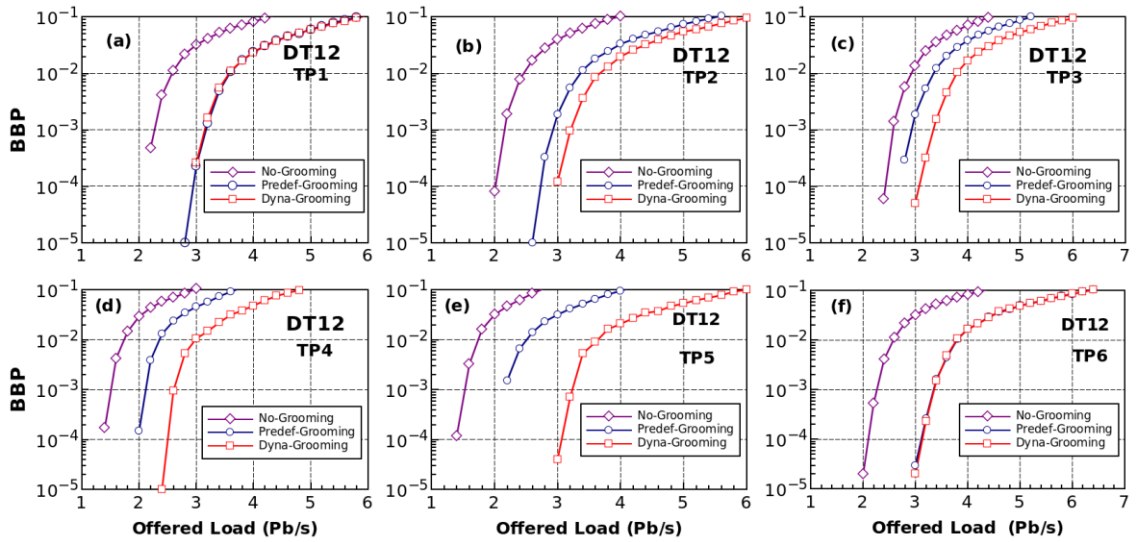

Fig. 3.16. BBP vs. Offered Load (in Pb/s) for different TPs, (top): fixed μ and increasing σ, (bottom): fixed σ and increasing μ

Regarding the second set of simulations, fixing σ=0.4 and varying μ, *dynamic* e2e-grooming benefits can raise up to 25% and 44% for TP4 and TP5, respectively, for 1% target BBP. Moreover, Fig. 3.16.d-f show the impact of the size of demands (in terms of bit-rate). As observed, the higher the bit-rate of demands, the higher the supported L (therefore, the network throughput) under the three strategies (no, *predefined* and *dynamic* e2e-grooming). For instance, for a 1% target BBP, L can increase up to 27%, 58% and 47% for no grooming, *predefined* and *dynamic* e2e-grooming, respectively, when μ value per TP ranges from 0.5 Tb/s –Fig. 3.16.d– to 2 Tb/s –Fig. 3.16.f –. Meanwhile, for a 10% BBP the same percentages raise up to 40%, 86% and 35%, respectively. Among the three strategies, the results show that *predefined* e2e-grooming is the most sensible to the size of demands.

Taking into account the joint impact of μ and σ values, the benefits of e2e-grooming are more significant for low/moderate bit-rate and heterogeneous demands, as observed for TP4 and TP5 –Fig. 3.16.d and Fig. 3.16.e–, whereas these benefits are reduced for high bit-rate and very heterogeneous demands, such as the case of TP3 –Fig. 3.16.c–. Specifically, for a 1% target BBP, for TP4 and TP5, the benefits of e2e-grooming are up to 50% for the *predefined* strategy, against an up to 120% for the *dynamic* one. Meanwhile, for TP3, the benefits are reduced by 15% and 27%, for *predefined* and *dynamic* e2e-grooming, respectively. Finally, according to the results, *dynamic* e2e-grooming does not yield benefits for high bit-rates and homogeneous or quasi-homogeneous TPs, as observed for TP1 and TP6.

3.2 Planning of optimal MIMO assignment for MCF-enabled networks

To overcome the negative effects of ICXT demonstrated in previous subsections 3.1.3.4 and 3.1.4.2, several strategies focused on ICXT management [41], [43], [110] and suppression by using MIMO equalization [111], [112] have been proposed in the literature. In JoS-enabled Flex-Grid/SDM networks since one spectrum range can be allocated across all spatial domain, the worst aggregate ICXT appears (i.e., no ICXT management apply in this scenario). So, this subsection is concentrated on the assignment of MIMO equalization to specific lightpaths of such networks in order to counteract ICXT negative effects.

MIMO-based ICXT suppression through DSP can be implemented at the receiver end, as an extension of the 2×2 MIMO for Polarization Multiplexing (PM) [113]. MIMO-DSP mitigates the negative effects of ICXT; however, its complexity [113], [114] and power consumption [115] are important aspects to be considered. Throughout this subsection, we will refer to MIMO for ICXT suppression solely. Note that the overall complexity order including the decoupling of both ICXT and polarization would be $2 \cdot A \times 2 \cdot A$, being A the number of coupled MCF cores. For instance, Fig. 3.17.a and Fig. 3.17.b show a simplified diagram of MIMO equalizer at the receiver for uncoupled (e.g., MF) and strongly-coupled SDM fiber, respectively, with 3 spatial channels. In the case of uncoupled SDM fiber, independent 2×2 MIMO scheme can be applied to each spatial channel. Therefore, at the end, $3 \cdot (2 \times 2)$ MIMO would be enough to decouple XY polarization. In contrast, if the three spatial channels are strongly-coupled (as represented in Fig. 3.17.b), they have to be jointly processed in a common DSP by using 6×6 MIMO scheme.

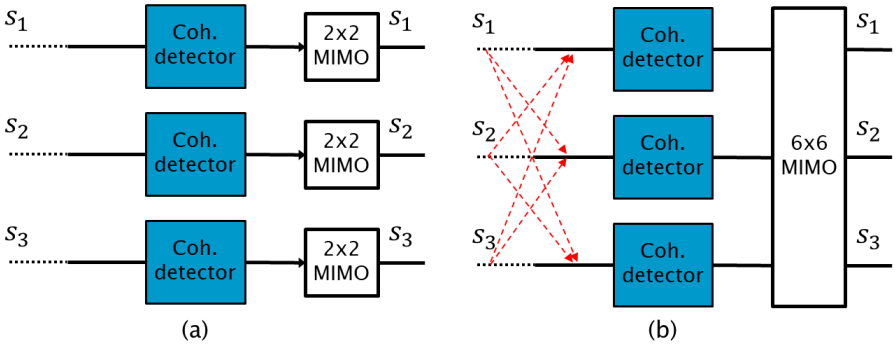

Fig. 3.17. MIMO-DSP for: (a) uncoupled and (b) strongly-coupled SDM fiber

MIMO-DSP helps recovering several signals coupled together, if all of them are jointly processed at a common receiver. So, in case of MCFs, if two or more cores are adjacent and they transmit optical signals on the same wavelength, ICXT between them can be suppressed if they are co-destined and MIMO is applied. Otherwise, the accumulated ICXT along the routing path has to be kept below a given threshold to properly recover them at the receiver [18].

As stated before, in weakly-coupled MCFs MIMO becomes optional. In fact, when a single robust (e.g., BPSK) modulation format is considered, e.g., as in traditional WDM networks, ICXT does not likely affect the network GoS making MIMO unnecessary. However, when high-order or distance-adaptive modulation formats are considered, like in Flex-Grid networks, significant performance gaps between MF –a crosstalk-free SDM fiber– and MCF solutions can appear. The fact is that, although low ICXT is present, it forces to employ more robust but less spectrally efficient modulation formats over long distance paths affecting the network GoS. Hence, the feasibility and convenience of MIMO equalization to compensate ICXT is an interesting case study from a network planning perspective.

On the first matter of feasibility, as said before, MIMO can be applied if the coupled signals are co-destined. For instance, in [112] it is assumed a network with 12-core MCFs, where lightpaths are carried on one routing path, using a single core and wavelength. Those coupled lightpaths directed to a common destination are equalized, while for the rest of them the accumulated ICXT threshold cannot be surpassed. This makes that the overall network performance (in terms of GoS) cannot approach the one of a crosstalk-free SDM fiber system, even though MIMO is applied. Regarding the convenience of using MIMO, as introduced before, JoS allows switching a spectrum range across all spatial channels at once (i.e., all sub-channels are co-destined), being possible to apply MIMO to all lightpaths (spatial SChs in this subsection). However, depending on the XT tolerance, applying MIMO to all lightpaths may not be necessary. So, in this scenario, one important question that arises is: *Which lightpaths would be convenient to be equalized in order to reduce the performance gap versus a crosstalk-free SDM benchmark solution?*

To the best of our knowledge, this subsection answers for the first time the question posed above for JoS-enabled Flex-Grid/MCF networks. We address the MIMO assignment jointly with the RMSA problem arising in EON networks, thus defining and targeting a new problem called Route, Modulation format, MIMO and Spectrum Assignment (RMMSA). To this aim, we propose an optimal solution based on two ILP formulations, and several sub-optimal solutions by means of heuristics. The rest of this subsection is organized as follows. Subsection 3.2.1 describes the RMMSA problem. ILP formulations for the joint RMMSA optimization are presented in subsection 3.2.2, while subsection 3.2.3 describes the proposed heuristics. Subsection 3.2.4 presents the numerical results in three lower-level subsections. Subsection 3.2.4.1 describes the scenario under study. The performance evaluation of the proposed heuristics is presented in subsection 3.2.4.2, whereas the relationship between MIMO equalization and spectral requirements is discussed in subsection 3.2.4.3 in large-scale Flex-Grid/MCF optical core networks. Finally, subsection 3.2.4.4 discusses MIMO complexity and crosstalk compensation aspects assuming a non-ideal MIMO.

3.2.1 Problem statement

The targeted RMMSA problem in JoS-enabled Flex-Grid/MCF optical core networks can be formally stated as:

Given:

1) A Flex-Grid/MCF network represented as a directed graph $\mathcal{G}(\mathcal{N}, \mathcal{E})$, where $\mathcal{N}$ is the set of optical nodes and $\mathcal{E}$ the set of unidirectional MCF links. All MCF links are assumed of $\mathcal{C}$ weakly-coupled cores with identical core layout.
2) A spectral grid consisting of an ordered set of FSs, denoted as $\mathcal{F}$, available in every MCF core. FSs have a spectral width (in Hz) equal to W.
3) A set of admissible modulation formats to be employed by node transceivers, denoted as $\mathcal{M}$. For a given $m \in \mathcal{M}$, ef_m denotes its efficiency (in bits/s·Hz).
4) A set of offered unidirectional demands to the network, denoted as $\mathcal{D}$. Each $d \in \mathcal{D}$ has associated a source (s_d) and a destination (t_d) node in $\mathcal{G}(\mathcal{N}, \mathcal{E})$ and a requested bit-rate (in b/s), denoted as r_d.

Find: a lightpath with or without MIMO equalization for supporting every offered demand in $\mathcal{D}$, subject to the following *constraints*:

1) *Spectrum contiguity*: spatial SChs must be allocated over a contiguous subset of FSs, the same in all cores of the traversed MCFs (i.e., they use the entire spatial dimension, so that JoS can be applied).
2) *Spectrum continuity*: in absence of spectrum conversion and regeneration (i.e., transparent transmission), FSs supporting a spatial SCh must be the same in all MCFs along the path from s_d to t_d.
3) *Spectrum clashing*: a given FS in any core of any MCF can only be allocated to one spatial SCh at most.
4) *Maximum number of lightpaths with MIMO* (η): in order to save DSP complexity and cost, this is the maximum amount of lightpaths to which MIMO-based ICXT suppression can be applied.

Objective: minimize the network spectral requirements by deciding on the most appropriate route, modulation format, MIMO necessity and spectrum assignment for all lightpaths needed to serve all demands.

The objective of the RMMSA problem is to allocate all demands, deciding on which lightpaths should be equalized by using MIMO to approach the performance (in terms of spectral requirements) of an equivalent MF scenario. Without loss of generality, we can assume that a network operator can afford a maximum number of lightpaths with MIMO η in the network, $0 \leq$

$\eta \leq |\mathcal{D}|$. When η=0, none of the lightpaths are equalized using MIMO and the TR (in km) of the optical signals is always limited by the accumulated ICXT and the OSNR (see subsection 3.1.1), as in a basic MCF optical network without MIMO-based ICXT suppression. Conversely, by applying MIMO at the receiver end to η>0 lightpaths, ICXT can be compensated. Assuming an ideal MIMO (i.e., full ICXT suppression), the TR restriction due to ICXT does not apply to those lightpaths anymore, being only limited by OSNR, like in the equivalent MF-based solution. Meanwhile, if a non-ideal MIMO suppression is implemented, the remaining ICXT needs to be evaluated if will or will not prevent an appropriate network performance. This raises the issue to investigate the trade-off between spectrum and MIMO requirements, which will be a key objective of this work. Indeed, there can exist an intermediate η value, $\eta = x$, $x \leq |\mathcal{D}|$, where identical spectral requirements as in an equivalent MF scenario can be achieved (assuming an ideal MIMO). We call this η value as the *sweet spot* from now on. As a matter of fact, some candidate lightpaths can trivially be discarded as candidates for MIMO from the very beginning, as they eventually require the same spectral resources with or without MIMO-based ICXT suppression. For instance, in Table 3.2 (presented in subsection 3.1.1), let us consider a path with a physical length of 800 km over 22-core MCFs with identical ICXT characteristics as the MCF prototype reported in reference [30]. There, the MSE modulation format for both MF (where transmission reach is only limited by OSNR) and MCF (considering ICXT as the overall transmission reach limiting factor) scenarios is the same, i.e., 16-QAM. Consequently, one lightpath served over this path, either in that MCF or equivalent MF scenario would require the same spectrum, making MIMO unnecessary.

3.2.2 Optimal problem solution

In this subsection, we present two ILP formulations to optimally solve the stated RMMSA problem. Using the first formulation (ILP1), the minimum number of FSs to serve all demands in $\mathcal{D}$ permitting at most η lightpaths with MIMO is found. The second formulation (ILP2) is used to find the minimum number of η lightpaths with MIMO required to achieve the same spectral requirements as in the equivalent MF solution. It is worth mentioning that ILP2 is not mandatory to solve ILP1, but can speed up the search for the sweet spot ($\eta = x$).

The following sets and input parameters have been defined for both ILP formulations:

- $\mathcal{P}_d$: Set of pre-computed candidate physical paths for demand $d \in \mathcal{D}$; z_p is the physical length (in km) of path p and h_p the number of hops that it traverses.
- $\mathcal{P}$: Set of all pre-computed candidate physical paths in the network ($\mathcal{P} = \cup_{d \in \mathcal{D}} \mathcal{P}_d$).
- $\mathcal{L}_d$: Set of pre-computed candidate lightpaths for supporting demand $d \in \mathcal{D}$.

- $\mathcal{L}$: Set of all candidate lightpaths in the network ($\mathcal{L} = \cup_{d\epsilon\mathcal{D}}\ \mathcal{L}_d$). We also denote as $\mathcal{L}_e$ those lightpaths traversing MCF link e, and $\mathcal{L}_e^f$ accounts for lightpaths traversing link e and using slot $f \in \mathcal{F}$.
- δ_l: Binary parameter, equal to 1 if MIMO is applied to candidate lightpath l, 0 otherwise. $l^{(1)}$ and $l^{(0)}$ account for lightpath l with and without MIMO, respectively.
- $m_{l^{(1)}}, m_{l^{(0)}}$: MSE modulation format assigned to lightpath l with and without MIMO, respectively.
- $nFS_{l^{(1)}}, nFS_{l^{(0)}}$: Number of FSs assigned to lightpath l with and without MIMO, respectively.
- GB: Guard-band width (in GHz) needed between adjacent spatial SChs to facilitate their filtering.
- W: Spectral grid granularity (i.e., 12.5 GHz according to the ITU-T recommendation [12]).

3.2.2.1 Candidate lightpath pre-computation

The allocation of a lightpath in the network requires deciding on the physical path that it will traverse from source to destination and the spectrum portion used. Moreover, in our scenario, we assign another attribute δ_l to lightpaths, indicating whether MIMO is applied to them or not. To let both ILP formulations decide on the RMMSA for each demand to be allocated in the network, we rely on the pre-computation of candidate lightpaths (i.e., candidate physical paths and candidate frequency slots with/without MIMO). Table 3.6 details the algorithm to this end.

According to candidate lightpath pre-computation algorithm, for every demand $d \in \mathcal{D}$ and path $p \in \mathcal{P}_d$, the MSE modulation format whose reach is equal or larger than z_p, either without ($m_{l^{(0)}}$) or with MIMO equalization ($m_{l^{(1)}}$) is selected. Then, assuming such modulation formats, the spectral width in FSs of a (candidate) lightpath l over that path p, either without ($nFS_{l^{(0)}}$) or with MIMO ($nFS_{l^{(1)}}$) is obtained (line 4 and 5). Note that, in order to minimize the required spectral width, we assume that the entire spatial dimension of the MCFs is used to configure a spatial SCh, similarly as in the FSA strategy presented in subsection 3.1.3.1. Thus, each core supports $r_d/\mathcal{C}$ b/s. This latter aspect makes a JoS-enabled Flex-Grid/MCF network equivalent to a Flex-Grid over single spatial channel from the routing point of view. Otherwise, the selected core index *i*-th must be also indicated in the lightpath l definition. Next, we find, in a sliding window fashion, all candidate lightpaths of $nFS_{l^{(0)}}$ adjacent FSs over that path, which are added to $\mathcal{L}_d$, namely, the set of candidate lightpaths without MIMO to carry demand d. The same is done to find all of them with MIMO, that is, of $nFS_{l^{(1)}}$ adjacent FSs. If there exist candidate lightpaths with and without MIMO that require the same number of FSs, we only keep in $\mathcal{L}$ those without MIMO equalization (MIMO is unnecessary).

Table 3.6: Candidate lightpath pre-computation algorithm

Input: $\mathcal{D}$, $\mathcal{P}_d$, $\mathcal{M}$, $\mathcal{C}$, W, GB

1: **for each** d in $\mathcal{D}$ **do**
2: $\mathcal{L}_d = \emptyset$
3: **for each** p **in** $\mathcal{P}_d$ **do**
4: $m_{l^{(0)}} \leftarrow$ Most efficient $m \in \mathcal{M}$ with reach>= z_p (w/o MIMO)
5: $m_{l^{(1)}} \leftarrow$ Most efficient $m \in \mathcal{M}$ with reach >= z_p (w/ MIMO)
6: $nFS_{l^{(0)}} = \left\lceil \left(r_d / (\mathcal{C} \cdot ef_{m_{l^{(0)}}}) + GB \right) / W \right\rceil$
7: $nFS_{l^{(1)}} = \left\lceil \left(r_d / (\mathcal{C} \cdot ef_{m_{l^{(1)}}}) + GB \right) / W \right\rceil$
8: **for** slotIndex = $nFS_{l^{(0)}}$ **to** $|\mathcal{S}|$
9: $\delta_l \leftarrow$ false
10: $l \leftarrow$ **newlightpath** (p, slotIndex – $nFS_{l^{(0)}}$, slotIndex, δ_l)
11: $\mathcal{L}_d \leftarrow \mathcal{L}_d \cup \{l\}$
12: **for** slotIndex = $nFS_{l^{(1)}}$ **to** $|\mathcal{S}|$
13: $\delta_l \leftarrow$ true
14: $l \leftarrow$ **newlightpath** (p, slotIndex – $nFS_{l^{(1)}}$, slotIndex, δ_l)
15: **if** $l \notin \mathcal{L}_d$ **then** $\mathcal{L}_d \leftarrow \mathcal{L}_d \cup \{l\}$
16: **End.**

As a last remark, note that all pre-computed candidate lightpaths already ensure both the spectral contiguity and continuity constraints pointed out in previous section (i.e., they employ the same set of contiguous FSs in all MCF links along the physical path p).

3.2.2.2 ILP formulations

For both ILP formulations, the following decision variables are introduced:

- x_l: Binary; equal to 1 if candidate lightpath $l \in \mathcal{L}_d$ is used to allocate demand $d \in \mathcal{D}$; 0 otherwise.
- y_{ef}: Binary; equal to 1 if FS $f \in \mathcal{F}$ is used in link $e \in \mathcal{E}$; 0 otherwise.
- y_f: Binary; equal to 1 if FS $f \in \mathcal{F}$ is used in any link of the network; 0 otherwise.

The ILP1 formulation to quantify the minimum number of FSs needed to serve all demands in $\mathcal{D}$ reads:

$$minimize \quad \Phi = \sum_{f \in \mathcal{F}} y_f \tag{3.3}$$

subject to:

$$\sum_{l \in \mathcal{L}_d} x_l = 1 \, , \forall d \in \mathcal{D} \tag{3.4}$$

$$\sum_{l \in \mathcal{L}_e^f} x_l \leq y_{ef} \, , \forall e \in \mathcal{E}, f \in \mathcal{F} \tag{3.5}$$

$$\sum_{e\in\mathcal{E}} y_{ef} \leq |\mathcal{E}| y_f \,, \forall f \in \mathcal{F} \tag{3.6}$$

$$\sum_{l\in\mathcal{L}} \delta_l \cdot x_l = \eta \tag{3.7}$$

Objective function (3.3) aims to minimize the total number of FSs used in any MCF link in the network (i.e., Φ, considered hereafter as the *spectrum usage* metric). Constraint (3.4) enforces that every offered demand is supported over a single lightpath. Constraint (3.5) is the spectrum clashing constraint, which ensures that any FS in any MCF link supports one lightpath at most. Constraint (3.6) assigns the value of variables y_f. Finally, constraint (3.7) limits the number lightpaths with MIMO to η.

Thus, by sweeping $\eta \in [0, |\mathcal{D}|]$ we can find the relationship between MIMO equalization and spectrum usage. One should expect that the higher the number of lightpaths with MIMO, the lower the number of required spectral resources. The upper (Φ_{MCF}) and lower (Φ_{MF}) bounds of the objective function (Φ) can be obtained if constraint (3.7) is not considered and candidate lightpath computation in algorithm 1 only includes the ones employing $m_{l^{(0)}}$ (i.e., without MIMO) or $m_{l^{(1)}}$ (i.e., assuming an ideal MIMO) modulation formats, respectively. Conversely, in order to compute the spectral requirements for $0 < \eta < |\mathcal{D}|$ values, it is necessary that set $\mathcal{L}$ includes all candidate lightpaths with and without MIMO equalization.

Moreover, in order to find out the sweet spot ($\eta = x$), where the spectrum utilization is the same as in the MF equivalent solution, ILP1 can be adapted as follows (ILP2):

$$minimize\ \eta = \sum_{l\in\mathcal{L}} \delta_l \cdot x_l \tag{3.8}$$

subject to constraints: (3.4), (3.5), (3.6), and

$$\sum_{f\in\mathcal{F}} y_f \leq \Phi_{MF} \tag{3.9}$$

In ILP2, objective function (3.8) aims to minimize the number of lightpaths with MIMO. Moreover, note that the value of ILP1 objective function for the MF solution (Φ_{MF}) feeds as an input parameter in constraint (3.9), in order to enforce that the total number of FSs used in any link does not exceed the value found for the MF-based solution. Therefore, ILP2 targets the opposite objective of ILP1.

3.2.3 Heuristic approaches

In this section, we introduce several heuristics in order to solve the RMMSA problem. It has been widely demonstrated in the literature that the RSA problem is Non-deterministic Polynomial (NP)-hard [73], [75], meaning, in few words and very informally, that the problem cannot be optimally solved in polynomial (deterministic) time by means of an algorithm. Furthermore, the additional modulation format and MIMO assignment sub-problems present in RMMSA increase

its computational complexity of RSA even more. For this reason, for large-scale problem instances, it is necessary to provide sub-optimal approaches employing heuristics in order to solve the RMMSA problem in polynomial times. In this subsection, we propose two greedy heuristics (i.e., algorithms choosing the partial solution that looks the best one at each stage, thus providing myopic or locally optimum solutions, not necessarily globally optimum) inspired in the Balanced Load Spectrum Allocation (BLSA) and Maximum Reuse Spectrum Allocation (MRSA) heuristics presented in [116]. Moreover, a third greedy heuristic is proposed, which selects from the set of candidate lightpaths the one with the lowest indexed starting FS, similarly to the RMSA heuristic presented in [73]. We call this latter heuristic as Lowest Indexed Spectrum Allocation (LISA). Our contribution is the introduction of the MIMO assignment sub-problem into these three greedy heuristics. These heuristics serve to obtain an initial solution of the addressed RMMSA problem instance, which is later on improved by means of a simulated annealing (SA)-based metaheuristic (SA-RMMSA), thus further approaching to the global optimum solution. Table 3.7 and Table 3.8 show the pseudo-code of these greedy heuristics. As BLSA and LISA only differ in the routing path selection, we present both heuristics in Table 3.7. Meanwhile, the MRSA heuristic is presented in Table 3.8.

According to Table 3.7, for each demand $d \in \mathcal{D}$ we select from $\mathcal{P}_d$ (e.g., K=3 SPs) the least congested (LC) or lowest indexed starting FS (LISFS) path p_j for BLSA and LISA, respectively. The rest of the code performs MSE modulation format assignment and FF MIMO and spectrum assignment. For the MIMO assignment, we pre-compute the candidate demands to be served with MIMO ($\mathcal{D}_{\text{MiMo\_Candidates}} \subseteq \mathcal{D}$) by discarding MIMO equalization for demands whose candidate paths report the same spectral requirements with or without it.

Regarding the MIMO assignment, we define a fitness function (f) as the savings (in terms of FSs) achievable by allocating a lightpath over the selected path p_j with MIMO (nFS_1) versus without MIMO equalization (nFS_2), multiplied by the number of hops of p_j, namely, $f = (nFS_2 - nFS_1) \cdot h_{p_j}$. Thus, the minimum f value is 0 (i.e., being the required FSs for a lightpath identical with or without MIMO), while its maximum value (*max*) can be computed for the longest shortest path (i.e., for the network diameter). In order to determine the goodness of assigning MIMO equalization to a lightpath, each computed f value has to be compared with a *reference value* (V). V is defined as the highest fitness value between 0 and *max*, namely, $V \in \{\mathbb{Z}^+ | \, 0 \leq V \leq max\}$ that allows getting at least η requested lightpaths with MIMO. V is pre-computed at the beginning of each simulation by decrementing it from *max* to 0. We run the heuristic for each V value and find the number of potential lightpaths to be served with MIMO. If this number is higher than η then we stop and set V. If V is very low, the goodness of the MIMO equalization could be poor, while if it is very high, it could occur that MIMO assignment is

extremely restrictive. Before deciding on the MIMO assignment, each demand d is firstly checked if it belongs to $\mathcal{D}_{\text{MiMo\_Candidates}}$ and if the number of allocated lightpaths with MIMO (l_{mimo}) is lower than η (line 9). If so, the fitness function is analyzed. Otherwise, the number of FSs in the MCF scenario without MIMO is considered for lightpath allocation. Lightpaths whose f value is higher than V (line 10) are equalized at the receiver. Finally, demand d is accommodated (line 21) in the network using path p_j, over *nFS* contiguous FSs, with/without MIMO (1/0).

Table 3.7: RMMSA LISA/BLSA heuristic

Input: $\mathcal{G}, \mathcal{D}, \mathcal{D}_{\text{MiMo\_Candidates}}, \mathcal{P}, \eta, V$

Output: $\mathcal{A}, \Phi$

1: $\mathcal{A} \leftarrow \emptyset$ **comment:** Set of established lightpaths
2: $l_{mimo} = 0$ **comment:** Number of allocated lightpaths with MIMO
3: **for** each d in $\mathcal{D}$ **do**
4: Select path p_j from $\mathcal{P}_d$ according to heuristic criterion (LISFS or LC)
5: $m_1 \leftarrow$ Most efficient $m \in \mathcal{M}$ with reach >= z_{p_j} (w/ MIMO)
6: $m_2 \leftarrow$ Most efficient $m \in \mathcal{M}$ with reach >= z_{p_j} (w/o MIMO)
7: $nFS_1 = \lceil (r_d/(\mathcal{C} \cdot ef_{m_1}) + GB)/W \rceil$
8: $nFS_2 = \lceil (r_d/(\mathcal{C} \cdot ef_{m_2}) + GB)/W \rceil$
9: **if** $d \in \mathcal{D}_{\text{MiMo\_Candidates}}$ and $l_{mimo} < \eta$ **then**
10: $f = (nFS_2 - nFS_1) \cdot h_{p_j}$
11: **if** $f > V$ **then**
12: $\delta \leftarrow$ true **comment:** binary parameter for MIMO (1/0)
13: $nFS = nFS_1$
14: $l_{mimo} = l_{mimo} + 1$
15: **else**
16: $\delta \leftarrow$ false
17: $nFS = nFS_2$
18: **else**
19: $\delta \leftarrow$ false
20: $nFS = nFS_2$
21: $(a, \Phi) \leftarrow$ accommodate $(\mathcal{G}, d, p_j, nFS, \delta)$
22: $\mathcal{A} \leftarrow \mathcal{A} \cup \{a\}$
23: **return** $(\mathcal{A}, \Phi)$
24: **End.**

Regarding Table 3.8, two iterative processes are followed to allocate lightpaths over the shortest disjoint path (SDP) in the first available and consecutive FSs. In each iteration *j* of the outer loop (line 2), the first pending demand in $\mathcal{D}$ is served over the shortest path p_j on the original network graph $\mathcal{G}$, computed, e.g., by means of the Dijkstra algorithm. After that, in the inner loop (line 7) each pending demand $d \in \mathcal{D}$ is served over the shortest path p_i, which is also disjoint with all already established routing paths $\mathcal{R}$ (line 8) in the current outer loop iteration j. The demands, for

which finding a SDP or available spectrum portion in the current iteration j is impossible, have the opportunity to be accommodated in subsequent iterations. As in LISA/ BLSA algorithm, MSE modulation format, FF MIMO and spectrum assignment are considered. Then, steps from 5 to 22 in LISA/BLSA algorithm are executed after the routing path selection. Again, MIMO assignment is based on fitness function *f*.

Table 3.8: RMMSA MRSA heuristic

Input: $\mathcal{G}, \mathcal{D}, \mathcal{D}_{\text{MiMo\_Candidates}}, \mathcal{P}, \eta, V$

Output: $\mathcal{A}, \Phi$

1: $\mathcal{A} \leftarrow \emptyset$ **comment:** Set of established lightpaths
2: **while** any pending demand in $\mathcal{D}$ **do**
3: $\mathcal{R} \leftarrow \emptyset$
4: Find SP p_j between s_d and t_d in $\mathcal{G}$
5: Execute steps from 5 to 22 of algorithm 2
6: $\mathcal{R} \leftarrow \mathcal{R} \cup \{p_j\}$
7: **for each** pending demand $d \in \mathcal{D}$ **do**
8: Find SP p_i and disjoint with all paths in $\mathcal{R}$ between s_d and t_d in $\mathcal{G}$
9: Execute steps from 5 to 22 of algorithm 2
10: $\mathcal{R} \leftarrow \mathcal{R} \cup \{p_i\}$
11: **return** $(\mathcal{A}, \Phi)$
12: **End.**

As for SA-RMMSA (Table 3.9), there are three versions of it, employing each one of the presented greedy heuristics. In fact, lines 4, 13 and 23 consist in the evaluation of the objective function by running LISA, BLSA or MRSA heuristics. The SA metaheuristic is inspired in the annealing processes to produce crystals [117]. We use this metaheuristic to change the order of elements in $\mathcal{D}$ aimed at improving objective function Φ. The initial solution (ω_o) is obtained sorting the demands in $\mathcal{D}$ in descending order, according to their required number of FSs over their shortest path. SA is also known as a LS-based metaheuristic, whose solutions evolve in the neighborhood (ω') of the current solution (ω) not only by accepting improving solutions (like, *hill climbing* movements), but also worse solutions (*uphill* movements) to provide diversification within the solution space. A neighboring solution (ω'), as intensification strategy, is defined as a swap movement (line 11) between two randomly chosen demands of the current order (ω) in $\mathcal{D}$. Thus, the process starts with an initial temperature $T(0)$ and it continues decreasing it in each iteration (line 20) with a cooling rate $\gamma \in (0,1)$, $\alpha = 0.9$ for us. The temperature affects the acceptance probability (P_{acc}) of non-improving solutions. In fact, the P_{acc} depends on the objective function worsening ($\psi = \Phi_{\omega'} - \Phi_{\omega}$) and the temperature, namely, $P_{acc} = e^{-\psi/T}$. For example, we initially decide to accept with probability 0.3 a solution yielding an objective function worsening in one FS. Then, $e^{-1/T(0)} = 0.3$, and $T(0) = -1/\ln(0.3)$ —line 6—. After the evaluation of each neighboring solution (ω'), if ω' improves the resulting Φ value of the

incumbent solution (ω^*), then this is updated ($\omega^* = \omega'$, line 17). This process ends after 20000 iterations (*maxIter*) or when the temperature reaches freezing state (e.g., 0). Finally, note that by changing the order of demands, different solutions for MIMO assignment can also be explored, as this resource is assigned on a FF basis.

Table 3.9: SA-RMMSA metaheuristic

Input: $\mathcal{G}, \mathcal{D}, \mathcal{D}_{\text{MiMo\_Candidates}}, \mathcal{P}, \eta$, V, γ, maxIter

Output: Φ_{ω^*}

1: $\omega_o \leftarrow \mathcal{D}$ sorted in descending order by their required *nFS* over SP
2: $\omega = \omega_0$ **comment:** Current solution
3: $\omega^* = \omega_o$ **comment:** Incumbent solution
4: $(\mathcal{A}, \Phi_\omega) \leftarrow$ RMMSA heuristic $(\mathcal{G}, \omega, \mathcal{D}_{\text{MiMo\_Candidates}}, \mathcal{P}, \eta, V)$
5: $\Phi_{\omega^*} = \Phi_\omega$ **comment:** Obj. function of the incumbent solution
6: $T(0) = -\frac{1}{\ln(0.3)}$, $T = T(0)$ **comment:** Initial temperature
7: iter = 0
8: **while** *iter*<*maxIter* and T>0 **do**
9: $d_x \leftarrow$ Select one demand randomly from $\mathcal{D}$
10: $d_y \leftarrow$ Select one demand randomly from $\mathcal{D}$ different than d_x
11: $\omega' \leftarrow$ **swap** (ω, d_x, d_y)
12: Release all established lightpaths $\mathcal{A}$ in $\mathcal{G}$
13: $(\mathcal{A}, \Phi_{\omega'}) \leftarrow$ RMMSA heuristic $(\mathcal{G}, \omega', \mathcal{D}_{\text{MiMo\_Candidates}}, \mathcal{P}, \eta, V)$
14: $\psi = \Phi_\omega - \Phi_{\omega'}$
15: $prob \leftarrow$ **random** [0,1) **comment:** Random probability
16: **if** $\Omega < 0$ or $prob < e^{-(\psi/T)}$ **then**
17: $\omega = \omega'$ **comment:** Jump to neighboring solution
18: **if** $\Phi_{\omega'} < \Phi_{\omega^*}$ **then**
19: $\Phi_{\omega^*} = \Phi_{\omega'}$ **comment:** Update incumbent
20: $T = \gamma \cdot T$ **comment:** Decrease temperature
21: iter = iter+1
22: Release all established lightpaths $\mathcal{A}$ in $\mathcal{G}$
23: $(\mathcal{A}, \Phi_{\omega^*}) \leftarrow$ RMMSA heuristic $(\mathcal{G}, \omega^*, \mathcal{D}_{\text{MiMo\_Candidates}}, \mathcal{P}, \eta, V)$
comment: Allocate demands with the incumbent solution
25: **return** Φ_{ω^*}
26: **End.**

3.2.4 Simulation results

This subsection presents the performance evaluation of the proposed solutions to solve the RMMSA problem. To this end, we firstly present the scenario under study. Next, we validate the performance of our proposed SA-based metaheuristics against the optimal solution of ILP1. Then, we evaluate the MIMO equalization and its spectral usage benefits in two large-scale optical core

network scenarios using the proposed SA-based metaheuristics. Finally, we discuss MIMO-DSP complexity and non-ideal crosstalk compensation.

3.2.4.1 Scenario under study

We consider the different topologies shown in Appendix A. In order to evaluate the performance of SA-based heuristics against ILP1, we use the TEST1 and TEST2 topologies of 6 and 9 nodes, respectively. Meanwhile, for larger problem instances, we consider the DT12 and NSF15 networks. Each network link is equipped with one weakly-coupled MCF of $C \in \{7, 12, 19, 22, 30\}$, whose characteristics match those of real MCF prototypes found in the literature [27]–[31]. These reported prototypes are the best single-mode MCFs (in terms of ICXT) and they have been selected in line the previous study of subsection 3.1.4. The measured worst aggregate ICXT of these MCF prototypes was shown in Table 3.1.

As for the TR of the optical signals, we adopt the method for MCF-enabled networks presented in subsection 3.1.1 and the values shown in Table 3.2. Looking at the overall TR values, we can appreciate that ICXT is not the limiting factor in 7- and 12-core MCFs, but it is in 19-, 22- and 30-core MCFs. Therefore, we do not consider in next subsections the 7- and 12-core MCFs since they do not require MIMO crosstalk compensation (i.e., 0% of MIMO requirements).

We also consider that each fiber/core has $|\mathcal{S}|$=320 FSs (corresponding to 4 THz C-Band discretized by W=12.5 GHz). Demands are allocated using spatial SChs with GB=7.5 GHz and they are switched at ROADMs using JoS. To form the spatial SChs we employ the entire spatial domain. Traffic is distributed uniformly between all source-destination node pairs. Moreover, demands request unidirectional connections of bit-rate $r_d \in \{400, 800, 1200, 1600, 2000\}$ Gb/s with the same probability of 1/5. The average requested bit-rate per demand is 1.2 Tb/s. Simulations were run on a 4-core Intel i7 3.4 GHz PC with 16 GB RAM, where the IBM ILOG CPLEX v. 12.6 solver [118] was installed and used for solving the ILP formulations.

3.2.4.2 Metaheuristic Performance Validation

In this subsection, we compare the performance of ILP1 versus the SA-based RMMSA metaheuristics. To this end, we consider the two MCF prototypes with the highest ICXT (19-core and 22-core MCFs) in order to assess the efficiency of metaheuristics under relevant ICXT levels. Table 3.10 to Table 3.13 show the different values of the objective function (Φ) for ILP1, as well as for the SA-based metaheuristics (SA-LISA, SA-BLSA, SA-MRSA). The CPLEX solver has been configured to finish the execution and return the result upon reaching an optimality gap lower or equal than 2% or a maximum execution time of 12 hours. Table 3.10 and Table 3.11 show the results in the TEST1 topology, while Table 3.12 and Table 3.13 show the results in the TEST2 topology. We obtain Φ for different η values in order to observe the influence of (ideal)

MIMO equalization in the spectrum usage. η=0 value represents, as stated in subsection 3.2.1, the results for a MCF-enabled network, where none of the lightpath are allocated with MIMO, while the last η value of each table corresponds to sweet spot *x*. This latter value, which yields the minimum spectrum usage, has been obtained using ILP2. Additionally, all tables show the execution times (in min.) for ILP1 and metaheuristics.

Table 3.10: Performance Validation in TEST1 topology with 19-core MCF

TEST1 Topology, $\mathcal{C}$ = 19, $\|\mathcal{D}\|$ = 600								
η	Φ				Exec. Time (min)			
	ILP1	SA-LISA	SA-BLSA	SA-MRSA	ILP1	SA-LISA	SA-BLSA	SA-MRSA
0	210	210 0%	210 0%	210 0%	48.7	1.3	2.6	3.3
33	195	198 1.5%	196 0.5%	197 1%	65.1	1.3	2.8	3.2
66	187	188 0.5%	187 0%	188 0.5%	43.3	1.3	2.6	3.1
99	178	180 1.1%	180 1.1%	181 1.7%	19.3	1.2	1.9	3.4
132	170	172 1.2%	173 1.8%	173 1.8%	23.2	1.2	1.7	3.4
167	161	166 3.1%	167 3.7%	167 3.7%	36.7	1.1	1.6	2.9

Table 3.11; Performance Validation in TEST1 topology with 22-core MCF

TEST1 Topology, $\mathcal{C}$ = 22, $\|\mathcal{D}\|$ = 800								
η	Φ				Exec. Time (min)			
	ILP1	SA-LISA	SA-BLSA	SA-MRSA	ILP1	SA-LISA	SA-BLSA	SA-MRSA
0	243	244 0.4%	243 0%	244 0.4%	28.9	1.2	4	8.1
31	228	231 1.3%	229 0.4%	231 1.3%	53.5	1.2	2.9	6
62	212	224 5.7%	225 6.1%	228 7.6%	35.3	1.2	2.5	5.9
93	204	220 7.8%	221 8.3%	212 3.9%	27.4	1.1	2.5	6.8
121	197	205 4.1%	204 3.6%	204 3.6%	31.2	1.1	2.4	6.2

Specifically, for the TEST1 topology (results of Table 3.10 and Table 3.11), we use a set of 600 and 800 demands with $\mathcal{C}$=19 and $\mathcal{C}$=22, respectively, which represent a medium offered load for different η values (lower than ~0.7 of spectrum occupation). The relative error between the results

of the metaheuristics and those of ILP1 is depicted under the Φ value. As observed, this error is below 8.3% (maximum observed one with the SA-BLSA metaheuristic) and even 0% in some cases. Regarding the execution times, ILP1 requires 38 min in average to find the optimal solution. The SA-based metaheuristics reduces significantly the execution times down to 1.2 min in average for SA-LISA. Indeed, among the three metaheuristics, SA-LISA presents the lowest execution time, while SA-MRSA the highest one, 4.8 min in average. SA-BLSA requires intermediate execution times between SA-LISA and SA-MRSA. Additionally, for $\mathcal{C}$=19 the sweet spot *x* is obtained with 167 lightpaths allocated with MIMO. The remaining 433 lightpaths do not need MIMO-based ICXT suppression. This means that, MIMO has to be applied to ~28% of lightpaths in order to meet the performance of the MF-based benchmark solution. As for $\mathcal{C}$=22, the percentage of lightpaths with MIMO required to meet the performance of equivalent MF solution is reduced to ~15% (121/800) due to its lower worst aggregate ICXT.

For the TEST2 topology (results of Table 3.12 and Table 3.13), we offer 800 demands for both $\mathcal{C}$=19 and $\mathcal{C}$=22 MCFs. This topology, with more nodes and links, increases the computational complexity of the ILP formulation. This is reflected in the results of ILP1, where for several η values ILP1 is not able to find any solution (cells with dotted lines) or the returned value has optimality gap higher than 2% (i.e., the ILP1 required more than 12 hours to be solved), which is also shown under the Φ value in the corresponding column of ILP1. For this reason, the relative error between ILP1 and SA-based metaheuristics only can be computed for a few cases, where errors lower than 6.6% are reported. Regarding the execution times, in those cases where optimal solutions were obtained, ILP1 requires up to 9.4 hours to find them. However, in most of the cases, after running for 12 hours, ILP1 does not return any solution. This situation occurs mostly for $\mathcal{C}$=19. The lower computational complexity with 22-core MCF can be explained not only by the fact that demands may require lower spectral resources facilitating the spectrum assignment sub-problem, but also because the ICXT introduced by 19-core MCFs is higher. Hence, as candidate lightpaths with and without MIMO require different number of FSs, the former ones cannot be removed from $\mathcal{L}_d$ (i.e., MIMO equalization can yield benefits in terms of spectral requirements). This latter aspect is more evident in long-haul networks, increasing the cardinality of the set of candidate lightpaths $\mathcal{L}$ (computed by algorithm 1) and, therefore, the number of decision variables. For instance, in the case of $\mathcal{C}$=22 and η=48 the number of candidate lightpaths ($|\mathcal{L}|$) is equal to 519267, while for $\mathcal{C}$=19 this number increases to 708841. SA-based metaheuristics reduce significantly the execution times, down to 1.7 min in average with SA-LISA. Like in the TEST1 topology, among the three metaheuristics, SA-LISA presents the lowest execution times, while SA-MRSA reports the highest one, 5 min in average. SA-BLSA requires intermediate execution times between SA-LISA and SA-MRSA. Additionally, for $\mathcal{C}$=19, the sweet spot *x* is obtained with 244 lightpaths served with MIMO. The remaining 556 lightpaths do

not need MIMO-based ICXT suppression. This means that, a ~31% of lightpaths with MIMO are required to meet the performance of the MF-based benchmark solution. When $\mathcal{C}$=22, this percentage falls down to ~12% (96/800) due to its lower ICXT. It is worth mentioning that, for $\mathcal{C}$=19 the sweet spot *x* was returned by ILP2 formulation after 12h of execution (optimality gap 22%).

Table 3.12: Performance Validation in TEST2 topology with 19-core MCF

TEST2 Topology, $\boldsymbol{\mathcal{C}}$ = 19, $\lvert\boldsymbol{\mathcal{D}}\rvert$ = 800								
$\boldsymbol{\eta}$	**Φ**				Exec. Time (min)			
	ILP1	SA-LISA	SA-BLSA	SA-MRSA	ILP1	SA-LISA	SA-BLSA	SA-MRSA
0	--	260	259	261	--	2	2.4	11.8
48	--	231	232	228	--	2.1	2.4	3.9
96	230 14%	214	216	210	>12h	1.8	2.2	3.9
144	--	204	209	203	--	1.2	2.3	5.7
192	200 10%	193	194	189	>12h	1.2	2.3	4.3
244	--	186	189	183	--	1.2	2.3	4.4

Table 3.13: Performance Validation in TEST2 topology with 22-core MCF

TEST2 Topology, $\boldsymbol{\mathcal{C}}$ = 22, $\lvert\boldsymbol{\mathcal{D}}\rvert$ = 800								
$\boldsymbol{\eta}$	**Φ**				Exec. Time (min)			
	ILP1	SA-LISA	SA-BLSA	SA-MRSA	ILP1	SA-LISA	SA-BLSA	SA-MRSA
0	215 6%	204	204	203	>12h	1.2	2.3	5
24	205 11%	193	198	192	>12h	2	2.3	4.5
48	179	185 3.4%	190 6.2%	186 3.9%	561.9	2.1	2.2	4.4
72	--	178	188	181	>12h	2.5	2.2	3.7
96	168	176 4.8%	179 6.6%	177 5.4%	206.3	1.2	2.2	3.7

Furthermore, it is interesting to observe the relationship between Φ and η. For instance, taking into account optimalsolutions in the TEST1 topology, where it has been possible to obtain results for all η values, we found that penalties in terms of spectral requirements increases slowly as the number of lightpaths with MIMO reduces. Thus, for $\mathcal{C}$=19, a 60% MIMO reduction (66 vs. 167) is translated only into a 16% increment in spectrum usage (187 vs. 161 FSs), and for $\mathcal{C}$=22 a 49% MIMO reduction (121 vs. 62) only entails an 8% increment in terms of spectrum usage (212 vs. 197 FSs). This aspect suggests us that the trade-off between MIMO equalization versus spectral

requirements (therefore, network GoS) is an important aspect to be analyzed in detail. If the goal is to save computational complexity and power consumption of MIMO-DSP, we can look for η values lower than sweet spot, even requiring moderately higher spectral resources. It should be assessed what is more economically attractive: whether to implement MIMO to increase GoS or to save MIMO costs at expenses of sacrificing network GoS.

3.2.4.3 MIMO equalization and spectral requirements benefits

This subsection aims to evaluate the benefits in terms of spectrum savings that MIMO equalization offers. To this end, we employ the proposed metaheuristics to illustrate quantitative results in the larger DT12 and NSF15 networks. Fig. 3.18.a-d show the spectrum usage (Φ) versus the number of lightpaths with MIMO (η). In line with the results previously shown in Table 3.10 to Table 3.13, we start from the MCF-enabled solution without MIMO (η=0) until finding the sweet spot *x* (where the MF baseline is reached), plotting several intermediate points. This MF baseline was obtained considering candidate lightpaths only employing $m_{l^{(1)}}$ modulation formats (i.e., with MIMO) or, what is the same, considering the OSNR as the only TR limiting factor. Note that this situation would occur if the input parameter η of heuristics is equal to $|\mathcal{D}|$. In turn, η should be modified with an appropriate granularity to obtain an accurate sweet spot. For this purpose, for each metaheuristic we plot several points (η, Φ) and the trend line over them.

Fig. 3.18.a-c show the results in the DT12 network with $\mathcal{C}$ equal to 19, 22 and 30, respectively, for 1000 offered demands. For $\mathcal{C}$=19, the number of demands that are candidates to be served with MIMO ($|\mathcal{D}|_{\text{MiMo\_Candidates}}$) is 650. As observed, in spite of the ICXT, the sweet spot is lower than $|\mathcal{D}|$ and $|\mathcal{D}|_{\text{MiMo\_Candidates}}$, close to 360, which represents the 36% (360/1000) of the total number of established lightpaths. For $\mathcal{C}$=22, the number of demands that are candidates to be served with MIMO is equal to 345 and the sweet spot *x* is close to 120, which represents the 12% of the total number of established lightpaths. Finally, for $\mathcal{C}$=30, $|\mathcal{D}|_{\text{MiMo\_Candidates}}$ is equal to 72 and the sweet spot *x* s around 24 representing the 2.4% of total established lightpaths. As observed, SA-LISA and SA-BLSA metaheuristics achieve very similar performance (in terms of spectrum usage) for different η values, while SA-MRSA outperforms both of them by approximately 10-20%. Observe that in Fig. 3.18.a-c are depicted two MF baselines (for SA-LISA&BLSA and SA-MRSA, respectively). The reason behind this behavior is that the diameter and the good connectivity (see values of Table A.1 in Appendix A obtained by *natural connectivity* definition presented in [119]) of the DT12 network allow SA-MRSA metaheuristic exploring longer paths for $\mathcal{C}$=19, $\mathcal{C}$=22 and $\mathcal{C}$=30 even in absence of MIMO equalization. Recall that MRSA heuristic explores disjoint paths in order to maximize the reuse of FS indexes. The higher the number of feasible disjoint paths, the higher the spectrum reutilization. Note that this behavior was not observed in the TEST1 topology (used in the previous subsection, which has

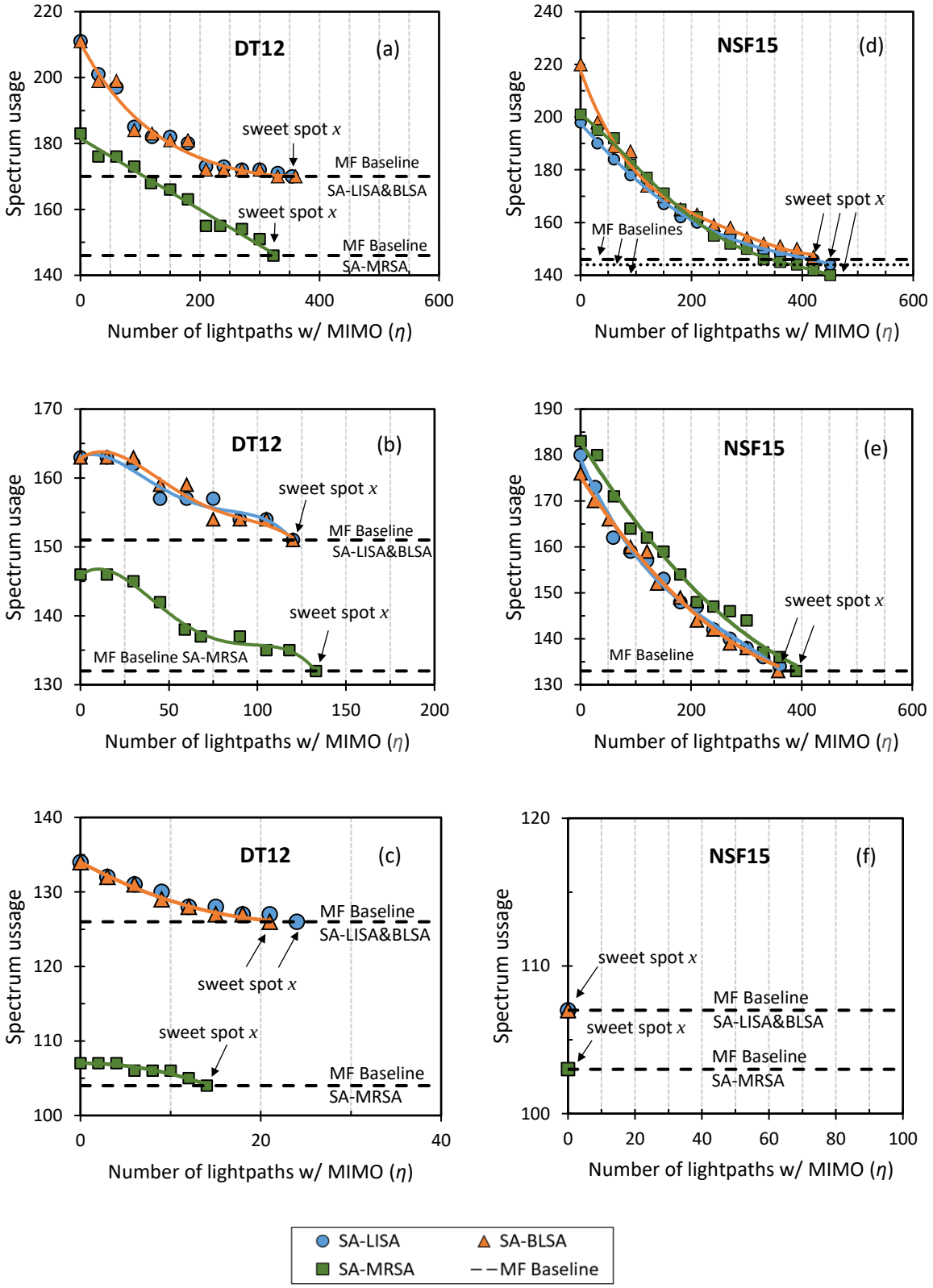

Fig. 3.18. Spectrum usage versus number of MIMO lightpaths for: (a) DT12 network with 19-core MCF, (b) DT12 network with 22-core MCF, (c) DT12 network with 30-core MCF (d) NSF15 network with 19-core MCF, (e) NSF15 network with 22-core MCF, and (f) NSF15 network with 30-core MCF.

also similar network diameter but lower network connectivity), since in this short topology (in terms of network nodes and links) there are not so many possibilities to find disjoint paths. Consequently, the results reveal that the performance of the SA-MRSA metaheuristic depends on the network diameter and connectivity.

Fig. 3.18.d-f show the results for NSF15 network with $\mathcal{C}$ equal to 19, 22 and 30, respectively, for 800 offered demands. For $\mathcal{C}$=19, the number of demands that are candidates to be served with MIMO ($|\mathcal{D}|_{\text{MiMo\_Candidates}}$) is 625. As observed, in spite of the negative effects of the ICXT in a larger network size (NSF15 vs. DT12), the sweet spot is lower than $|\mathcal{D}|$ and $|\mathcal{D}|_{\text{MiMo\_Candidates}}$. In fact, we have found that sweet spot *x* is close to 450, which represents the 56% (450/800) of the total number of established lightpaths. For $\mathcal{C}$=22, the number of demands that are candidates to be served with MIMO is equal to 650 and the sweet spot *x* is close to 360 representing the 45% of the total number established lightpaths. Finally, for $\mathcal{C}$=30, $|\mathcal{D}|_{\text{MiMo\_Candidates}}$ is equal to only 3, and there is no need for MIMO equalization (0% MIMO requirement). This result confirms previous findings presented in subsection 3.1.4.2 about ICXT impact. The fact is that ICXT impact depends on a combination of several topological characteristics (network diameter, average path length, network connectivity, etc.) and traffic distribution. In our scenario, considering the NSF15 network without MIMO, almost all transmission distances use the same modulation formats as with MIMO equalization. This is the reason why only 3 demands are candidates to be served with MIMO, which do not affect the spectrum usage at all. Moreover, for each metaheuristic we also plot several points (η, Φ) and the trend line over them. As observed, for $\mathcal{C}$=19 the three metaheuristics SA-LISA, SA-BLSA and SA-MRSA, experiment similar performance with some differences between MF baseline of each metaheuristic. Conversely to what happens in the DT12 network, SA-MRSA does not outperform the other options so significantly. The reason is that the diameter of NSF15 with $\mathcal{C}$=19, 22, 30, hinders exploring feasible disjoint paths (recall that we consider transparent transmission) in order to maximize the reutilization of FSs.

Regarding the execution times, as in the previous subsection, the lowest execution times are reported for SA-LISA, while the highest ones are those of SA-MRSA. There is no case where longer time than 1.8 min and 7.4 min is reported for SA-LISA and SA-MRSA, respectively. Likewise, SA-BLSA experiments intermediate execution times between SA-LISA and SA-MRSA metaheuristics. It is worth highlighting the low execution times of all lightweight metaheuristics, demonstrating their suitability to solve the RMMSA problem even in large-scale instances.

Finally, in order to save on computational complexity and power consumption of MIMO-DSP we can look for η values lower than sweet spot. For example, for the best results of Fig. 3.18.a-e a

50% of MIMO reduction is translated into a 5-15% of penalty in spectrum usage. That is, the spectral requirements evidences a slow decrement as the η increases, as highlighted when analyzing ILP1 results in previous subsection.

3.2.4.4 MIMO complexity and crosstalk compensation

The effectiveness of MIMO-DSP to undo crosstalk mainly depends on the filter characteristics and some physical layer impairments. For instance, in case of Multi-Mode Fibers (MMFs), the number of taps per carrier increases with the Differential Mode Delay (DMD) and transmission distance. This, as stated in [120], leads to a hard convergence and an unstable adaptation of the MIMO equalizer. As a result, in the presence of relevant DMD, regardless of the filter length, crosstalk remains after MIMO equalization. Since strongly-coupled MCFs are considered a form of MMFs (equivalent to one core with several so-called super-modes) [24], for this SDM fiber, the impact of DMD on the complexity and effectiveness of MIMO-DSP is also relevant. Taking as an example the experiment carried out in [111], six column filters with 100 taps were needed to remove a -4 dB accumulated crosstalk almost completely in a 3-core strongly-coupled MCF, after 24 km of propagation for a target 10^{-3} BER. This conclusion suggests us that a remaining crosstalk after MIMO equalization, although small, was evidenced.

As in weakly-coupled MCFs all cores are not coupled together, while DMD can be negligible under certain conditions [121], the MIMO-DSP complexity can be relaxed by reducing the number of filters as well as their length, respectively. To illustrate how the number of filters can be reduced, let us consider the 7-core MCF depicted in Fig. 3.19.a. The center core #1 is coupled with 6 neighboring cores, while the outer cores from #2 to #7 are only coupled with 3 cores. Therefore, a full 7×7 MIMO (without polarization decoupling) would not be needed to compensate ICXT, but rather the MIMO equalizer matrix shown in Fig. 3.19.b would be enough, where *h* accounts for the adaptation coefficient of the filter in position *i*,*j*. Core #1 is equalized with all the rest of the cores, core #2 is only equalized with cores #1, #3, and #7; and so on. As a result, instead of 49 (7x7) filters, only 31 (7+6·4) would be enough, which means a ~37% complexity reduction in terms of the number of filters. In general, we can compute the required number of filters of a MIMO equalizer as $\sum_{q=1}^{|\mathcal{C}|}(\text{number of neighboring cores}_q + 1)$. Applying the same analysis for the 19-core MCF prototype (cf. Fig. 1(a) in [29]), the number of required filters would be 91 against 361 (19x19), i.e., ~75% of complexity reduction.

On the other hand, non-ideal MIMO compensation in weakly-coupled MCFs could be assumed for those desirable lightpaths to be equalized, either due to intrinsic limitations of MIMO-DSP or an intentional relaxation to further reduce its complexity. In such a case, the remaining crosstalk might be so low to let network performance totally unaffected or, even affecting it to a certain degree, it might suffice to approach the performance of an equivalent crosstalk-free SDM fiber

solution. For instance, for the same 19-core MCF prototype [29], if we concentrate on the ICXT reduction between the center core #1 and its neighbors from #2 to #7, again the same MIMO equalizer matrix of Fig. 3.19.b should be considered instead of a full 7 × 7 MIMO. In such a case, after applying MIMO to these cores from #1 to #7, the crosstalk compensation margin (per km) should be around 3 dB, since the worst aggregate ICXT now will be reported for outer cores from #8 to #19 (having 3 neighboring cores each), where the aggregate crosstalk is around -43 dB per 30 km (i.e., -57.8 dB/km instead of -54.8 dB/km). This reduces the complexity (in terms of the number of filters) by around 37% and 91% versus full 7 × 7 and 19 × 19 MIMO, respectively.

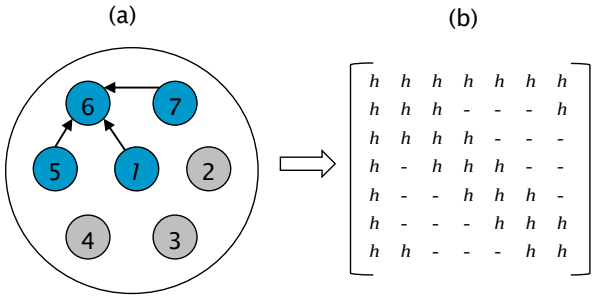

Fig. 3.19. 7-core MCF: (a) cross-sectional view (b) MIMO equalizer matrix

The previous results presented in subsections 3.2.4.2 and 3.2.4.3 were obtained considering ideal MIMO able to completely suppress the ICXT. In this subsection, we aim to evaluate non-ideal MIMO by assuming a compensation margin of crosstalk from 1 dB to 6 dB per 1 km of fiber propagation, which correspond to a 20-75% of coupled power reduction. Note that, from the experiment in [111], much larger compensation margins should be obtained to almost completely suppress a large -4 dB accumulated crosstalk. For this set of experiments, LISA, BLSA and MRSA algorithms shown in Table 3.7 and Table 3.8 are the same, only changing the reference scenario in the selection of the MSE modulation format with MIMO $m_{l^{(1)}}$, therefore, the fitness function *f* and the reference value *V*. This means that our proposal of minimizing the number of lightpaths with MIMO aiming to improve the network throughput is valid even in case of non-ideal MIMO equalization.

Specifically, in this subsection we consider the MCF prototype with the worst aggregate ICXT, namely, the 19-core MCF with the same set of demands $\mathcal{D}$ used in previous subsection 3.2.4.3. Fig. 3.20.a and Fig. 3.20.b show the spectrum usage (Φ) as a function of the number of lightpaths with MIMO equalization (η) using SA-MRSA for DT12 and NSF15 networks, respectively. In each graph, three curves are shown for three compensation crosstalk margins, namely, 1 dB/km, 3 dB/km and 6 dB/km. As observed, in the DT12 network, results shown in Fig. 3.20.a disclose that 1 dB/km and 3 dB/km crosstalk compensation do not reach the MF baseline, demanding 6 dB/km crosstalk compensation to reach it. Indeed, 6 dB/km crosstalk compensation yields the same results as the ones depicted in Fig. 3.18.a. This means that, the impact of ICXT below -60

dB/km (not included) is irrelevant (as also corroborated in [122]). Initially, the performance gap between the considered MCF- and equivalent MF-based solution is ~25% (183/146) without MIMO. Then, by applying MIMO-DSP yielding 1 dB/km crosstalk compensation to ~13% (125/1000) of the lightpaths, the performance gap is reduced to ~18%. Meanwhile, for a MIMO-DSP yielding 3 dB/km crosstalk compensation, this gap downs to ~4% when ~28% (275/1000) lightpaths are equalized. Note that, similarly to the sweet spot *x*, curves for 1 dB/km and 3 dB/km of crosstalk compensation present a point η_i, beyond which the spectrum usage does not decrease, since more equalized lightpaths do not provide any spectrum savings.

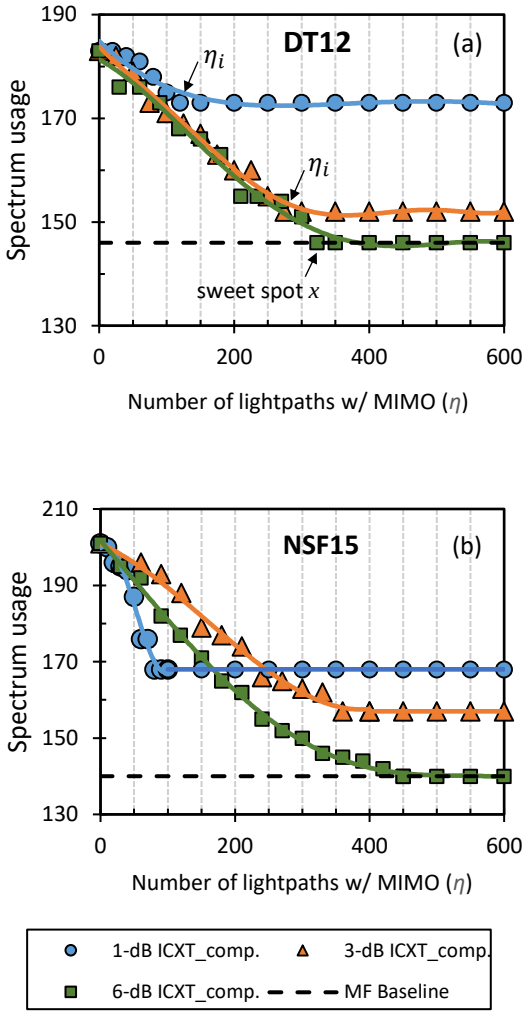

Fig. 3.20. Spectrum usage vs. number of lightpaths with 1-dB/km, 3-dB/km and 6-dB/km MIMO ICXT compensation in the (a) DT12 (b) NSF15 network.

As for the NSF15 network, results shown in Fig. 3.20.b are slightly different, especially with 1 dB/km crosstalk compensation. This crosstalk compensation margin seems yielding better spectrum usage benefits than 6 dB/km before reaching η_i. The fact is that, the higher the crosstalk compensation, the larger $|\mathcal{D}|_{\text{MiMo\_Candidates}}$, which hinders the search of global optimum solutions in a polynomial time. For example, for 1 dB/km crosstalk compensation,

$|\mathcal{D}|_{\text{MiMo\_Candidates}}$ is equal to 203, whereas for 6 dB/km $|\mathcal{D}|_{\text{MiMo\_Candidates}}$ raises up to 625. In particular, the initial performance gap between the considered MCF- and equivalent MF-based solution decreases from ~44% to ~20% and ~12% when MIMO-DSP yielding 1 dB/km and 3 dB/km crosstalk compensation is applied to 21% (168/800) and 45% (360/800) of lightpaths, respectively. Finally, again a 6 dB/km crosstalk compensation would be enough to reach the MF baseline.

According to the results of subsection 3.2.4.3 and 3.2.4.4, the performance of a crosstalk-free SDM solution can be met even in case of non-ideal MIMO. For this purpose, the remaining crosstalk has to be lower than -60 dB/km (not included). That is, around 6 and 4 dB/km of crosstalk compensation is enough for the 19- and 22-core MCFs, respectively, considered in this work.

Finally, even with the potential complexity reduction of MIMO-DSP in weakly-coupled MCFs against strongly-coupled ones, real-time DSP implementation is still an open question for long-haul communications. Nevertheless, techniques like DMD fiber management [123], [124], unconstrained frequency-domain equalization to accelerate the convergence during filter adaptation against time-domain one [113], or bit-width reduction in floating point operations of Field Programmable Gate Arrays (FPGAs)/Application-Specific Integrated Circuits (ASICs) [125] foresee successful real-time DSP equalization. In fact, the first real-time 6×6 MIMO-DSP SDM transmission experiment was carried out in 2015 [126] for 3-core strongly-coupled MCF. The challenge for researchers is to continue putting efforts in key aspects that lead to further complexity reductions aimed at supporting real-time MIMO-DSP in backbone networks.

3.3 Conclusions

This chapter has focused on the operation and planning of spatially fixed Flex-Grid/SDM optical networks. This kind of networks is characterized by using a fixed spatial granularity per SCh, e.g., the entire spatial domain in the most rigid form, where the JoS operation is possible to be applied.

To start with, as MF and MCF SDM fibers have been considered in this PhD thesis, TR estimations under the most relevant physical impairments have been presented. These values have been useful to evaluate different RA strategies and ICXT impact (in the case of MCFs).

Spa-SChs, the expected allocation strategy over spatially fixed Flex-Grid/SDM networks, have been largely studied. Firstly, the GB impact on network performance has been assessed. The results have disclosed that depending on the topology diameter, network performance can increase by ~80-160% reducing GB width from 12.5 GHz to 0 GHz (ideal case). Next, a cost-effective Spa-SCh configuration called PSA, when flexible baud-rate per OC is considered, has been proposed based on avoiding spectral wastage and minimizing the number of assigned spatial

channels (therefore, transceivers). This strategy can be applied to both planning and operation scenarios.

Then, by using the PSA strategy, it has been studied the SCh allocation in spatially fixed Flex-Grid/SDM networks taking into account the spectral-spatial gaps left by each lightpath. These gaps can be leveraged by co-routed lightpaths, performing end-to-end spatial traffic grooming (e2e-grooming). Thus, by means of this SCh allocation strategy, it has been found that network throughput does not always grow as the spatial multiplicity increases due to unfilled spectral-spatial gaps even e2e-grooming is performed.

Regarding this e2e-grooming operation, it has been also proposed a mechanism called *dynamic* spatial traffic grooming to increase the network GoS (therefore, the network throughput). This mechanism has been demonstrated that yields high benefits for moderate traffic profiles in terms of bit-rate and heterogeneity.

Throughout this chapter, it has been considered five weakly-coupled MCF prototypes available in the literature. Some of these prototypes have extremely low ICXT values (e.g., the MCFs with low core count of 7 and 12), which do not affect the TR at all (i.e., the limiting factor are the intra-core impairments). Meanwhile, other prototypes such as 19-, 22-, 30-core MCFs evidence certain performance penalties depending on the network size because, in these cases, the TR limiting factor is ICXT. Among them, the 19-core MCF has the worst ICXT, therefore it has been reported the highest penalty in optical core networks. The fact is that more robust but lower spectrally efficient modulation formats require to assign both/either more spectral and/or spatial resources per Spa-SCh. For instance, up to 50% of throughput penalties have been evidenced for 19-core MCF versus the equivalent MF solution in both national and continental backbone networks.

Finally, for a network planning scenario, the problem of optimal MIMO assignment for MCF-enabled networks has been solved by means of ILP formulations, as well as metaheuristics, to counteract the performance penalties introduced by ICXT. It has been demonstrated that this problem can be jointly solved with the well-known RMSA studied in Flex-Grid over SMFs by applying MIMO equalization to the least amount of lightpaths, where no so high order MIMO is expected to counteract or cancel the ICXT effect. Assuming ideal MIMO compensation, our results have revealed that up to 56% lightpaths require MIMO-based ICXT suppression in order to match the spectral requirements of a crosstalk-free SDM solution. In the case of non-ideal MIMO, considering e.g., a 3 dB/km crosstalk compensation, this percentage decreases down to 28%, with up to 12% of performance gap versus the crosstalk-free benchmark scenario.

Chapter 4

4 Operation of Spectrally and Spatially Flexible Optical Networks (SS-FONs)

In previous chapter 3, the spatial dimension was considered rigid, driving the so-called spatially fixed Flex-Grid/SDM optical networks. In this chapter, a flexible spatial dimension is taken into account in order to assess its impact on SCh configuration and network throughput scalability. As presented before, Spa-SChs are mandatory to be allocated when the spatial dimension is rigid. Moreover, this rigidity causes some spectral wastage issues, which, in turn, causes to a lack of correspondence between throughput increment and spatial multiplicity. This chapter is aimed at evaluating what happens when flexibility is applied to both spatial and spectral dimensions, i.e., as in the SS-FONs case. For this purpose, firstly, section 4.1 studies SCh allocation in SS-FONs. In fact, since different SChs are possible to be allocated by using various spectral and spatial channels, a methodology to select one or a combination of them is proposed in subsection 4.1.1. This methodology will allow not only asses the throughput scalability vs. spatial multiplicity, but also different hardware requirements especially from the BVTs point of view. Besides, the ponderation of both metrics provides a tool for network operators in order to select a proper SCh configuration tailored to their needs. For example, the one yielding the best trade-off between performance and network cost.

The performance of SS-FONs is presented in section 4.2 by using two reference networks and several traffic scenarios. Specifically, subsection 4.2.1 assesses the impact of SCh configuration on network throughput by testing several valid forms of allocating connections. Then, by choosing interesting use cases, the scalability of SS-FONs in terms of throughput versus spatial multiplicity is evaluated in subsection 4.2.2, taking as benchmark scenario those results presented in previous chapter 3 and subsection 3.1.4. Further, for the same selected scenarios, the complexity of BVT configuration is analyzed in detail in subsection 4.2.3.

Finally, last section 4.3 provides the main conclusions of this chapter.

4.1 SCh allocation in SS-FONs

In the Spa-SCh configuration presented in previous chapter 3, the spatial dimension is considered fixed, and if there are Spa-SChs that do not employ the entire spatial dimension S, the aggregation of traffic demands with common source-destination nodes can be allowed. This obviously

simplifies the ROADM architecture, since JoS reduces the number of SSSs; however, these SSSs could require a high-port-count [55]. In contrast, in order to introduce flexibility in the spatial domain, it is required a more complex switching technique, like InS (w/ or w/o LC support), as introduced in chapter 2. This flexibility in the spatial domain means that we can accommodate SChs using a flexible number of spatial channels (n_s) with the minimum granularity and if some spatial channels remain unused ($n'_s = S - n_s$) in the same or different spectrum range, these spectral-spatial resources can be assigned to other traffic demands, regardless of their s_d and t_d nodes.

Let us take the previous example in Fig. 3.11 again, where demand d_2 could not be allocated in the same spectrum range assigned to demand d_1 (in spatial channels s_4 to s_7) due to the restrictions of the JoS technique. However, in SS-FONs, this demand d_2 is not only allocated over these spectral-spatial resources, but would also use 1 FS (as d_2 requires) employing another BVT with one OC at a central frequency different than f_i. Obviously, the complexity and cost of both SDM-ROADM and BVT designs enabling spectrally-spatially flexible SCh configurations are higher [50], [58].

Depending on the n_s value, different SCh allocation policies can be configured, namely, Spe-SCh, SC Spa-SCh or MC Spa-SCh. For instance, if $n_s = 1$, we have a Spe-SCh (Fig. 4.1), while a SC Spa-SCh (Fig. 3.1.a) or an MC Spa-SCh (Fig. 3.1.b) could be allocated with higher n_s values depending on the spectral width of each Sb-Ch (Δ_{Sb}), i.e., R_B. Starting from $n_s = 1$ (i.e., a Spe-SCh generated with MCs), if n_s increases, n_{fs} can start decreasing until only SC may be needed (Spa-SCh).

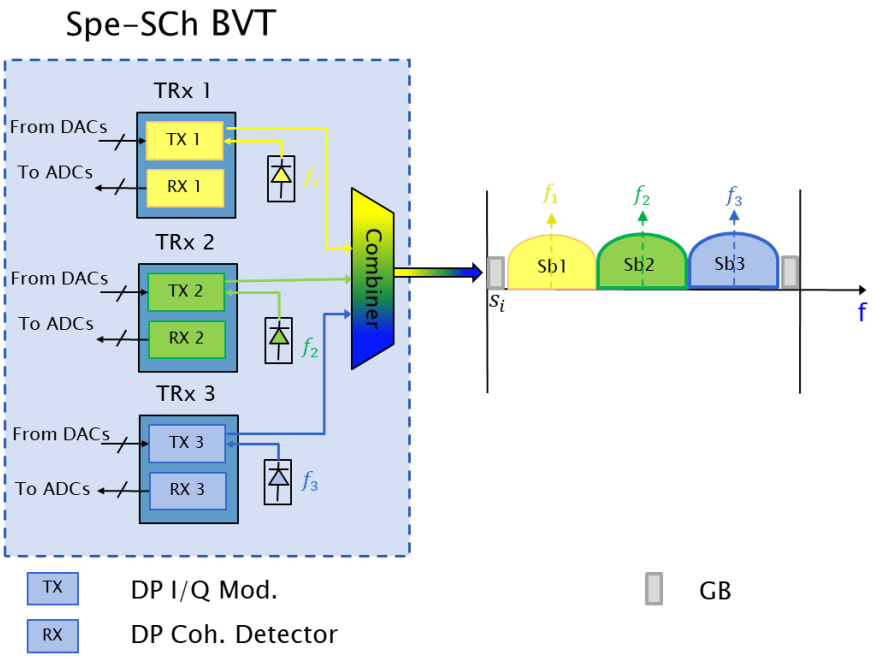

Fig. 4.1. Simplified diagram of integrated Spe-SCh BVT

4.1.1 Weighted Spectral and Spatial Allocation (WSSA)

As we have a wide range of possibilities to form SChs (i.e., different n_{fs} versus n_s options) in SS-FONs, it can be useful to choose the proper configuration (n_s, n_{fs}) based on a function that weights the minimization of spectral and spatial resources per SCh. We call this methodology as Weighted Spectral and Spatial Allocation (WSSA).

WSSA requires, for each demand bit-rate r_d, to compute all candidate SCh configurations as a form of (n_s, n_{fs}) tuples, given a modulation format and the total spatial channel count S. These tuples are gathered in a so-called solution space ($\boldsymbol{\Omega}$) set, which is populated in the same manner as in the strategy presented in subsection 3.1.5 by means of equation (3.2). That is, starting from $n_s = 1$ to $n_s = S$, we compute the corresponding n_{fs} and the *i*-th tuples yielding identical n_{fs} value than (*i*-1)-th tuples are directly discarded. Subsequently, for each tuple *i* is computed its resultant b_i value by means of equation (4.1), where $\alpha \in [0,1]$ is the weighting parameter.

$$b_i = \alpha . n_{fs} + (1 - \alpha) . n_s \tag{4.1}$$

If the priority is to minimize the spectral resources per SCh, α=1 has to be set, while if it is to minimize spatial resources, α has to be equal to 0. All b_i values are added to set β and the selected SCh configuration (Ω_i) will be the *i*-th element yielding the lowest b_i value. Fig. 4.2 shows the example of three α values: 0 (Fig. 4.2.a), 0.5 (Fig. 4.2.b) and 1.0 (Fig. 4.2.c) with transceivers of 32 GBaud ($\max \Delta_{Sb} = 32$ GHz). We have three demands, d_1 = 1 Tb/s, d_2 = 100 Gb/s, and d_3 = 400 Gb/s, employing DP-64QAM, DP-16QAM, DP-QPSK, respectively. Given S=7, the $\boldsymbol{\Omega}$ sets for demand d_1, d_2 and d_3 are:

$\Omega_1 = \{(1,8), (2,4), (\mathbf{3}, \mathbf{3}), (5,2)\}$

$\Omega_2 = \{(\mathbf{1}, \mathbf{2}), (3,1)\}$

$\Omega_3 = \{(1,9), (2,5), (3,4), (\mathbf{4}, \mathbf{3}), (6,2)\}$

In Fig. 4.2.a, when $\alpha = 0$ the prioritization will be to minimize the number of allocated spatial channels n_s per SCh and WSSA strategy will select the first tuple in the respective Ω set, i.e., $\Omega(1)$. Conversely, when $\alpha = 1$ (Fig. 4.2.c) the objective is to minimize the allocated spectral resources, thereby the selected tuple is the last element in Ω, i.e., $\Omega(|\Omega|)$. However, when $\alpha \in (0,1)$, e.g., $\alpha = 0.5$ (Fig. 4.2.b), β sets for demand d_1, d_2 and d_3 are:

$\beta_1 = \{4.5, 3.0, \mathbf{3.0}, 3.5\}$,

$\beta_2 = \{\mathbf{1.5}, 2.0\}$,

$\beta_3 = \{5.0, 3.5, 3.5, \mathbf{3.5}, 4.0\}$.

In this case, for $\alpha = 0.5$ the lowest b_i for each demand are shown in boldface and the selected tuple $\Omega(i)$ is different for each d. In fact, $\Omega(3)$ is the selected element for d_1, $\Omega(1)$ for d_2, and $\Omega(4)$ for d_3. This WSSA approach implies that a mix of different SCh configurations (Spe-SCh, SC/MC Spa-SCh) can be allocated to satisfy the offered traffic.

It can occur that two or more elements in set β have the same b_i value. In these cases, WSSA methodology selects the element requiring the least amount of spectral resources, because it also aims to minimize the number of OCs (n_{OC}) in the case of MC SChs (Spe-SChs or S2-SChs), due to potential cumulative coherent crosstalk between contiguous Sb-Chs.

Regarding the n_{oc} OCs needed (per spatial channel) to configure the SChs, it mainly depends on the baud-rate (R_B) of the transceivers with maximum baud-rate (R_B^{max}). In turn, when flexible baud-rates are considered, the gross R_B at the Nyquist limit with dual polarization can be computed by means of equation (4.2). Hence, n_{OC} OCs will be equal to $\left\lceil \frac{R_B}{R_B^{max}} \right\rceil$.

$$R_B = \frac{r_d}{2 \cdot n \cdot n_s} \text{ [Baud]} \tag{4.2}$$

The aggregate traffic (r_d) is equally split into n_s spatial channels and n_{OC} OCs, i.e., $r_d/n_s \cdot n_{OC}$ b/s are transmitted per Sb-Ch. In the example of Fig. 4.2.b, for $d_1 = 1$ Tb/s DP-64QAM, $\alpha = 0.5$ and $n_s = 3$, the resulting baud-rate is 27.78 GBaud $[1000 \div (2 \cdot 6 \cdot 3)]$ and n_{OC} equal to 1. Therefore, the bit-rate transmitted per each Sb-Ch is 333.33 Gb/s $[1000 \div (3 \cdot 1)]$. Note that when MC SChs have to be allocated, we consider that these MCs are modulated with the same modulation format, thus transmitting an aggregate SCh bit-rate equal to the requested traffic demand, as denoted in equation (4.3).

$$r_d = 2 \cdot R_B \cdot n \cdot n_s \cdot n_{OC} \text{ [b/s]} \tag{4.3}$$

In Fig. 4.2.a for $\alpha = 0$, for each demand is allocated one Spe-SCh, namely, SCh1, SCh2 and SCh3 for d_1, d_2 and d_3, respectively. Each Sb-Ch is modulated over one OC at different operational central frequency. Therefore, one tunable laser source per OC are required (see simplified diagram of integrated Spe-SCh BVT in Fig. 4.1) or, as other alternative, one frequency comb plus one Arrayed Waveguide Grating (AWG) [67]. For example, in Fig. 4.2.a we should employ 8 laser sources. As α value increases, the possibility of sharing the laser source between Sb-Chs also increases, thanks to the spatial BVT designs [107]. For instance, with $\alpha = 0.5$ and $\alpha = 1$, we can observe in Fig. 4.2.b and Fig. 4.2.c that Spa-SChs allow to reduce the number of laser sources to 3. Blanks in these figures are free spectral and spatial resources to be assigned to other demands that fit into them. Moreover, with $\alpha = 1$ the total number of Sb-Chs (therefore, transceivers) to allocate SCh1, SCh2, SCh3 are higher than those with $\alpha = 0$ and $\alpha = 0.5$ (14 vs. 8), whilst the operational R_B of the transceivers is lower with $\alpha = 1$ than those with $\alpha = 0$ and $\alpha = 0.5$. For example, 16.67 GBaud vs. 27.78 GBaud for d_1. It is worth observing that, like in the case of our

example for $\alpha = 0.5$, it should exist an α value where the number of Sb-Chs and the spectral width per each are equal to $\alpha = 0$, with the difference that the Sb-Chs are accommodated over the spatial domain rather than the spectral one.

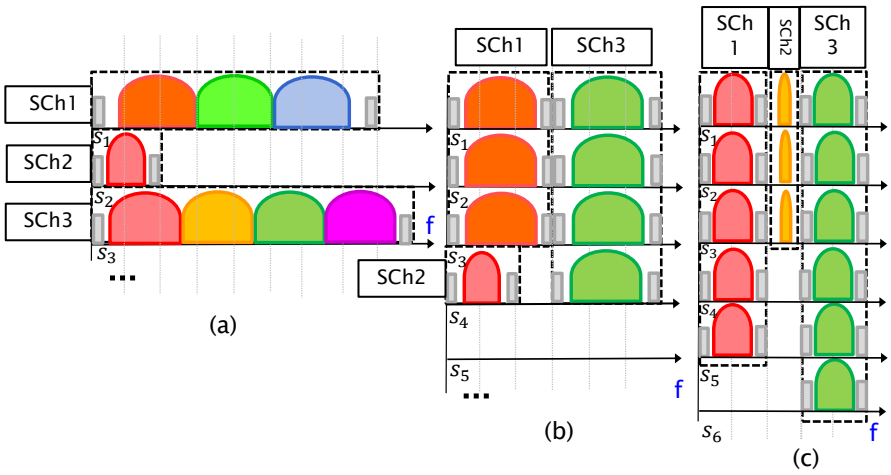

Fig. 4.2. SCh allocation for d_1=1 Tbps, d_2=100 Gbps, d_3=400 Gbps with PM-64QAM, PM-16QAM, PM-QPSK, respectively, S=7 with: (a) α=0, (b) α=0.5 and (c) α=1.

$\alpha = 0$ is the unique value that ensures that a single allocation policy (pure Spe-SCh) is employed for every traffic demand, regardless the traffic profile, network size, fiber type and S. However, a mix of Spe-SChs with SC/MC Spa-SChs can be configured with higher α values, including $\alpha = 1$ because, as seen, n_{OC} depends, among other factors, on the R_B^{max} of the transceivers.

4.1.2 RMSSA greedy heuristic for SS-FONs

Table 4.1 shows the RMSSA greedy heuristic that we propose for spectrally-spatially flexible super-channel configuration using WSSA methodology and InS with LC support switching strategy at SDM-ROADMs. In general, when a new demand d_i arrives at the network, K=3 SPs are computed as feasible candidate paths. For each candidate path (p), the MSE modulation format, with a TR equal or higher than the physical path length, is selected. Then, all candidate configurations for SCh composition (Ω) are computed by means of algorithm shown in Table 4.2 (line 7), which returns the selected tuple (n_s, n_{fs}) based on the alpha parameter. Finally, if there exist n_{fs} FSs available in n_s spatial channels along p, demand d_i is allocated. Otherwise, subsequent candidate paths are analyzed. If no candidate path can allocate d_i, it is finally blocked.

The analysis of the time complexity of the presented RMSSA heuristic for SS-FONs can be presented as follows. Firstly, the algorithm computes the K-SPs by using Yen's algorithm whose complexity was already mentioned in previous chapter 3, subsection 3.1.4.1. Later on, for each $p \in P$ the MSE modulation format (from $|M|$ possible ones) is assigned followed by the selection of the SCh configuration over S available spatial channels, therefore, the time complexity of this step is bounded by $|P|(|M| + S)$. To this time complexity has to be added the one of searching

through all $|P|$ feasible candidate paths (worst-case) free spectral resources in F over up to S spatial channels per link $e \in E$. So at the end, the overall time complexity of RMSSA greedy heuristic per arrival connection for SS-FONs is $\mathcal{O}(K|N|(|E| + |N| \cdot log|N|) + |P|(|M| + S + |F||S||E|))$. Compared to the RMSSA heuristic for spatially fixed Flex-Grid/SDM networks presented in subsection 3.1.4.1, the time complexity of this RMSSA heuristic for SS-FONs increases by S times in one of its terms, being necessary to search free spectral resources in F not only over the first spatial channel but also over up to S spatial channels per link. This fact gives us an idea of the complexity increment that the control plane would have to handle during the SCh provisioning tasks in SS-FONs versus those required in fixed Flex-Grid/SDM networks.

Table 4.1: RMSSA heuristic for SS-FONs

Input:
G=(N,E) // Physical Network
GB // Assumed guard-band per Spe-SCh
d_i *// Demand arriving at the network*
F // Set of FSs per spatial channel
S // Total number of spatial channels of MF or MCF.
α // Alpha value
M // Set of modulation formats
Begin:
  P ←Compute *K*=3 candidate SPs between s_d and t_d in *G*
  X_i ←*false // binary flag to determine if* d_i *is blocked or accepted*
  For each *p* in *P* **do**
    Find the most efficient modulation format $m \in M$ with $TR \geq$ Physical length of *p* [km]
    $(n_s, n_{fs}) \leftarrow$ **Compute SCh configuration** (d_i, S, α)
    If the same continuous and contiguous n_{fs} FSs in *F* are free in n_s spatial channels along *p* **then**
      Allocate the spatial and spectral resources
      X_i ←*true*,considering d_i as served
      break
    end if
  end for
  If X_i is false **then**
    Consider d_i as blocked
  end if
End.

Table 4.2. Compute SCh configuration

Input:
d_i *// Demand arriving at the network*
S // Total number of spatial channels of MF or MCF
α // Alpha value ∈ [0,1]
Begin:

3: $n_s = 1$, $n_{fs\_aux} = 320$ // *Big initial value*
4: **While** $n_s \leq S$
5: Compute $n_{fs} \leftarrow \lceil (r_d/(n_s \cdot SE) + GB)/W \rceil$
6: **If** $n_{fs} < n_{fs\_aux}$ **then**
7: $\Omega \leftarrow \Omega \cup \{(n_s, n_{fs})\}$
8: $b_i \leftarrow \alpha \cdot n_{fs} + (1-\alpha) \cdot n_s$
9: $\beta \leftarrow \beta \cup \{b_i\}$
10: **end if**
11: $n_{fs\_aux} \leftarrow n_{fs}$
12: $n_s \leftarrow n_s + 1$
13: **end while**
14: $i = arg\ [\min(\beta)]$ // index *i* of the $\min(\beta)$ element.
15: **return** $(n_s, n_{fs}) \leftarrow \Omega_i$ // Select *i-th* tuple of Ω set.
16: **End.**

4.2 Performance of SS-FONs

This subsection aims to present some simulation results of SS-FONs performance regarding throughput and BVT complexity. To this end, subsection 4.2.1 studies the impact of different SCh configurations (that can be allocated following the WSSA methodology proposed in previous subsection 4.1.1) on network throughput. Next, in order to compare the capacity of spatially fixed Flex-Grid/SDM networks and SS-FONs, subsection 4.2.2 presents the results of network throughput vs. spatial multiplicity. It is worth mentioning that network throughput results of these subsections are obtained by considering InS with LC support nodes (the ones with the highest flexibility, therefore, the ones yielding the best-expected performance). Moreover, the generation/detection of different SCh configurations is directly related with the BVT design. Some aspects of this design for the appropriate operation of SS-FONs are finally discussed in subsection 4.2.3.

4.2.1 Impact of SCh configuration on network throughput

As explained in subsection 4.1.1, different candidate SCh configurations (n_s, n_{fs}) can be obtained depending on the $\alpha \in [0,1]$ value. In order to illustrate the effect of SCh configuration, we choose a network scenario where both MF and equivalent MCF solutions can be contrasted. Both 7- and 12-core MCF prototypes have the same TR as the equivalent MF solutions (as presented in Table 3.2). So, ICXT is not the TR limiting factor. In contrast, the 19-core MCF prototype evidences lower TR than the equivalent MF solution. Moreover, this prototype shows the most restrictive TR compared to the 22-core and 30-core MCF ones. Hence, we find interesting to evaluate the effect of the SCh configuration by varying the weighting parameter α

of WSSA methodology in both reference networks, considering all links equipped with 19-core MCFs [29]. Fig. 4.3.a and Fig. 4.3.b show the network throughput (for a BBP≈1%) versus $\alpha \in [0,1]$, with 0.02 granularity, in DT12 and US26 reference networks (see Appendix A), respectively. The mean bit-rate per connection is 800 Gb/s.

Please recall that $\alpha = 0$ forces allocating all demands over pure Spe-SChs, where the overhead due to GBs is lower than in other SCh configurations. This aspect may suggest that the highest network throughput is always obtained with α=0, describing a monotonically decreasing behavior from then on. However, observing Fig. 4.3, we see that network throughput experiences short increments or becomes constant with some high α value intervals. This means that, even though other SCh configurations (n_s, n_{fs}) introduce higher GB overhead, they could be appropriate (especially in dynamic scenarios where fragmentation plays an important role) for increasing the number of allocated connections, thus improving network throughput.

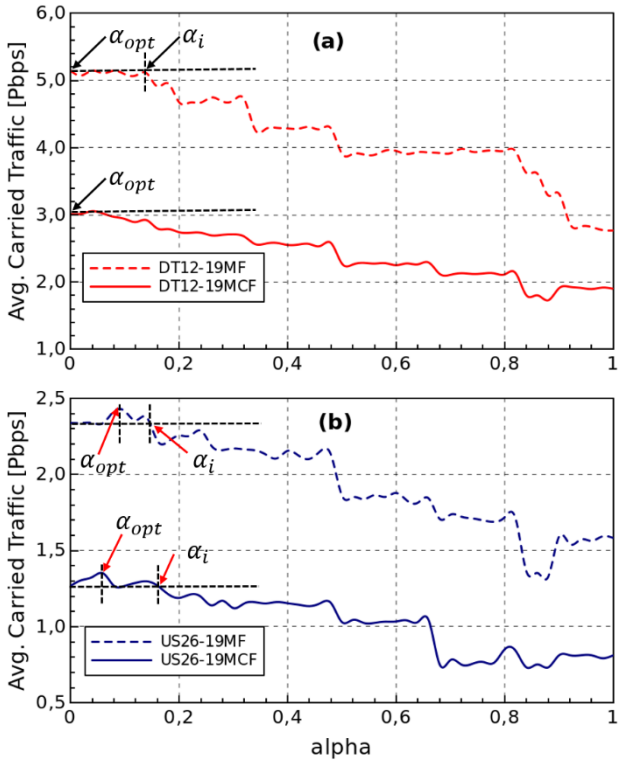

Fig. 4.3. Network throughput versus α with S=19 MF&MCF solutions in: (a) DT12 network, and (b) US26 network.

The above-described situation can be more relevant in cases where demands require a large number of FSs using a single spatial channel, hindering their allocation along the routing path, as both spectral continuity and contiguity constraints must be ensured end-to-end. Consequently, it may be easier to find less spectral resources, although employing more than one spatial channel (i.e., using SC/MC Spa-SChs). In MCF-enabled networks, we also have to recall that the higher the ICXT and the larger the network size, the higher the amount of spectral resources to be

allocated, as less efficient modulation formats are mandatory. This is evidenced in Fig. 4.3.b for both 19MF (dotted blue line) and 19MCF (solid blue line) solutions, where $\alpha = 0.08$ and $\alpha = 0.06$ allows increasing the network throughput compared to the one obtained with $\alpha = 0$. We define this increment as throughput gain (in %), which is equal to 3.4% (2.42 Pbps vs. 2.34 Pb/s) and 6.3% (1.35 Pbps vs. 1.27 Pbps), respectively. These α values yielding the highest network throughput we denote them as optimum values (α_{opt}), as highlighted in Fig. 4.3. Meanwhile, in the scenarios where the network diameter is not significant (like in DT12 network) the initial alpha equal to 0 can lead to the maximum throughput (i.e., $\alpha_{opt} = 0$). We can also see in this figure that the network throughput vs. α function is not linear, but rather like a step function. There are intervals where no significant changes occur when incrementing α, and some points where the network throughput drops abruptly. Another interesting point from Fig. 4.3 to be observed is the one denoted in this work as the *break-even point* (α_i), which is defined as the maximum α value after α_{opt} yielding identical network throughput to $\alpha = 0$ (i.e., throughput gain = 0%). The situations where network throughput is not affected by α increments can offer benefits in the BVT complexity (and therefore in cost), which will be discussed later on in subsection 4.2.3. According to the results, throughput reductions up to 48% and 38% are reported for MF and MCF solutions, respectively, when comparing $\alpha = 0$ vs. $\alpha = 1$. Finally, comparing MCF versus MF solutions, we can see that in the DT12 network with $\alpha = 0$, throughput differences up to 2.1 Pb/s are reported (equivalent to 42% of penalty due to ICXT), while for $\alpha = 1$ they lower to 0.9 Pb/s (33% penalty). In the case of the US26 network, these differences are around 1.1 Pbps (46% penalty) and 0.8 Pb/s (50% penalty) with $\alpha = 0$ and α=1, respectively.

Another aspect to study is how the network throughput gain is affected by the TP. To shed light on this, Fig. 4.4 shows the throughput gain for different mean bit-rates per connection (μ), namely, 0.4 Tb/s, 2 Tbps and 4 Tb/s, in both reference topologies. We can see that, in the US26 network there are throughput gains for both MCF and MF solutions and for the three traffic profiles. These gains rise as the mean bit-rate per connection increases, becoming up to 40% in the MCF scenario under $\mu = 4$ Tb/s. That is, for long-haul backbone networks with ICXT-limited TR, the higher the μ value, the higher the throughput gain obtained by using the α_{opt}. This happens because, as we stated before, large demands can motivate the exploration of SCh configurations with $n_s > 1$, in order to find out alternatives to accommodate them. Moreover, the higher the n_s value, the higher the laser source sharing factor, as explained in previous subsection 4.1.1.

In Fig. 4.4, spaces where no bars are depicted mean that the throughput gain is null (0%), i.e., $\alpha_{opt} = 0$. For example, considering the allocation of traffic demands with $\mu = 0.4$ Tb/s and $\mu = 2$ Tb/s in the DT12 network, $\alpha = 0$ is the optimal value for both MF and equivalent MCF solutions. For $\mu = 4$ Tb/s, the MCF solution with $\alpha_{opt} = 0.03$ reports a 7% of throughput gain,

whilst the MF solution does not evidence any gain. Although in the MF solution $\alpha_{opt} > 0$ does not occur, the benefits of replacing some Spe-SChs by Spa-SChs by increasing alpha should be analyzed. For example, in this case we obtain by simulation that $\alpha = 0.08$ yields identical network throughput to the one with $\alpha = 0$ (i.e., *break-even point* $\alpha_i = 0.08$). According to [58], the total SDM network cost can be considered as the sum of the ROADMs and BVTs costs. The former can be disaggregated in the sum of bypass part, A/D module and amplifiers costs, thus obtaining equation (4.4).

$$\text{Total SDM network cost} = cost_{bypass} + cost_{A/D} + cost_{amp} + cost_{BVTs} \quad (4.4)$$

Among these network elements, BVTs contribute to the total network cost in the range from 45% to 58% [58], i.e., BVTs are the major network equipment cost. It has been also reported that the use Spa-SCh BVTs can reduce the cost in 5-20% versus Spe-SCh BVTs with 2-10 Sb-Chs, thanks to the integration and sharing of network elements (e.g., the laser sources). Moreover, when Spa-SChs are allocated, the joint digital signal processing [68] of spatial sub-channels at the receivers by means of integrated chips could further reduce the power consumption and cost of the SDM networks. Therefore, using higher α values in dynamic scenarios may not only increase the network throughput, but also reduce the overall SDM network cost. Some statistics about BVT configuration with different alpha values corroborating the last affirmation are more detailed in the results of the next subsection 4.2.3.

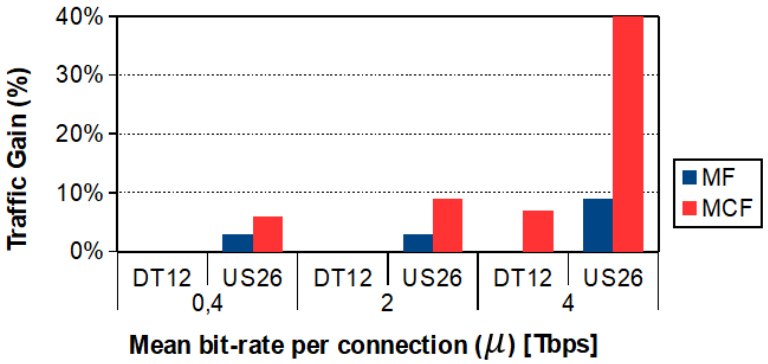

Fig. 4.4. Throughput gain (%) for α_{opt} vs. $\alpha = 0$ in DT12 and US26 networks with 19-core MCFs.

To end this subsection, we illustrate in Fig. 4.5 the different SCh configurations that can be obtained with α_{opt}, showing the n_s histogram. For the US26 backbone network (Fig. 4.5.a-c), we consider the MCF solution and all μ values assumed before, whilst for the DT12 network in Fig. 4.5.d, we contemplate the MF solution and $\mu = 4$ Tb/s. As mentioned before, this latter scenario is an interesting case where no traffic gain exists; however, alternative SCh configurations than Spe-SCh can potentially reduce overall network cost.

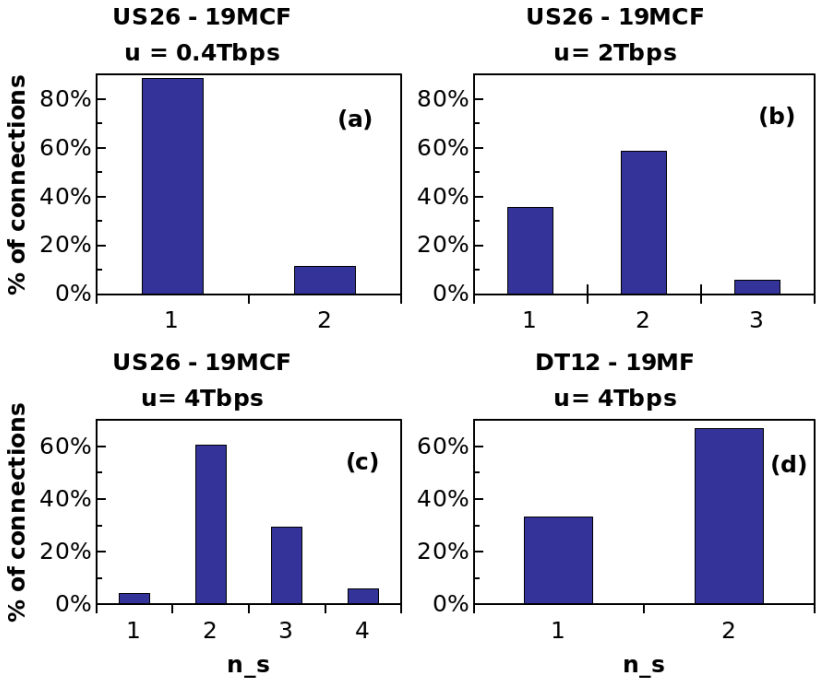

Fig. 4.5. n_s Histogram with S=19 (MCF), α_{opt} , US26 for: (a) μ=0.4 Tbps, (b) μ=2 Tbps,(c) μ=4 Tbps; and (d) S=19 (MF), α_i, DT12, μ=4 Tbps.

As observed, higher μ values demand increasing n_s as well. In the US26 network, under $\mu = 0.4$ Tb/s the ~90% of connections employ $n_s = 1$, whilst for $\mu = 2$ Tb/s the percentage of connection with $n_s = 1$ downs to ~35%. Finally, for $\mu = 4$ Tb/s just ~5% of connections employ $n_s = 1$. As μ increases from 0.4 to 4 Tb/s, the maximum n_s goes from 2 to 4. These results highlight that a considerable number of Spe-SChs can be replaced by SC/MC Spa-SChs with throughput gains and cost reduction implications, as stated before. Moreover, the previous described scenario in Fig. 4.4 for DT12 network with MF and $\mu = 4$ Tb/s, reported that, whereas there is no $\alpha > 0$ that provides throughput gain, there exists an α_i value (α_i =0.08) that yields cost reduction in BVTs, keeping the same network throughput as $\alpha = 0$. In such case, ~33% of connections have been allocated with Spe-SChs and the remaining ones employ Spa-SChs with $n_s = 2$, as appreciated in Fig. 4.5.d.

4.2.2 Network throughput vs. spatial multiplicity analysis

In subsection 3.1.4.2, we observe that throughput increment of spatially fixed Flex-Grid/SDM networks does not correspond with the spatial multiplicity. This subsection is aimed to study this relation of spatial multiplicity versus network throughput when spatial flexibility is considered, i.e., in SS-FONs. To this end, we consider same assumptions presented in subsection 3.1.4.2 for comparison purposes including the two reference networks and TPs (TP1 and TP2), but following the RMSSA heuristic presented in subsection 4.1.2.

Fig. 4.6 shows network throughput in function of the spatial multiplicity. As in subsection 3.1.4.2, the network throughput results for different SCh configurations in SS-FONs are obtained with a BBP≈1%. Moreover, we scale up the spatial multiplicity from 7 to 30 spatial channels including MF as well as MCF solutions. For comparison purposes, network throughput of spatially fixed Flex-Grid/SDM networks, specifically, the case of JoS-enabled Flex-Grid/SDM networks with e2e-grooming (JoS-Gr plots) previously evaluated in subsection 3.1.4.2 is also added in Fig. 4.6. As observed, for SS-FONs, we depict the throughput for three alpha values, namely, $\alpha = 0$, $\alpha = 1$ and α_{opt} (the value between 0 and 1, which produces the highest network throughput).

It is worth mentioning that the ROADM design (bypass part, A/D module, amplifiers) for SS-FONs is the same regardless of the α value. However, as we stated in previous subsection 4.2.1, the selected α value has to be associated with the corresponding complexity and cost of the BVTs. For example, $\alpha = 0$ (blue curve with triangle markers) in the DT12 network (Fig. 4.6.a,b) yields the highest network throughput, but at expenses of higher complexity and cost derived from using Spe-SCh BVTs. Conversely, $\alpha = 1$ (red curve depicted with square markers) yields the lowest network throughput, but with low complexity and cost due to integrated design of the Spa-SCh BVTs [58], [107]. In the case of the US26 network (Fig. 4.6.c,d), α_{opt} (red curve with triangle markers) not only yields higher network throughput than the one with $\alpha = 0$, but also lower complexity and cost by replacing some Spe-SChs (e.g., ~12% of connections for US26 backbone network, TP2 and S =19) by SC/MC Spa-SChs.

Furthermore, for DT12 network, MF/MCF solutions, and TP1/TP2 the results show that α_{opt} is equal to α =0, because higher-order modulation formats allow reducing the spectrum occupation in a single spatial channel. Meanwhile, in the US26 network, α_{opt} is higher than 0, particularly, $\alpha_{opt} \in (0,0.1]$. Throughput gain (α_{opt} vs. $\alpha = 0$) raises as the spatial multiplicity and TP increase (e.g., we demonstrated in previous subsection 4.2.1 up to 40% of traffic gain with high TPs). Particularly, under TP1, throughput gain keeps lower than 2%, while under TP2, throughput gain raises up to 6%. Throughput gain dependence on the spatial multiplicity can be explained as follows. The smaller the spatial multiplicity, the higher the relative overhead. As the spatial multiplicity increases, the impact of the overhead becomes compensated by the increment of the potential network capacity in terms of spectrum. We also observe that for both considered networks, regardless of the TP, the curves for SS-FON with α_{opt} and $\alpha = 1$ are divergent. They start (in S=7) with a short difference in terms of network throughput (lower than 50%), whilst they end (in S=30) with a difference up to 130%.

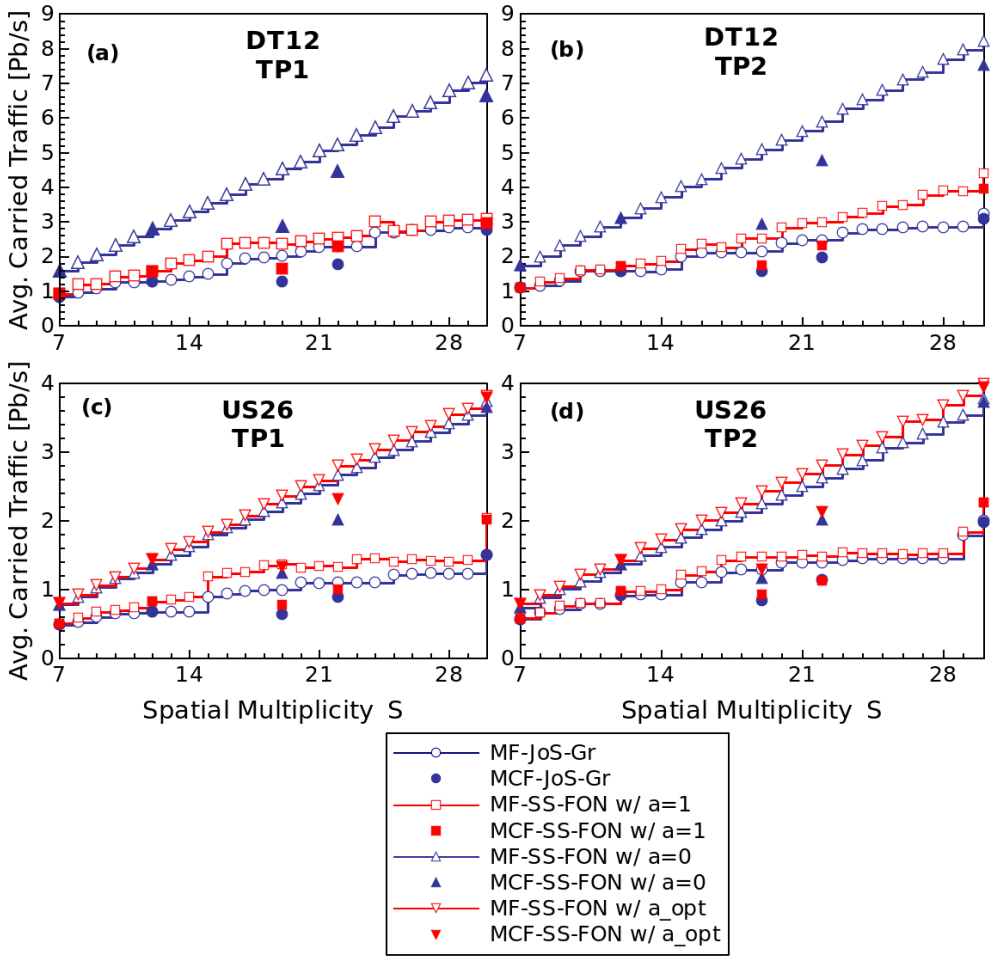

Fig. 4.6. Network Throughput (in Pb/s) versus S with spectrally-spatially flexible SChs for: (a) DT12 under TP1, (b) DT12 under TP2, (c) US26 under TP1, (d) US26 under TP2.

Regarding MCF solutions, it is important to recall that ICXT may cause a huge amount of required spectral resources per SCh, being necessary to split the optical signals in more spatial channels. In these cases, the α granularity is relevant to find out the optimal value as we have more elements in the solution space (Ω). For example, for 19-MF $\alpha_{opt} = 0.09$, while for 19-core MCF $\alpha_{opt} = 0.04$. Besides, note that network throughput with the 19-core MCF is lower or equal than with the 12-core MCF one due to the higher ICXT, meaning that although the 19-core MCF offer more capacity, the spectral and spatial resources are rapidly consumed by traffic demands employing less efficient modulation formats.

The results of Fig. 4.6 also report that in SS-FONs for a 4.3x spatial multiplicity factor (S=30 vs. S=7) with α=0 or α_{opt}, throughput scales up to a similar factor (e.g., 5x and 4.1x in the best –US26 TP2– and worst case –DT12 TP1–, respectively) for MF and MCF solutions, showing a more clear correspondence with the potential network capacity increment driven by spatial multiplicity. Moreover, the network throughput of MCF solution scales up to a close factor to MF one (penalty lower than 10% against MF solution is observed) in both national and continental

backbone networks, which indicates the feasibility of MCF deployments in the assessed spatial multiplicity interval. In the case of $\alpha = 1$, this α value entails the same complexity and cost in BVTs for spatially fixed Flex-Grid/SDM networks and SS-FONs. Under this scenario, differences (in terms of throughput) between both networks are at most 52% and even 0% in some cases. That is, spatially fixed Flex-Grid/SDM networks can carry an acceptable amount of throughput compared to SS-FONs (when $\alpha = 1$) with the advantage of cost reduction in the ROADM design (specifically, in the bypass part, as explained in chapter 2 and subsection 2.3.1). It is worth mentioning that, for spatially fixed Flex-Grid/MCF networks end-to-end MIMO compensation can be applied to entire spatial dimension, while for MCF-enabled SS-FONs MIMO could not always be applied. This additional advantage of spatially fixed Flex-Grid/MCF networks can reduce the differences against MCF-enabled SS-FONs. For example, note that for 19-core MCF, MIMO equalization in spatially fixed Flex-Grid/MCF networks would yield a throughput higher than the one of MCF-enabled SS-FONs with $\alpha = 1$, and the differences with equivalent MF-enabled SS-FONs would be shorter (penalties lower than 25%).

So far, Fig. 4.6 showed the performance of SS-FONs in terms of throughput while evaluating the spatial multiplicity scalability. Besides, it is also interesting to observe their performance in terms of BBP when increasing the offered load (i.e., fixing the IAT and increasing the HT). To this end, Fig. 4.7 shows the BBP vs. Offered Load (in Pb/s) for some relevant scenarios. In particular, we consider for this analysis the US26 network (where ICXT effects are more relevant), S=12 and S=22 (some intermediate spatial multiplicities where there exists a MCF prototype), traffic profile TP2 (which has shown throughput gains for the considered 7-30x spatial multiplicity range). Fig. 4.7.a,b show the results for SCh configurations with α=0 and α_{opt}, while Fig. 4.7.c,d with α=1. According to the results, when MF-based solutions are considered, throughput gains (α_{opt} vs. α=0) up to 8% are obtained for low offered loads yielding 0.01% BBP Fig. 4.7.b. However, under offered loads yielding a BBP higher than 1% and lower or equal to 10%, throughput gains are almost inappreciable. Regarding MCF-based solutions, as ICXT of the 12-core MCF has no impact on the TR, its performance is identical to 12-MF equivalent solution, whereas for the 22-core MCF throughput gains up to 10% are obtained for a 0.01% target BBP. Fig. 4.7.c,d show the same performance analysis for SCh configurations with α=1. In this case, JoS-Gr plots are also added, and as observed, for MF-based solutions the performance differences between SS-FONs and spatially fixed Flex-Grid/SDM networks are lower than 14%. Meanwhile, when ICXT is relevant (the case of 22-core MCF) the performance differences between both networks are almost inappreciable (i.e., these performance differences, when ICXT is relevant, can be lowered down to 0%). This is due to the long distance paths, high bit-rate connections and ICXT impact, where the unused spectral-spatial resources left by lightpaths cannot be assigned to other traffic demands in spite of the spatial flexibility, unless traffic demands are accordingly split into several chunks.

Finally, Fig. 4.7 clearly shows the differences in the supported offered load between SCh configuration with α=0, α_{opt} and α=1. For example, for a maximum 10% BBP, networks allocating SChs with α=0 or α_{opt} can support up to 2.2x more offered load than when they allocate SChs with α=1, due to spectrum savings of GBs.

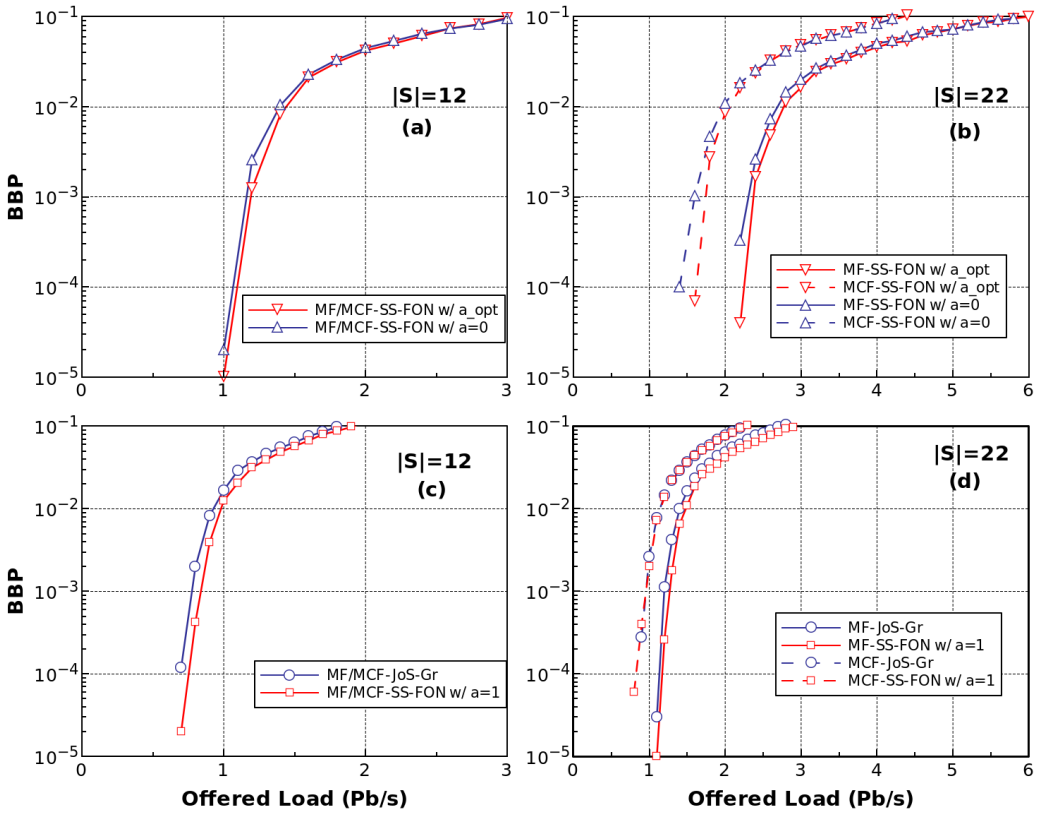

Fig. 4.7. BBP versus Offered Load (in Pb/s) for US26 network and TP2: (a) $\alpha = 0, \alpha_{opt}$, S =12, (b) $\alpha = 0, \alpha_{opt}$, S =22, (c) $\alpha = 1$, S =12 and (d) $\alpha = 1$, S =22

4.2.3 BVT complexity analysis

This subsection analyzes the BVT complexity for different SCh configurations in SS-FONs as well as in spatially fixed Flex-Grid/SDM networks for comparison purposes. To this end, we have obtained additional metrics, namely, the average number of OCs per SCh ($\overline{n_{OC}}$) (which is equal to the average number of tunable laser sources per Spa-SCh BVT), the average number of transceivers per SCh/BVT ($\overline{n_{TRx}}$) and the average baud-rate per transceiver (R_B). This latter metric can be taken as a key indicator of the electronic complexity of DSP. Table 4.3 and Table 4.4 show these metrics for MF and MCF solutions with 19 spatial channels, respectively, in DT12 and US26 networks under TP2. In addition, we consider the SCh configurations (α values) for JoS-Gr and SS-FONs plots shown in Fig. 4.6. For both reference networks, regardless of the SDM fiber type, the results show that with $\alpha = 0$ we have BVTs with the largest number of OCs and equal to the number of transceivers per BVT. Conversely, when $\alpha = 1$, BVTs have only one OC (except for US26 with 19-core MCFs, as there exist cases where 2 Tb/s demands with long-

distance paths require 2 OCs). That is, Spe-SCh BVTs (α =0) require in average up to 5.8x and 9.6x more laser sources than Spa-SCh BVTs (α =1) for 19-MCF&DT12 and 19-MCF&US26 networks, respectively. In contrast, Spa-SCh BVTs (α =1) require in average up to 2.9x and 2.1x more transceivers than Spe-SCh BVTs (α =0). However, for Spa-SCh BVTs (α =1), their transceivers are operating at lower baud-rate than Spe-SCh BVTs (α =0), e.g., up to 62% and 51% of baud-rate reduction is reported with $\alpha = 1$ against $\alpha = 0$ for DT12 and US26 networks, respectively.

This latter aspect supports even more the fact that Spa-SCh BVTs reduces the network cost by not only optical *integration* and *sharing* but also by reducing the electronic processing at DSPs. Therefore, lower amounts of throughput with higher α values (see Fig. 4.3) must be contrasted with cost reduction. Moreover, for α_{opt} 4-11% less laser sources and 2-4% less transceivers are required per BVT with the same baud-rate, compared to the obtained metrics with $\alpha = 0$. As we stated before, for DT12 network α_{opt} is equal to zero, regardless of the SDM fiber type. So, the values for $\alpha = 0$ are not repeated in the corresponding column. Table 4.3 and Table 4.4 also show BVT statistics with the previous introduced α_i value for US26 network. These results help better understanding the benefits of the proposed mechanism to configure SChs. A 30-32% less laser sources and 6-9% less transceivers per BVT with α_i yields the same network performance (in terms of throughput) with $\alpha = 0$. For DT12 network, this α_i value yields the same BVT statistics than $\alpha = 0$, then the column for α_i in DT12 network is not shown.

Finally, when longer network sizes are considered (e.g., US26 vs. DT12) and lower TRs are obtained (e.g., MCF solution vs. MF one), less efficient modulation format are required to be employed. In turn, less efficient modulation formats determine to transmit lower bit-rates per Sb-Ch. Therefore, in order to satisfy one traffic demand more Sb-Chs (consequently more transceivers, baud-rates and laser sources) may be required. This is the case in the results of Table 4.3 and Table 4.4 when we compared the different metrics for US26 vs. DT12 networks and for MCF vs. MF solutions.

Table 4.3: Metrics for Different SCh Configurations for DT12 and US26 networks with S=19 (MF) and TP2

Metric	**JoS-Gr**		**SS-FON**					
	$\alpha = 1$		$\alpha = 0$		$\alpha = 1$		$\alpha_{opt} = 0.09$	α_i
	DT12	**US26**	**DT12**	**US26**	**DT12**	**US26**	**US26**	**US26**
$\overline{n_{OC}}$	1	1	3.8	5.4	1	1	4.8	3.8
$\overline{n_{TRx}}$	10.9	11.2	3.8	5.4	10.9	11.2	5.2	5.1
R_B	9.5	13.7	25.2	28	9.5	13.7	28	28

Table 4.4: Metrics for Different SCh Configurations for DT12 and US26 networks with S=19 (MCF) and TP2

Metric	JoS-Gr				SS-FON			
	$\alpha = 1$		$\alpha = 0$		$\alpha = 1$		$\alpha_{opt} = 0.04$	α_i
	DT12	**US26**	**DT12**	**US26**	**DT12**	**US26**	**US26**	**US26**
$\overline{n_{OC}}$	1	1.1	5.8	9.6	1	1.1	8.9	6.5
$\overline{n_{TRx}}$	11.3	13.7	5.8	9.6	11.3	13.7	9.4	8.8
R_B	14.5	19.9	28.4	29	14.5	19.9	29	29

4.3 Conclusions

This chapter has focused on the operation of SS-FONs. In this kind of networks, flexibility in the spectral and spatial dimension opens some questions like *how to configure SChs?, What are the implications of these configurations on performance and hardware requirements?*. This chapter has contributed to answering these questions, by considering MF and MCF SDM fibers, different network topologies and traffic conditions. Specifically, regarding SCh configuration, a novel methodology called WSSA strategy has been provided in order to explore different allocation possibilities, ranging from pure Spe-SCh to pure SC Spa-SCh (if possible). Results have disclosed that a mix of SCh configurations (Spe-SChs, SC/MC Spa-SChs) during network operation tasks can yield better or at least equal performance than the allocation with best-expected results (i.e., with pure Spe-SChs). As for hardware requirements of BVTs, according to the literature, integrated Spa-SCh BVTs are cheaper than Spe-SCh BVTs thanks to sharing laser sources avoiding frequency combs and AWGs. In this sense, it has been also demonstrated that when a mix of SCh allocation configurations is considered in long-haul backbone networks, the same throughput than pure Spe-SCh allocation can be obtained, while an average of 30-32% less laser sources and 6-9% less transceivers per BVT is evidenced. Other further economic BVT configurations are possible with lower network performance (in terms of throughput) than pure Spe-SCh, thereby a trade-off between performance and cost can be analyzed in detail by network operators leveraged on the WSSA methodology.

Furthermore, this chapter has been studied the throughput scalability against spatial multiplicity in SS-FONs. Results have revealed that, conversely to what happens in spatially fixed Flex-Grid/SDM networks, in SS-FONs there exists a straightforward correspondence between spatial multiplicity factor and throughput increment. Specifically, a 4.3x spatial multiplicity factor in either MF or MCF solution yields a 4.1x (in the worst case) scaling factor in the network throughput considering the optimum SCh configuration. Nevertheless, as stated throughout this chapter, throughput gains have to be contrasted with network cost related to more complex SDM-ROADM architecture and BVT configuration than those employed in spatially fixed Flex-

Grid/SDM networks. For instance, differences from 0 to 52% in network throughput between spatially fixed Flex-Grid/SDM and SS-FONs with equivalent configuration (therefore, cost) in BVTs are reported.

Finally, as an outcome of this chapter and previous chapter 3, the results have shown that regardless of spatial flexibility, the MCF solution is a feasible implementation given the extremely low ICXT of the current laboratory prototypes and the very small differences in terms of network throughput for all cases, except for the 19-core MCF [29]. This prototype is expected to be improved with a fabrication technology and design like the 22-core MCF, which provides better network performance.

Chapter 5

5 SDM-ROADMs without spatial conversion for SS-FONs

In previous chapter 4, the performance of SS-FONs by using InS with LC support (see subsection 2.3.1) at SDM-ROADMs was discussed. Indeed, in analogous way to networks where spectrum conversion is permitted, such SDM-ROADMs are the ones allowing spatial conversion (switching from one spatial channel index to another at intermediate nodes). However, aiming to reduce such costly nodes by trading some flexibility for superior cost-efficiency, this chapter proposes to introduce the so-called Space Continuity Constraint (SCC) during provisioning tasks as suggested by InS w/o LC support SDM-ROADMs (see subsection 2.3.1), i.e., nodes without spatial conversion. In this way, in addition to the *spectrum continuity* and *spectrum contiguity* constraints imposed by transparent Flex-Grid optical networks, the SCC will have to be considered by assigning spectrum channels to lightpaths in the same spatial channel index *i*-th along the end-to-end routing path.

For this purpose, firstly, SDM-ROADM architectures with and without spatial conversion are presented in subsection 5.1. Then, the impact of spatial conversion on the network performance of SS-FONs as well as on their cost is evaluated in planning and operation scenarios in subsection 5.2. For the former ones, the RA problem under SCC is formally stated by means of an ILP formulation in subsection 5.2.1.2, and then, a lightweight heuristic is proposed in order to address large-problem instances in subsection 5.2.1.3. The comparison between performance under SDM-ROADM with and without spatial conversion is discussed in subsection 5.2.1.4 by using various reference networks and traffic profiles. As for network operation scenarios presented in subsection 5.2.2, where the fragmentation plays an important role, the same analysis carried out in planning scenarios is taken into account in order to demonstrate this cost-effective solution by deploying SDM-ROADMs without spatial conversion.

The work for this chapter was carried out in collaboration with the UPCT. The first part, for the network planning scenario (subsection 5.2.1), was implemented in the Net2Plan simulator [11], [127]; while the second part, for the network operation scenario (subsection 5.2.2), it was implemented in the Java-based ad-hoc simulator, presented in subsection 1.3.

5.1 SDM-ROADM architectures with/without spatial conversion

This subsection is aiming to analyze SDM-ROADM architectures with and without spatial conversion (synonym terms for InS with and without "lane change" support, respectively, in the literature [49], [50] and introduced in chapter 2).

Fig. 5.1 shows an SDM-ROADM with spatial conversion, which includes one Colorless, Directionless and Contentionless (CDC)-capable (by means of a multicast switch [48]) A/D module to inject/extract channels originated/terminated at the node without any internal blocking. The architecture has i input/output fibers ports (two degrees are shown for simplicity), each one carrying j spatial channels. The CDC architecture allows that any wavelength can be directed from/to any input/output fiber port and without contention at the A/D module. At the input fiber ports an SDM MUX (e.g., a FAN-OUT device in the case of MCFs [49], [51]) separates the spatial channels and to each of them, two device options can be connected. Specifically, either a power splitter or an SSS can be placed within the white boxes of Fig. 5.1, for B&S or R&S scheme, respectively, as shown in Fig. 5.3. For B&S scheme, the incoming optical signals from adjacent nodes are broadcasted to all available directions' modules within the ROADM by a power-loss-passive device, while in R&S scheme, SSSs allow to switch the input signals to the desired direction. Thanks to that, isolation is increased and signal attenuation caused by the broadcast operation is eliminated. Meanwhile, at the output fiber port, the opposite process is carried out by placing an SSS per spatial channel in order to multiplex different wavelengths and, then, an SDM MUX (e.g., a FAN-IN device in the case of MCFs) is used to pack (or join) all spatial channels in one output SDM fiber port.

Specifically about SDM-ROADM design with B&S scheme, the remarkable features extracted from Fig. 5.1 are summarized as follows:

- The number of passive splitters and SSSs is $i \cdot j$, i.e., it grows linearly with the node degree and spatial channel count.
- The number of SSS ports is $(i-1) \cdot j + 2$ considering at least one port for adding operation, i.e., it also grows linearly with the node degree and spatial channel count.
- Splitting losses are $10 \cdot log\{(i-1) \cdot j + 1\}$ considering at least one port for dropping operation. They grow logarithmically with the node degree and spatial channel count.

As for R&S scheme, the number of SSSs is doubled because passive splitters at input ports are replaced by SSSs, thereby also eliminating the splitting losses. Meanwhile, the number of ports per SSS is the same as in B&S scheme.

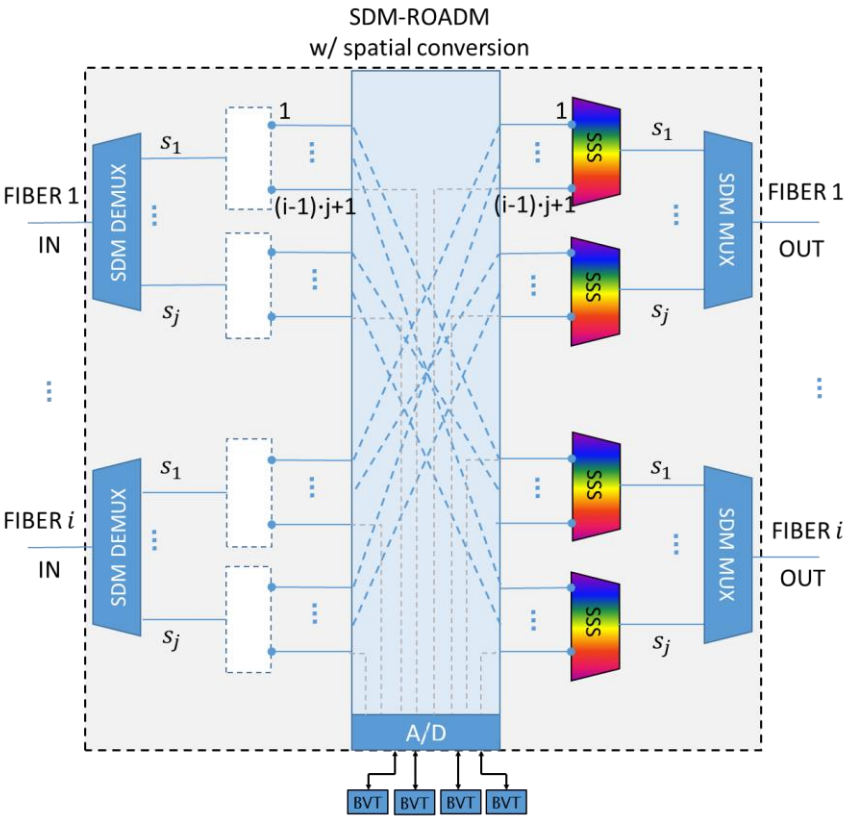

Fig. 5.1. Simplified SDM-ROADM architecture with spatial conversion. Two degrees are shown for simplicity.

Fig. 5.2 shows an SDM-ROADM without spatial conversion divided into two parts. In the first part (Fig. 5.2.a), a regular ROADM for standard SMF fiber is shown. The architecture has i input/output fibers ports (two degrees are shown for simplicity) and to each input fiber port two device options can be connected, namely, either a power splitter or an SSS can be placed within the white boxes of Fig. 5.2.a, for B&S or R&S scheme, respectively (see Fig. 5.3). In the second part (Fig. 5.2.b), this regular ROADM is used for designing the SDM-ROADM without spatial conversion, i.e., the architecture can be built as a parallel deployment of j (one per spatial channel) regular ROADMs for SMFs. According to Fig. 5.2.b, at the input fiber ports a SDM MUX (e.g., a FAN-OUT device in the case of MCFs [49], [51]) separates the spatial channels and each of them is connected to its corresponding ROADM. Meanwhile, at the output fiber port, the opposite process is carried out by placing an SDM MUX (e.g., a FAN-IN device in the case of MCFs) to pack (or join) spatial channels, one from each ROADM in one output SDM fiber port.

Specifically for B&S scheme, we can observe by means of Fig. 5.2 that:

- The total number of splitters and SSSs per ROADM is i, i.e., it grows linearly with the node degree regardless of the spatial channel count.
- The number of SSS ports is $i + 1$ considering at least one port for adding operation, i.e., it grows linearly with the node degree regardless of spatial channel count.

- Splitting losses are $10 \cdot \log\{i\}$ considering at least one port for dropping operation, i.e., they grow logarithmically with the node degree regardless of the spatial channel count.

As for R&S scheme, again the number of SSSs is doubled, splitting losses are eliminated and the number of ports per SSS is the same as in B&S scheme.

Comparing both SDM-ROADM architectures with and without spatial conversion, we can observe that the spatial conversion flexibility is obtained at the cost of higher splitting ratios or SSS size, for B&S and R&S, respectively. That is the reason why the number of cross-connections significantly increases in SDM-ROADMs with spatial conversion versus the ones not supporting it, as seen in Fig. 5.1 and Fig. 5.2. In view of that, large splitting losses supporting spatial conversion hinder B&S scheme implementation in such SDM-ROADMs. The higher the losses, the higher the required amplification and so the ASE noise introduced. For example, assuming an EDFA with amplification gain of 20 dB, S=12, the nodal degree would be limited to 8. In the same example, SDM-ROADMs without spatial conversion could handle up to 100 nodal-degree. That is, SDM-ROADMs without spatial conversion favor the B&S scheme implementation, thus saving costs. On the other hand, according to the analysis carried out in [47], the maximum splitting ratio in a B&S scheme may be limited to a factor of 9, requiring R&S for higher values. Thus, the scalability of SDM-ROADMs with spatial conversion under B&S scheme would be much compromised, while in SDM-ROADMs without spatial conversion, as the splitting ratio only depends on the nodal degree, not so high isolation is demanded.

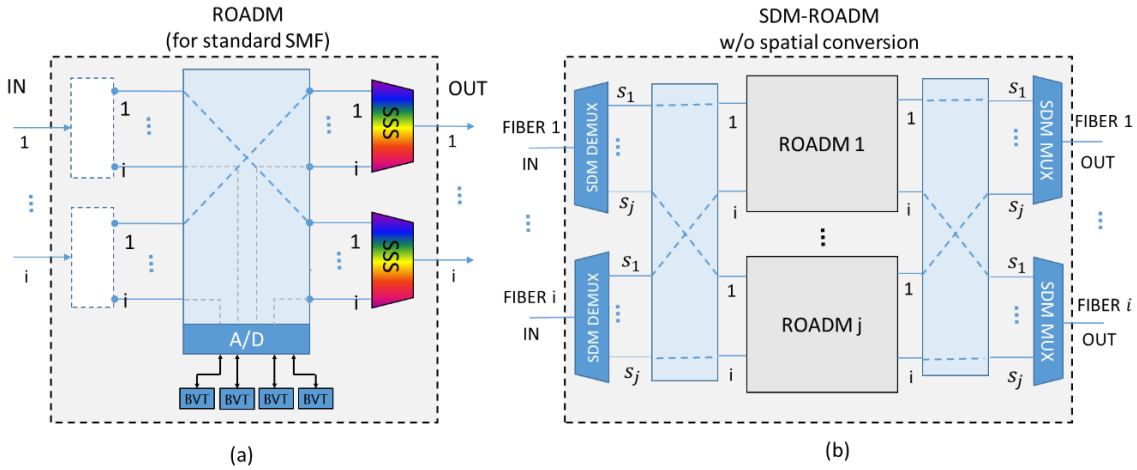

Fig. 5.2. Simplified architecture for: (a) ROADM for standard SMFs, (b) SDM-ROADM without spatial conversion. Two degrees are shown in both cases for simplicity.

Furthermore, Table 5.1 shows the number of input ports required in the SSS devices for nodes with and without spatial conversion considering different spatial channel count and nodal degree. In order to contextualize, the largest size of state-of-the-art SSSs is 1x35 [63]. The shadowed cells in Table 5.1 are those that exceed 35 ports. As we can observe, several settings

for SDM-ROADMs with spatial conversion overcome this limitation, while in SDM-ROADMs without spatial conversion the number of ports is way below it. Note that for a given nodal degree, the SSS size is fixed regardless the spatial channel count.

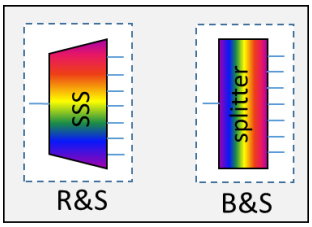

Fig. 5.3. Device connected at input ports of (SDM)-ROADMs by using: (a) a SSS for R&S scheme, and (b) a power splitter for B&S scheme.

Table 5.1: Number of Required Input Ports per SSS

S	**SDM-ROADM w/ spatial conversion**			**SDM-ROADM w/o spatial conversion**		
	***D*=2**	***D*=4**	***D*=8**	***D*=2**	***D*=4**	***D*=8**
7	8	22	50	2	4	8
12	13	37	85	2	4	8
19	20	58	134	2	4	8

Table 5.2 summarizes the main characteristics of SDM-ROADMs with and without spatial conversion. The scalability of SDM-ROADMs with spatial conversion is much compromised under both B&S and R&S schemes, due to the high demanded splitting ratios and SSS size. Meanwhile, the scalability of SDM-ROADMs without spatial conversion is better, even under B&S scheme because it does not depend on the spatial channel count, thus saving further costs.

Table 5.2: Summary of SDM-ROADM characteristics under B&S and R&S schemes

SDM-ROADM	**B&S**	**R&S**
w/ spatial conversion	Splitting ratios < 9	↑ spatial channel count → ↑ SSS size
w/o spatial conversion	$D < 9$	SSS size independent of spatial channel count

5.2 Impact of spatial conversion on the performance and cost of SS-FONs

This subsection analyzes the impact of spatial conversion at the network nodes on the performance and cost of SS-FONs. To this end, we consider both planning and operation scenarios with different reference networks and traffic conditions. It is worth mentioning that for performance impact assessment of spatial conversion, the unique additional constraint in RA process is the so-called SCC regardless of the scheme (B&S or R&S) implemented at the SDM-ROADM and presented in previous subsection 5.1. This means internal losses at SDM-ROADMs

have not been considered in the TR estimation. The impact would have been higher for B&S SDM-ROADMs with spatial conversion given the larger splitting ratios. In contrast, in order to analyze the network cost impact, the SDM-ROADM design is important to be considered.

5.2.1 Network planning scenario

For this scenario, both problems with and without spatial conversion at network nodes are firstly stated and then, its performance in terms of network throughput is compared.

5.2.1.1 Problem statement

The RA process with and without spatial conversion at network nodes is tackled as a Route, Transponder, Space and Spectrum Assignment (RTSSA) problem, which can be formally stated as follows:

Given:

1) A Flex-Grid/SDM network represented as a directed graph $\mathcal{G}(\mathcal{N}, \mathcal{E})$, where $\mathcal{N}$ is the set of optical nodes and $\mathcal{E}$ the set of unidirectional SDM fiber links. All SDM fiber links $e \in \mathcal{E}$ are assumed with the same set $\mathcal{S}$ of spatial channels.
2) A spectral grid consisting of an ordered set of FSs, denoted as $\mathcal{F}$, available in every spatial channel. FSs have a spectral width (in Hz) equal to W (i.e., 12.5 GHz according to the ITU-T recommendation [12]).
3) A set of offered unidirectional demands to the network, denoted as $\mathcal{D}$. Each $d \in \mathcal{D}$ has associated a source (s_d) and a destination (t_d) node in $\mathcal{G}(\mathcal{N}, \mathcal{E})$ and a requested bit-rate (in b/s), denoted as r_d.
4) Set of transponder types available in the network. For each transponder type t, r_t is the line-rate of the transponder, l_t is the TR, and n_t is the number of FSs (including GBs) needed to be allocated for this transponder.

Objective: minimize the network-wide spectral requirements allocating the most suitable route, transponder, space and spectrum resources for every offered demand in $\mathcal{D}$, subject to the following *constraints*:

1) *Traffic demand fulfillment:* every demand must be served and its requested bit-rate r_d can be satisfied by establishing one or more lightpaths. The sum of the associated line rate r_t for each lightpath has to be equal or higher than r_d.
2) *Spectrum continuity*: in absence of spectrum conversion and regeneration (i.e., transparent transmission), FSs supporting an optical channel must be the same in all spatial channels along the path from s_d to t_d.

3) *Spectrum contiguity*: optical channels must be allocated over a contiguous subset of FSs, the same in the traversed fiber links and spatial channels.
4) *Spectrum clashing:* a given FS f of one SDM fiber link e can be allocated up to S lighpaths, but a given FS f of one SDM fiber link e and spatial channel s_i can only be allocated to one lightpath at most.
5) *Space continuity* (if applied)*:* a lightpath can only use one spatial channel index i-th along the end-to-end routing path (i.e., no spatial conversion at intermediate nodes is permitted).

5.2.1.2 Optimal problem solution

The optimal solution for RTSSA problem stated in the previous subsection can be addressed by means of an ILP formulation. In this case, we present both formulations considering nodes with and without spatial conversion capabilities, respectively. For these formulations, the following sets and input parameters have been defined:

- $\mathcal{P}_d$: Set of pre-computed candidate physical paths for demand $d \in \mathcal{D}$; z_p is the physical length (in km) of path p and h_p the number of hops that it traverses.
- $\mathcal{P}$: Set of all pre-computed candidate physical paths in the network ($\mathcal{P} = \cup_{d\epsilon\mathcal{D}}\ \mathcal{P}_d$). We also denote as $\mathcal{P}_e$ those paths traversing SDM fiber link e.
- $\mathcal{T}_p$: Set of pre-computed candidate transponders whose TR z_t is higher or equal to z_p in order to satisfy a demand $d \in \mathcal{D}$.
- $\mathcal{T}$: Set of all pre-computed candidate transponders in the network $\left(\mathcal{T} = \cup_{p\in\mathcal{P}}\ \mathcal{T}_p\right)$.
- $\mathcal{O}_t$: Set of all pre-computed candidate optical channels to allocate the n_t FSs required for one transponder $t \in \mathcal{T}$. We also denote as $\mathcal{O}_t^f$ those channels containing FS $f \in \mathcal{F}$.
- $\mathcal{O}$: Set of all pre-computed candidate optical channels in the network ($\mathcal{O} = \cup_{t\in\mathcal{T}}\ \mathcal{O}_t$)

For both ILP formulations, as presented in [128], the pre-computation of candidate optical channels is necessary, which is shown in Table 5.3. For a given demand d, its corresponding set of candidate paths $\mathcal{P}_d$, set of candidate transponders per path $p \in \mathcal{P}_d$, namely, $\mathcal{T}_p$, and set of available FSs $\mathcal{F}$ per spatial channel, all candidate optical channels $\mathcal{O}_t$ of n_t contiguous FSs over each path $p \in \mathcal{P}_d$, are found in a sliding window fashion

Note that with this pre-computed candidate optical channels, we are indeed, ensuring the *spectrum continuity* and *contiguity* constraints along each path $p \in \mathcal{P}$.

5.2.1.2.1 ILP formulation for RTSSA with spatial conversion

In this subsection, we present the details of the proposed ILP formulation for RTSSA problem

with spatial conversion, where we introduce the following decision variable:

Table 5.3: Candidate optical channels pre-computation algorithm

Input: $\mathcal{F}, d, \mathcal{P}_d, \mathcal{T}_p$

for each p **in** $\mathcal{P}_d$ **do**
  for each t in $\mathcal{T}_p$ **do**
    $\mathcal{O}_t = \emptyset$
    for slotIndex = n_t **to** $|\mathcal{F}|$
      $o \leftarrow$ **newchannel** (slotIndex $-n_t$, slotIndex)
    $\mathcal{O}_t \leftarrow \mathcal{O}_t \cup \{o\}$
End.

x_{pto}: binary decision variable; 1 if path $p \in \mathcal{P}$ has a transponder assigned $t \in \mathcal{T}$ and channel $o \in \mathcal{O}$ to serve one demand $d \in \mathcal{D}$; 0 otherwise.

$$\min \sum_{p\in\mathcal{P},t\in\mathcal{T},o\in\mathcal{O}} n_t \cdot h_p \cdot x_{pto} \tag{5.1}$$

subject to:

$$\sum_{p\in\mathcal{P}_d,t\in\mathcal{T}_p,o\in\mathcal{O}_t} r_t \cdot x_{pto} \geq r_d\,, \forall d \in \mathcal{D} \tag{5.2}$$

$$\sum_{p\in\mathcal{P}_e,t\in\mathcal{T}_p,o\in\mathcal{O}_t^f,} x_{pto} \leq S, \forall e \in \mathcal{E}, f \in \mathcal{F} \tag{5.3}$$

Objective function (5.1) minimizes the total number of FSs used in the network. Constraint (5.2) represents the traffic demand fulfillment: the sum of the operational line rates r_t: $t \in \mathcal{T}$ assigned to one path $p \in \mathcal{P}$ is at least the requested bit-rate r_d: $d \in \mathcal{D}$. Finally, constraint (5.3) represents the *spectrum clashing* constraint*:* one FSs $f \in \mathcal{F}$ of one SDM fiber $e \in \mathcal{E}$ can be assigned to S lightpaths at most (one per spatial channel), where $S = |\mathcal{S}|$ (spatial channel count per SDM fiber) in order to maintain the nomenclature used in previous chapters. Note that in this formulation we do not tackle the specific spatial channel assignment for a particular SDM fiber link e due to the aforementioned spatial conversion flexibility at SDM-ROADMs.

5.2.1.2.2 ILP formulation for RTSSA without spatial conversion

In this subsection, we present the details of the proposed ILP formulation for RTSSA problem using SDM-ROADM without spatial conversion, where we introduce the following decision variable:

x_{ptso}: binary decision variable; 1 if path $p \in \mathcal{P}$ has a transponder assigned $t \in \mathcal{T}$, spatial channel $s \in \mathcal{S}$, and spectral channel $o \in \mathcal{O}$ to serve one demand $d \in \mathcal{D}$; 0 otherwise.

$$\min \sum_{p\in\mathcal{P},t\in\mathcal{T},s\in\mathcal{S},o\in\mathcal{O}} n_t \cdot h_p \cdot x_{ptso} \tag{5.4}$$

subject to:

$$\sum_{p\in\mathcal{P}_d,t\in\mathcal{T}_p,s\in\mathcal{S},o\in\mathcal{O}_t} r_t \cdot x_{ptso} \geq r_d\,, \forall d \in \mathcal{D} \tag{5.5}$$

$$\sum_{p\in\mathcal{P}_e, t\in\mathcal{T}_p, s\in\mathcal{S}, o\in\mathcal{O}_t^f} x_{ptso} \leq 1, \forall e \in \mathcal{E}, s \in \mathcal{S}, f \in \mathcal{F} \quad (5.6)$$

Similarly to previous ILP formulation, objective function (5.4) minimizes the total number of FSs used in the network. Constraint (5.5) represents the traffic demand fulfillment: the sum of the operational line rates $r_t: t \in \mathcal{T}$ assigned to one path $p \in \mathcal{P}$ over one spatial channel $s \in \mathcal{S}$ is at least the requested bit-rate $r_d: d \in \mathcal{D}$. Finally, constraint (5.6) represents the *spectrum clashing* constraint*:* one FSs $f \in \mathcal{F}$ of one SDM fiber $e \in \mathcal{E}$ and spatial channel $s \in \mathcal{S}$ can be only assigned to one lightpath at most. Note that in this formulation, unlike the previous formulation for RTSSA with spatial conversion, we tackle the specific spatial channel assignment for a particular SDM fiber link *e* in both constraints (5.5) and (5.6), which, in fact, ensure the *space continuity* constraint.

By means of these ILP formulations, we can appreciate that depending on the necessity, lightpaths cannot be only defined by the physical path p and the optical channel o associated to, but also with other resources like transponder t and spatial channel s, as denoted in this ILP formulation and explained in subsection 2.3.

5.2.1.3 Heuristic approach

This subsection presents a heuristic algorithm for solving the RTSSA problem in large Flex-Grid/SDM network scenarios employing SDM-ROADMs either with or without spatial conversion. Its pseudo-code is shown in Table 5.4.

The algorithm targets to maximize the carried traffic attempting to satisfy fully the traffic demands. This algorithm is based on the local search technique, in which a performance metric is used to evaluate the goodness of a solution within a main loop. Before entering the loop, it is necessary to compute the *K*-SPs as candidate physical paths $\mathcal{P}_d$ for all available traffic demands $\mathcal{D}$ (i.e., between their s_d and t_d) and candidate transponders $\mathcal{T}_p$ according to the TR ($z_t > z_p: p \in \mathcal{P}_d$). During this calculation, some paths may have no available transponder for a node pair that falls within its TR, and will not be included as valid option for that node pair.

Secondly, the algorithm enters into the main loop. Unserved demands are sorted in descending order according to the percentage of remaining traffic to be carried (line 4), and stored in $\mathcal{D}_{NotSat}$. As a result, the demand with the highest unserved traffic proportion will be the first one for which the RTSSA will be tried. Later, for each demand d in $\mathcal{D}_{NotSat}$, the algorithm calculates how to allocate a lightpath for each path $p \in \mathcal{P}_d$ and transponder $t \in \mathcal{T}_p$ taking into account the FF spectrum assignment for n_t continuous and contiguous FSs. If SCC is considered (line 9), it is mandatory to test over the same spatial channel index *i*-th along p (line 10); otherwise, the algorithm is free to test over different spatial channels in each link $e \in \mathcal{E}$ traversing path p. The sequence of spatial channels for OAM tasks are stored in $\mathcal{S}'$ (line 12), which cardinality coincides

with h_p. Each potential lightpath l to be allocated is represented by a performance metric consisting in its spectral efficiency (line 14), where cost of the transponder has been set to n_t value. In this way, the algorithm is aware of the optimization of spectrum resources available in the network. For a demand d, the lightpath l with highest performance metric is allocated (line 22). After this allocation, if demand r_d is fulfilled, demand d is removed from $\mathcal{D}_{NotSat}$. This process is repeated while there exists at least one new lightpath l allocated in the network. In other words, until all the demands are satisfied ($\mathcal{D}_{NotSat} = \emptyset$) or all the feasible possibilities have been analyzed.

Table 5.4: Heuristic algorithm pseudo-code for RTSSA w/ and w/o spatial conversion

1: **Input:** $\mathcal{G}, \mathcal{D}, \mathcal{P}, \mathcal{T}$
2: $\mathcal{D}_{NotSat} = \mathcal{D}$
3: **do**
4: Sort $\mathcal{D}_{NotSat}$ in descending order by the relative blocked traffic
5: **for** each d in $\mathcal{D}_{NotSat}$ **do**
6: $bestMetric = 0$
7: **for** each p in $\mathcal{P}_d$ **do**
8: **for** each t in $\mathcal{T}_p$ **do**
9: **if** SCC is considered **then**
10: FF spectrum assignment of n_t continuous and contiguous FSs in any spatial channel s_i along p
11: **else**
12: FF spectrum assignment of n_t continuous and contiguous FSs over h_p spatial channels ($\mathcal{S}'$) along p
13: $carriedTraffic \leftarrow$ Compute carried traffic after potential allocation
14: $currMetric \leftarrow carriedTraffic/cost(t)$
15: **if** $currMetric > bestMetric$ **then**
15: $bestMetric = currMetric$
17: **if** SCC is considered **then** $l \leftarrow$ **newlightpath** (p, t, s_i)
18: **else** $l \leftarrow$ **newlightpath** (p, t, $\mathcal{S}'$)
19: **end**
20: **end**
21: **if** ∃ new lightpath l **then**
22: Allocate l in the network
23: **if** r_d is fulfilled **then** $\mathcal{D}_{NotSat} \leftarrow \mathcal{D}_{NotSat} \setminus \{d\}$
24: **end**
25: **while** (∃ at least new lightpath l in the network)
26: **End.**

5.2.1.4 Simulation results

In this subsection, we present the results about performance validation of heuristic explained in previous subsection and the impact of spatial conversion on SS-FONs performance.

5.2.1.4.1 Scenario under study

Results presented in this subsection are obtained for different reference networks whose topologies are available in [127], [129]. Table 5.5 summarizes the main characteristics of these reference networks (note that I2 topology is also shown in Appendix A with the *TEST2* name). Furthermore, we consider that each network link is equipped with a weakly-coupled MCF with identical core count ($|\mathcal{C}|$), namely, $|\mathcal{C}| \in \{7, 12, 19\}$ [27], [29]. Each core has a total available spectrum $|\mathcal{F}|$=120 FSs of 12.5 GHz spectral width (W). To satisfy the offered demands, a set of available transponders is defined, operating at line rate $r_t \in \{40, 100, 400\}$ Gb/s, using different modulation formats (BPSK, QPSK, 16-QAM, 64-QAM) and flexible baud-rate (maximum 35 GBaud). Each transponder has different TR l_t according to the modulation format and MCF considered (ICXT values presented in Table 3.1 are taken into account). Table 5.6 shows TR for different line rates where shadow cells represent invalid combinations. Moreover, each transponder occupies a certain number of slots n_t, which includes a 10 GHz GB [5] and it reads $\left\lceil \frac{line\_rate/SE+GB}{W} \right\rceil$.

Table 5.5: Main characteristics of reference networks

Name	Nodes $\|N\|$	Links $\|E\|$	Avg. Node Degree D	Diameter (km)
Top 7 Spain (T7S)	7	16	2.29	920
Internet 2 (I2)	9	26	2.89	4,116
Poland (POL)	12	36	3.00	810
Germany50 (GER)	50	176	3.52	934
NSFNet (NSF)	14	42	3.00	4,500
European Optical Network (EON)	18	66	3.67	3,837

Table 5.6: TR in km for different r_t in Gb/s according to the considered modulation format and MCF type

Line rate	64-QAM		16-QAM		QPSK		BPSK	
	$\|\mathcal{C}\| = 7, 12$	$\|\mathcal{C}\| = 19$	$\|\mathcal{C}\| = 7, 12$	$\|\mathcal{C}\| = 19$	$\|\mathcal{C}\| = 7, 12$	$\|\mathcal{C}\| = 19$	$\|\mathcal{C}\| = 7, 12$	$\|\mathcal{C}\| = 19$
40					9,000	2,383	20,000	4,755
100			2,000	599	9,000	2,383		
400	600	150						

Both ILP and heuristic algorithms have been implemented in a network design and planning tool, Net2Plan [11], [127], which includes the JOM library, a Java-based interface for CPLEX solver [130], used in the execution of the ILP algorithm. Fig. 5.4 depicts an example of using Net2Plan as a framework to emulate a Flex-Grid/MCF network scenario. The emulated network is modelled by a set of geo-positioned nodes interconnected by MCF links (Fig. 5.4.a). Transponders connected to A/D ports of SDM-ROADMs has been also modelled by using different parameters, such as: the line rate, n_t FSs, cost, modulation format and its TR aware of ICXT. The carried

traffic using optimized lightpaths (which include the sequence of core indexes and FSs) to minimize spectrum requirements is also shown (Fig. 5.4.b). Green color means that a traffic request is satisfied.

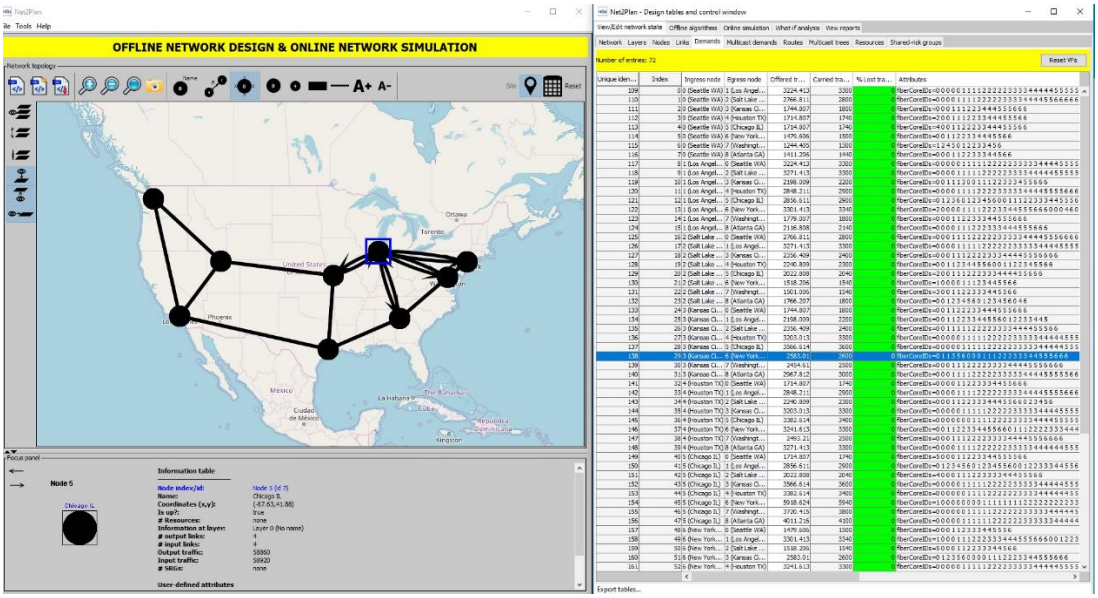

(a) (b)

Fig. 5.4. Net2Plan framework in a Flex-Grid/MCF scenario. (a) geo-positioned nodes interconnected by MCF links, and (b) carried traffic using optimized lightpaths

5.2.1.4.2 Heuristic performance validation

The results of this subsection were obtained from simulations run in a personal computer with 8-core i7 CPU and 16 GB of RAM. The JOM library was configured so that if the optimal solution is not found after one hour, the best feasible solution so far was returned, if any. The one-hour limit is only hit with SCC. The constraint structure in the RTSSA ILP without spatial conversion seems to be simpler and more favorable for the internal solver branch-and-bound optimizations, and the optimum solution is always returned before an hour; thus, it can be used as a performance upper bound to estimate the sub-optimality of the results with spatial conversion.

For testing the performance of the heuristic two reference topologies have been chosen, namely, T7S and I2 networks, while for modeling the traffic, we assume an offered IP traffic represented by a population-based seminal traffic matrix, where the offered traffic between two nodes is proportional to the product of their populations. To satisfy the offered demands, a set of available transponders is defined, according to the line rates r_t defined in previous subsection with TR for different modulation formats (see Table 5.6). For a same line rate r_t, the transponder with the MSE modulation format is always selected based on the TR values. The ILP formulations and the proposed heuristic can choose different lightpaths with different transponders to satisfy the same

IP demand. The candidate path list stores the K=5 shortest paths (in km) for each demand. Over these paths, candidate lightpaths are subsequently computed for each candidate transponder.

Fig. 5.5 depicts the obtained results with the ILP formulations and heuristic in terms of spectrum occupation (in terms of FSs) for growing IP traffic load. The process stops when one $r_d: d \in \mathcal{D}$ cannot be completely fulfilled, and thus we assume that the network capacity limit is reached. Both ILP and heuristic results are presented with (w/) and without (w/o) spatial conversion (which is translated in whether applying SCC or not) in the two reference topologies aforementioned.

Results show that there is not significant difference between any of the settings analyzed for $|\mathcal{C}|$=7 and $|\mathcal{C}|$=12. The fact that the curves for 7 and 12 cores have almost the same slope means that the spectrum allocation is very similar with these two MCFs. However, for $|\mathcal{C}|$=19 more problems appear when trying to allocate the lightpaths due to the ICXT, that implies a TR reduction.

Besides, Fig. 5.5 shows an increasing slope changing close to the throughput limit, especially noticeable in the T7S network (Fig. 5.5.a and Fig. 5.5.c). This change in the spectrum occupation trend appears because both strategies mainly choose the shortest path to allocate the lightpath under low traffic loads. Nevertheless, as the network traffic increases, shortest paths may become fully occupied, being necessary to explore longer paths, therefore, transponders with less efficient modulation formats, thus increasing the spectrum occupation.

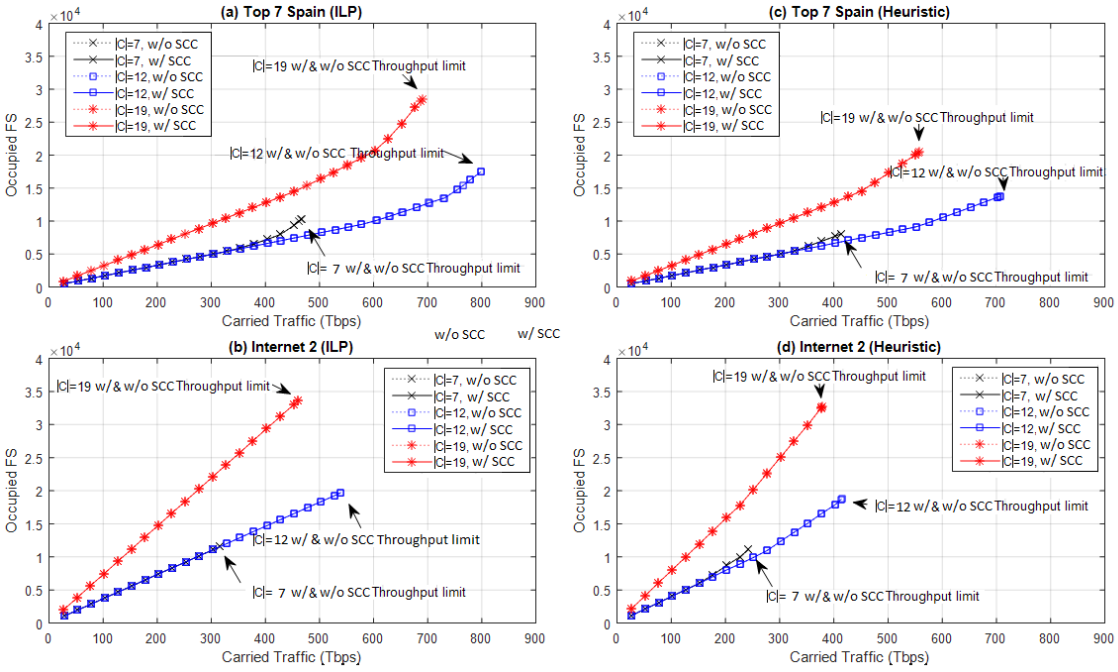

Fig. 5.5. Occupied FSs vs. throughput for: (a) Heuristic in T7S, (b) ILP in T7S, (c) Heuristic in I2 and (d) ILP in I2

It is important to note that results are very sensitive to the traffic matrix. Therefore, it would be inappropriate to get a general conclusion when comparing behaviors in different topologies.

Table 5.7 and Table 5.8 show the network throughput (maximum total carried traffic with zero blocking) when using the ILP/heuristic with and without spatial conversion (i.e., w/ and w/o SCC). The values for the ILP with spatial conversion are measured in Tb/s, while the rest of the values account for relative performance degradation against former ones. For instance, a value of -10.7% represents that using such an approach the network throughput is a 10.7% less than the analogous network (same core count) using SDM-ROADMs with spatial conversion and computed with an ILP.

Table 5.7: Maximum throughput in T7S network using ILP vs. Heuristic (in Tb/s)

	$\|\mathcal{C}\|$=7		$\|\mathcal{C}\|$=12		$\|\mathcal{C}\|$=19	
	w/ SCC	**w/o SCC**	**w/ SCC**	**w/o SCC**	**w/ SCC**	**w/o SCC**
ILP	460.0	0.0%	798.7	-0.1%	689.7	-0.5%
Heuristic	-10.7%	-10.7%	-11.4%	-11.6%	-19.2%	-19.5%

Table 5.8: Maximum throughput in Internet 2 network using ILP vs. Heuristic (in Tb/s)

	$\|\mathcal{C}\|$=7		$\|\mathcal{C}\|$=12		$\|\mathcal{C}\|$=19	
	w/ SCC	**w/o SCC**	**w/ SCC**	**w/o SCC**	**w/ SCC**	**w/o SCC**
ILP	315.6	-0.1%	539.6	-0.1%	460.3	-0.2%
Heuristic	-23.1%	-23.1%	-23.2%	-23.3%	-17.8%	-18.2%

Comparing the results of the ILPs against the ones obtained with the heuristic, ILPs naturally provide better performance although, as explained before, at an expense of a large computational complexity. For example, the heuristic can carry, at most, -19.53% in T7S and -23.3% in Internet 2 less traffic than its equivalent settings in the ILP. However, only a few seconds are needed to execute the algorithm instead of an hour for the ILP.

Comparing w/ and w/o SCC cases, differences in terms of maximum network throughput are minimal, only slightly noticeable as the number of cores grows, i.e., the spatial conversion option became more significant as $|\mathcal{C}|$ increases.

5.2.1.4.3 Spatial conversion impact analysis

The results of this subsection were obtained from simulations performed in an 8-core and 16 GB RAM computer. The heuristic algorithm has been tested in four reference topologies with different node degree and network diameter, namely, POL, GER, NSF and EON topologies (see Table 5.5). Two of these have a diameter less than 1000 km. Hence, they could be considered small networks. The other two have a diameter close to the largest TR of a transponder over 19-core MCFs, where the highest limitation is found.

In this part, incoming IP traffic demands are generated by a uniform random (0,1) distribution for each node pair. The rest of the assumptions are the same as those presented in previous subsection

5.2.1.4.1. Maximum network throughputs are shown in Fig. 5.6, obtained using the proposed heuristic in the four considered network topologies As expected, we can see that topologies with lower diameter can carry a larger amount of traffic with the same link capacity. Specifically, the larger the diameter of the network the lower the average spectrum efficiency due to TR limitations in MCFs. In addition, a slight difference can be noticed in those networks with a larger number of links. In fact, in networks with a similar diameter, more links facilitate finding available paths to solve the RTSSA problem. This is more visible in EON vs. NSF than in GER vs. POL topologies, but it is very dependent to the traffic matrix. There are not major differences (even inexistent) when comparing the network performance by deploying SDM-ROADMs with and without spatial conversion, as happened in the previous subsection. This highlights the profit-cost balance in favor of deploying such SDM-ROADMs in Flex-Grid/SDM networks.

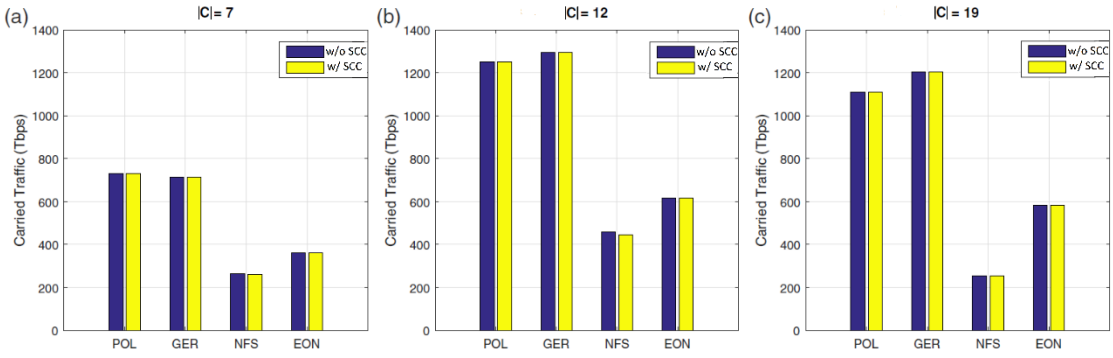

Fig. 5.6. Maximum carried traffic by heuristic algorithm for different topologies and core count: (a) 7, (b) 12 and (c) 19 cores.

To evaluate the performance of the heuristic in the different topologies, a *network economic efficiency* metric is presented as the ratio between the maximum network throughput in Tbps and the total number of cores in the network ($|\mathcal{C}| \times |\mathcal{E}|$). The role of this metric is capturing the trade-off between profit (network throughput) and cost (links and cores). Our interest is using it for comparing their values among different settings.

Economic efficiency helps us to evaluate the merits of each alternative. As an example, although the GER topology has a significantly higher throughput than POL, the economic efficiency in GER is clearly lower as it needs a much higher investment in number of links to achieve similar revenues. This effect is smoothed in NSF vs. EON for $|\mathcal{C}|$=7 and 12 because despite that the carried traffic in EON network is higher than in NSF one, the EON topology has many more links, so the balance between profit and cost is similar in both cases. However, in this last comparison, for $|\mathcal{C}|$=19 the trend is inverted, as in this case, the lack of options to carry traffic in long-haul paths for NSF is decisive in the network economic efficiency (in comparison with the EON value, for example).

Table 5.9 shows that in the $|\mathcal{C}|$=19 scenario, the *network economic efficiency* value drops in all the networks, but this does not happen in $|\mathcal{C}|$=7 and $|\mathcal{C}|$=12 cases. This is a direct consequence of the higher ICXT values, and therefore the TR reduction.

Table 5.9: Network economic efficiency

Topology	$\|\mathcal{C}\|$=7	$\|\mathcal{C}\|$=12	$\|\mathcal{C}\|$=19
POL	2.9	2.9	1.6
GER	0.6	0.6	0.4
NSF	0.9	0.9	0.3
EON	0.8	0.8	0.5

5.2.2 Network operation scenario

In previous subsection 5.2.1, we assessed in network planning scenarios a SDM-ROADM architecture without spatial conversion trading spatial channel switching for superior cost-efficiency. This architecture implements the SCC, i.e., it forces to employ the same spatial channel index along the end-to-end routing path. This SDM-ROADM is called "space-wavelength switching granularity without SDM lane change" in [50], [65]. Particularly, the obtained results presented in previous subsection 5.2.1 revealed minor network throughput reductions (up to 10% at most) in exchange of very important complexity reductions deploying this SDM-ROADM versus the SDM-ROADM with spatial conversion.

As a follow-up to previous subsection 5.2.1, in this subsection we consider two benchmark SDM-ROADM architectures, namely, SDM-ROADM with spatial conversion and JoS (introduced in chapter 2), to evaluate for the first time to the best of our knowledge, the impact of SDM-ROADM without spatial conversion in network operation (i.e., dynamic) scenarios. This is a crucial needed validation, since in dynamic scenarios spectrum fragmentation is an intrinsic issue [65] affecting the overall network performance of Flex-Grid/SDM networks, even if fragmentation-aware heuristics are considered [82], [97]. Previous works evaluate the performance of different architectures under network planning [56], [61], [88] and operation [57], [59] scenarios. Reference [57] states that the performance (in terms of blocking probability) of different SDM-ROADMs are influenced by the traffic profile. In addition to this, we aim to analyze the impact of the spatial multiplicity. For this purpose, we scale the spatial channel count from 7 to 30 (first SDM region to be explored [109]), considering not only crosstalk-free SDM fibers (like in all previous works [56], [57], [59], [61]), but also SDM fibers with the presence of ICXT, corresponding to MCF laboratory prototypes available in the literature [27]–[31]. We also account for Sb-Chs arranged over both the spectral domain (i.e., Spe-SCh) and over spatial domain (i.e.,

Spa-SCh). Finally, we contrast the performance (in terms of throughput) of different SDM-ROADMs versus their hardware requirements, especially at the bypass part.

The remainder of this subsection is structured as follows. Subsection 5.2.2.1 presents a heuristic mechanism for resource allocation considering SCC. Next, numerical results and subsequent discussion are presented in two subsections. Subsection 5.2.2.2 presents the impact of spatial conversion on the network performance under Spe- and Spa-SCh allocation, while subsection 5.2.2.3 presents the impact analysis of spatial conversion on network cost.

5.2.2.1 RMSSA heuristic

In this subsection, we present a greedy heuristic for solving the RMSSA problem associated to the allocation of an incoming Spe-SCh/Spa-SCh request in a Flex-Grid/SDM optical network, considering the SCC. The details of the heuristic are shown in Table 5.10.

For a given incoming demand d, the K=3 candidate Shortest Paths (SPs) are computed between its source (s_d) and destination (t_d) nodes, taking their physical length (z_p) as the metric. For each one of them, the MSE modulation format meeting the TR requirements is selected. Following the procedure, the necessary n_{fs} FSs is calculated according to equation (3.2). Obviously, $n_s = 1$ in the case of a Spe-SCh, while for Spa-SCh we compute it based on the PSA strategy presented in chapter 3. Next, for each spatial channel index (s_i) of the SDM fiber, the candidate path is tested for the allocation of the computed n_{fs} FSs in s_i along the routing path, fulfilling both the *spectrum continuity* and *contiguity* constraints of the Flex-Grid networks. If the path has enough spectral resources in at least n_s spatial channels, the demand is considered served. Otherwise, the next candidate path is explored until no more candidates are available (in such a case, the demand is considered blocked). Note that a FF strategy is used in the route, space and spectrum assignment, similar to approaches described in [55]. Our goal is to evaluate SDM-ROADMs without spatial conversion with a basic and lightweight resource allocation scheme, although other more advanced (out of the scope of this work), especially for spatial resource allocation can be explored, e.g., least congested routing path in order to balance the network load among the vast amount of spectral-spatial resources.

It is worth highlighting that, the RMSSA heuristic has been carefully designed providing, in average, execution times lower than 1 ms per demand in a large continental backbone network (e.g. in EON16 shown in Appendix A) with 30 spatial channels. That is, a lightweight heuristic has been designed, meaning that although the additional constraint introduced (SCC) for Flex-Grid/SDM networks, this does not suppose a substantial computational complexity increase.

Table 5.10: RMSSA heuristic without spatial conversion considering Spa-SCh and Spe-SCh

1: **Input:**
G=(|N|,|E|*) // Physical Network*
GB // Assumed guard-band per SCh
$d(s_d, t_d, r_d)$ *// Demand arriving at the network represented as a triplet*
n_s *// Number of spatial channels needed to build the SCh.*
2: **Begin:**
3: $P \leftarrow$Compute *K*=3 candidate SPs between s_d and t_d in *G*
4: *X* ←*false // binary flag to determine if d is blocked or accepted*
5: **For** each p in P **do**
6: Find the most efficient modulation format with TR $\geq z_p$ $[km]$
7: Compute $n_{fs} \leftarrow \left\lceil \frac{r_d/(n_s \cdot SE)+GB}{W} \right\rceil$
8: $n \leftarrow 0$ *// init value for the spatial channels counter*
9: $A \leftarrow \emptyset$ *// Set of feasible candidate spatial channels*
10 **For** each s_i of the SDM fiber **do**
11: **If** continuous and contiguous n_{fs} FSs are free in s_i along p **then**
12: $n \leftarrow n + 1$
13: $A \leftarrow A \cup \{s_i\}$
14: **If** $(n = n_s)$ **then** break
15: **end if**
16: **end for**
17: **If** $(n = n_s)$ **then**
18: Allocate the n_{fs} spectral resources in the |*A*| spatial channels
19: *X*←*true*, considering *d* as served
20: break
21: **end if**
22: **end for**
23: **If** *X* is false **then**
24: Consider d as blocked
25: **end if**
26: **End.**

5.2.2.2 Impact of spatial conversion on network performance

In order to evaluate the impact of spatial conversion on network performance (in terms of throughput) we have carried out several simulations. In particular, we consider demands arrive to the network following a Poisson distribution with given mean IAT and HT. The traffic is distributed uniformly between all pairs of source-destination nodes. Upon arrival, demands request for a bidirectional lightpath, with a bit-rate selected among two different traffic profiles: TP1={100, 400, 1000} Gb/s and TP2={400, 1000, 2000} Gb/s, with the same probabilities of {0.4, 0.3, 0.3}. Note that the average requested bit-rate per demand under TP1 is 460 Gb/s, while

under TP2 it raises to 1.06 Tb/s. That is, TP2 represents a 2.3x increase in size of the connections regarding TP1.

To obtain the numerical results, we have considered the continental EON16 and the national DT12 networks, whose main characteristics are shown in Appendix A. Each fiber/core is assumed to have 320 available FSs with W=12.5 GHz, while the GB width value has been set to 7.5 GHz, as recommended in chapter 3 and subsection 3.1.2. TR values presented in Table 3.2 and three degrees of flexibility in BVTs are considered, namely, modulation format, baud-rate (max. 32 GBaud) and Sb-Ch multiplicity, thus obtaining different operational line rates. In other words, a SCh transmits an aggregate bit-rate r_a according to equation (4.3).

5.2.2.2.1 Evaluation considering spectral super-channel allocation

In this subsection, we assess the impact of the spatial conversion on network throughput considering Spe-SCh allocation. To this end, results with and without SCC (i.e., network performance by deploying SDM-ROADMs with/without spatial conversion) are plotted in Fig. 5.7. There, the average network throughput for different spatial multiplicities is shown. Specifically, we scale S from 7 to 30 spatial channels including MF and the cases where there exists a MCF prototype. For MF-based solutions 1-spatial channel granularity is considered, while for MCF-based ones the five best single-mode MCF prototypes found in the literature are taken into account, i.e., $S \in \{7, 12, 19, 22, 30\}$ [27]–[31]. Different offered loads (L=HT/IAT) are simulated by fixing the IAT and incrementing the HT until we obtain a BBP close to 1% for each spatial multiplicity value. Therefore, the average network throughput (*Avg. Carried Traffic*) can be computed by averaging all instantaneous carried traffic after each connection is established along the entire simulation. To get statistically relevant results, we offer $5x10^5$ demand requests per execution. As in results presented in chapter 3 and subsection 3.1.4.2, this allows having relevant time of observation compared to the transient one (i.e., initial period before getting the steady state because of the Poisson process).

The results show that there are not major differences (<2%) in terms of throughput by considering the SCC in a national network like in the DT12 one. Conversely, in a continental network as the EON16, quite higher differences, up to 14%, are observed. The fact is that demands in larger networks may require more spectral resources (i.e., less efficient modulation formats are mandatory), hindering the SCh allocation since meeting the SCC gets more complicated. In the EON16 network, it is more clearly evidenced the impact of the spatial multiplicity, namely, the higher the spatial multiplicity S, the higher the spatial conversion impact in terms of throughput (i.e., curves w/ and w/o SCC are divergent), which was expectable due to the intrinsic SCC limitation in space channel assignment. Another finding that can be appreciated is the TP sensitivity in the DT12 network's throughput, carrying up to 14% more traffic for a 2.3x

(TP2/TP1) traffic profile increment (in terms of its average bit-rate per connection). Meanwhile, the TP sensitivity is almost unappreciated in EON16 network.

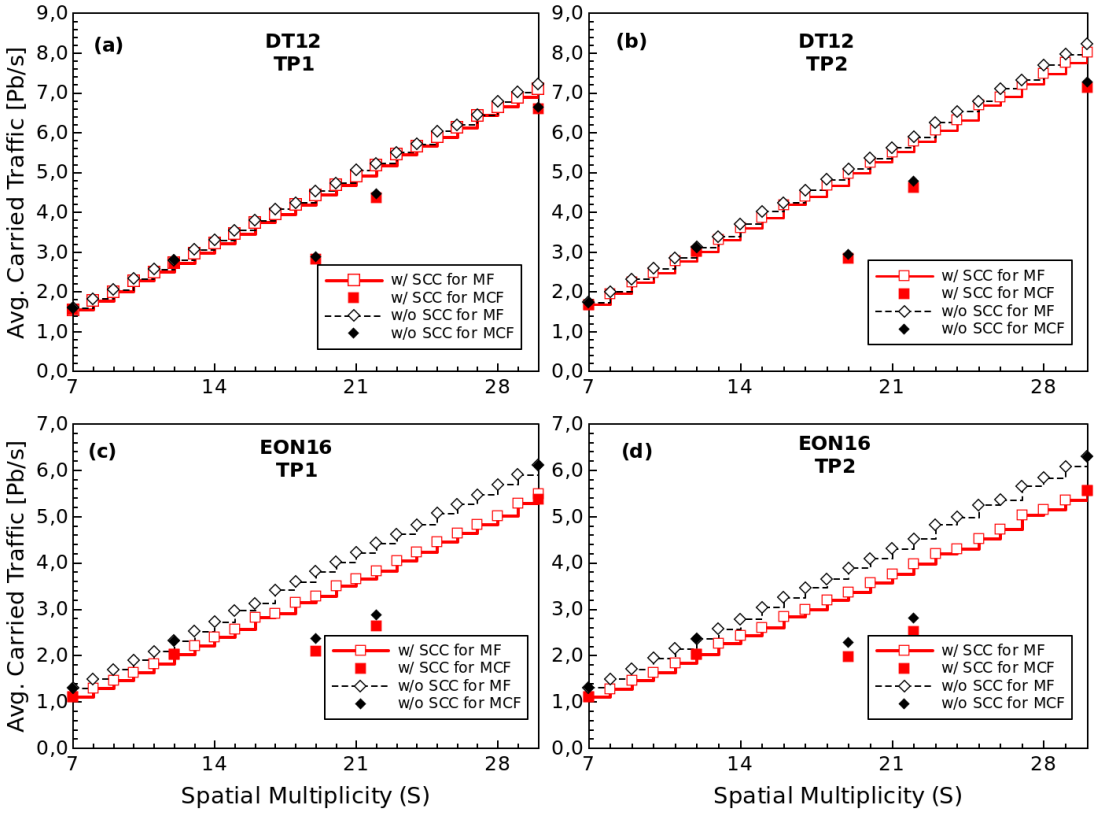

Fig. 5.7. Average Carried Traffic (in Pb/s) vs. spatial multiplicity with Spe-SChs in DT12 network under (a) TP1, (b) TP2, and in EON16 network under (c) TP1 and (d) TP2.

In particular, 7- , 12-core MCFs achieve the same performance as the equivalent MF solutions, since their extremely low ICXT does not become the TR limiting factor, being the OSNR instead as in the equivalent MF solutions. In its turn, 30-core MCF yields very close performance between MCF- and MF-based solutions because although the ICXT is the TR limiting factor, this is not so much different than the one imposed by the OSNR. However, 19- and 22-core MCFs perform noticeably worse than the equivalent MF solutions due to higher ICXT introduced. Between these two MCFs, the performance degradation of 19-core MCF is the most significant because it presents the highest ICXT level, resulting in a network throughput very close to that with 12-core MCF. Indeed, the differences between the 19-core MCF and the equivalent MF solution in terms of network throughput are up to 70% for DT12 and up to 50% for EON16 network (in the worst cases). The influence of the network diameter in the ICXT impact can be explained as follows. In larger networks, path lengths impose less efficient modulation formats by themselves. In addition, as the order of the modulation formats decreases, the TR margin between them increases. For example, according to Table 3.2 with a 22-core MCF, the TR margin between the 64-QAM and 16-QAM modulation format is 623 km (832-209 km), while between the 16-QAM and QPSK this margin increases to 2479 km (3311-832 km). The larger margins contribute to increasing the

number of connections that match the selected modulation format for either MF or MCF equivalent solutions.

On the other hand, Fig. 5.8 shows the impact of spatial conversion in terms of BBP for increasing traffic (i.e., increasing the offered load in Pb/s) under Spe-SCh allocation for some relevant scenarios. In particular, we consider the EON16 network (where ICXT effects are more relevant), S=12 and S=22 (some intermediate spatial multiplicities where there exists a MCF prototype) and the most stringent traffic profile TP2. According to the results, when Spe-SChs and MF-based solutions are considered, the penalties (in terms of BBP) considering SCC ranging from 0.2 to 2 orders of magnitude for an offered load interval yielding a BBP from 10^{-1} to 10^{-5}, respectively. As for MCF-based solutions, since ICXT of the 12-core MCF is not the limiting factor on the TR, its performance is identical to 12-MF equivalent solution, whereas for the 22-core MCF the penalties range from 0.2 to 1.3 orders of magnitude in terms of BBP. These results also show that, as stated before, the penalties with SCC is reduced when 22-core MCFs are considered.

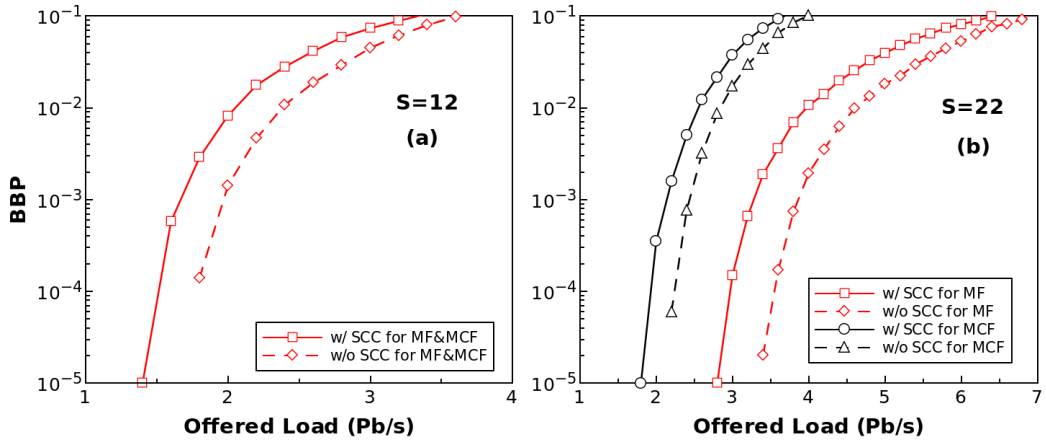

Fig. 5.8. BBP versus Offered Load (in Pb/s) for EON16 network and TP2 when Spe-SCh are allocated with (a) S=12, (b) S=22.

5.2.2.2.2 Evaluation considering spatial super-channel allocation

In turn, Fig. 5.9 shows the impact of the spatial conversion on network throughput considering Spa-SCh allocation. In this case, since Spa-SChs are also supported by JoS SDM-ROADMs (see Table 2.1), the performance results with *predefined* e2e-grooming of such SDM-ROADMs are also plotted in Fig. 5.9 as a benchmark scenario. Note that these "JoS" results are the lower bound of spatially fixed Flex-Grid/SDM networks where the SCC is implicit. As observed, regardless the SCC, an S increase does not always entail throughput increase. That is, the monotonically increasing behavior of throughput versus spatial multiplicity for Spe-SCh allocation is not evidenced when Spa-SChs are allocated. This is caused by two factors: (i) the spectral grid constraint. For example, for r_d = 400 Gb/s, S=7, GB=7.5 GHz and DP-16QAM the resulting n_{fs} is 2, and when S=8 the n_{fs} continues being equal to 2; and (ii) the spectral and spatial assignment

of Spa-SCh has a greedy behavior, i.e., for a given demand if an S increment yields lower spectral resources, this SCh configuration (n_{fs}, n_s) is preferred. It may happen that sometimes the unused spatial resources (left by the greedy spatial assignment policy of Spa-SChs) for a given spectrum portion cannot be used by other lightpaths, because they do not suitably fit into them unless they are accordingly divided in several chunks. These two aspects, the spectral grid constraint and the unused spectral-spatial resources, cause the step-like shape in the three throughput curves (i.e., non-monotonically increasing behavior) whether SCC is or not considered. We also observe that the impact of spatial conversion is practically inexistent (differences lower than 1% are reported between w/ SCC and w/o SCC curves) in both MF and MCF scenarios. Finally, the before stated greedy behavior (in spectral-spatial resources assignment) of Spa-SCh as S increases, causes not only that some points do not yield any throughput increment, but also a throughput drop. Hence, for Spa-SCh allocation, it seems that in some cases it may be convenient to explore MC-based Spa-SChs (see Fig. 3.1.b), i.e., Spa-SChs with higher n_{fs} instead of preferring Spa-SChs with large n_s, although not considered in this work.

The results with Spa-SCh allocation, as the ones with Spe-SChs, also evidence TP sensitivity. As demonstrated in [57], [59], [61], the network performance with different SDM-ROADMs is influenced by the size and diversity of connections. Indeed, according to [57] when large connections are considered the performance of three SDM-ROADMs (InS without LC support, FJoS, JoS introduced in chapter 2) are practically equal. The argument seems to be somewhat obvious, with large demands the unallocated spectral-spatial resources are not able to be assigned regardless SDM-ROADM architecture. Similar to results in [57], we have also found that, for low spatial channel count (see e.g., Fig. 5.9.d and S=12) and large demands, the performance (in terms of blocking probability for [57] or in terms of throughput for this work) of two SDM-ROADMs without spatial conversion and JoS is almost identical. As a contribution of this work, we show that the network performance deploying SDM-ROADMs with spatial conversion (in spite of its flexibility) could also become identical to the one offered by the former architectures. Nevertheless, according to our results, for higher spatial channel count (e.g., S= 18 in Fig. 5.9.d) –upgrade necessary e.g., due to the increment of the offered connections– this similarity in outcomes is not evidenced. In fact, the performance of SDM-ROADMs with/without spatial conversion for SS-FONs in dynamic scenarios outperforms (up to 40%) the one of JoS for spatially fixed Flex-Grid/SDM networks even enhancing its performance by applying *predefined* e2e-grooming, as result of flexibility provided by the former architectures. Then, the results from Fig. 5.7 and Fig. 5.9 reveal that the performance of SDM-ROADMs depends on both the traffic profile and the spatial multiplicity under Spe-SCh and Spa-SCh allocation.

Specifically for MCF cases, as in previous subsection, 19- and 22-core MCFs report significant differences versus the MF equivalent solutions. Focusing on the 19-core MCF, i.e., the one with

the highest ICXT, differences in terms of network throughput of up to 58% are observed in both networks, DT12 and EON16, compared to the equivalent MF solution. In the EON16 network, the throughput gain of the 19-core MCF versus the 12-core one is in the best cases up to ~22% and ~13% for TP1 and TP2, respectively, while for DT12 network is up to ~5% and ~2%. That is, these results also evidence TP sensitivity. The higher the traffic demands, the higher the number of spatial channels that can be assigned to Spa-SChs, reducing the possibility that spatial and spectral resources are left unused (wasted). Consequently, the highest TP (i.e., the TP2 one) improves the network resources usage and evidences a ~16% of network throughput increment regarding TP1 in EON16 for S = 30, while for DT12 up to ~42% network throughput increment is evidenced scaling the traffic profile from TP1 to TP2. It is important to highlight in Fig. 5.9.d the network performance for the 19- and 22-core MCFs (the ones with the highest ICXT). As observed, when these MCFs are considered in long-haul (in terms of physical distance) and large (in terms of bit-rate) communications under Spa-SChs, the ICXT dominates over the SDM-ROADM architecture. That is, whereas for MF-based solutions the network performance by deploying SDM-ROADMs with/without spatial conversion outperform the one with JoS SDM-ROADMs, for MCF-based solutions the network performance by deploying the three SDM-ROADMs are very similar. This happens because unused spectral-spatial resources per SCh cannot be assigned to other traffic demands, regardless of what switching strategy is considered.

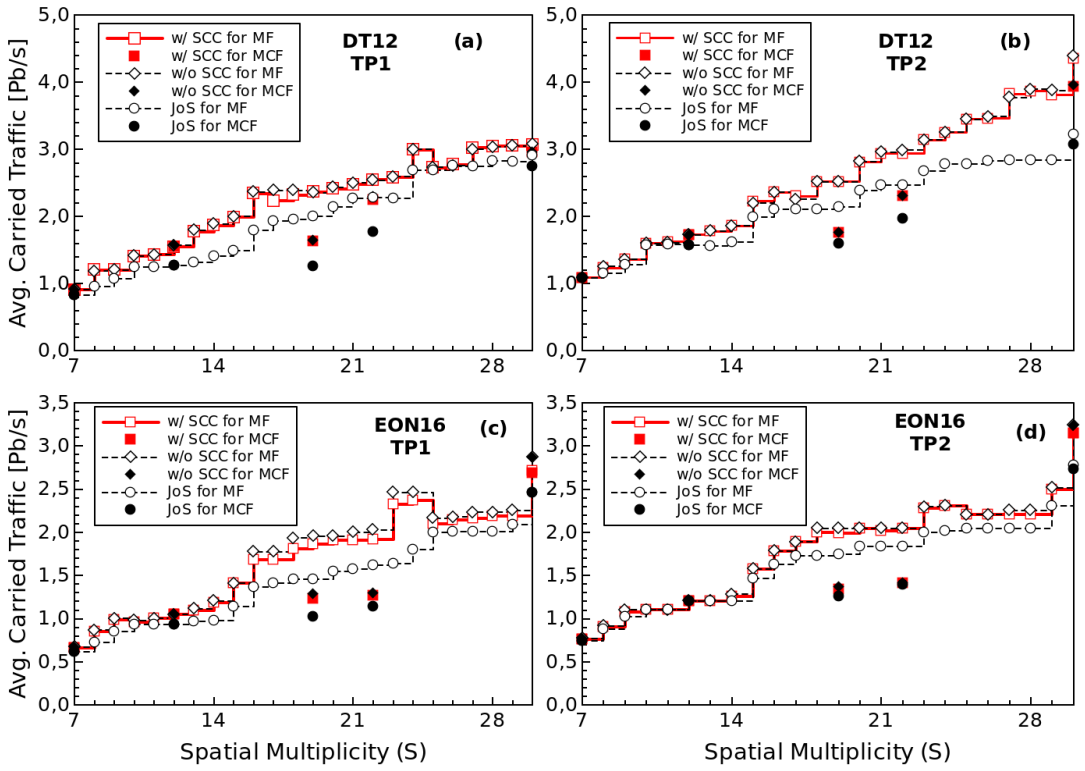

Fig. 5.9. Average Carried Traffic (in Pb/s) vs. spatial multiplicity when supporting Spa-SChs in DT12 network under (a) TP1, (b) TP2, and in EON16 network under (c) TP1 and (d) TP2.

Fig. 5.10 shows the impact of spatial conversion in terms of BBP for increasing traffic (i.e., increasing the offered load in Pb/s) under Spa-SCh allocation for the same cases considered in Fig. 5.8. As observed, the penalties of SCC is practically non-existent (i.e., no impact of spatial conversion). Finally, contrasting the results shown in Fig. 5.8 versus the ones shown in Fig. 5.10, we can clearly appreciate the differences in the offered load between Spe- and Spa-SChs. For instance, for a maximum 10% BBP, networks allocating Spe-SChs can support up to 2x more offered load than when they allocate Spa-SChs, due to spectrum savings of GBs and potential fragmentation caused by unused spectral-spatial resources, where Spa-SChs have not been able to be accommodated.

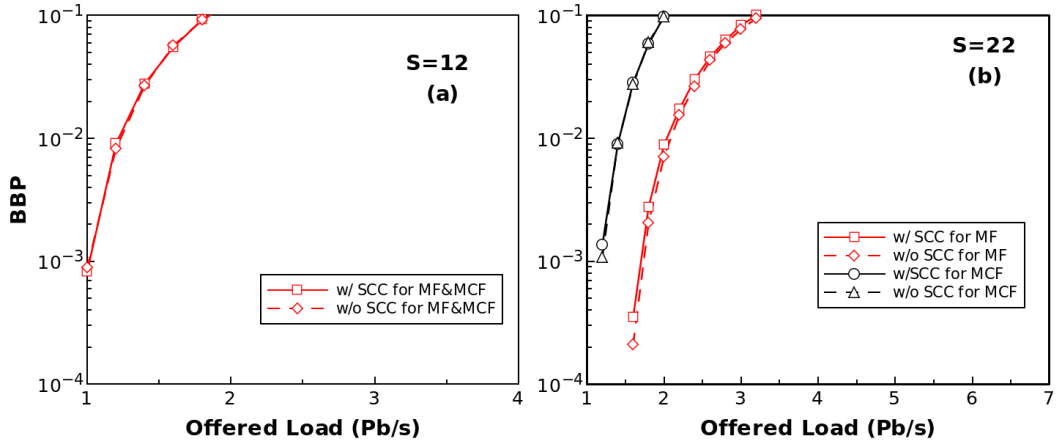

Fig. 5.10. BBP versus Offered Load (in Pb/s) for EON16 network and TP2 when Spa-SCh are allocated with (a) S=12, (b) S=22.

5.2.2.3 Impact of spatial conversion on network cost

In this subsection, we analyze the impact of spatial conversion on network cost, specifically in the bypass part of different SDM-ROADM designs in order to give insight into the trade-off between network throughput and hardware cost. This cost analysis does not intend to be exhaustive because there are other important costs to be considered, e.g., the BVTs cost (the major network equipment cost in SDM networks [58]). To this end, the cost model presented in [60] regarding the SSSs and summarized in Table 5.11 is taken into account. The last row for 1x320 SSS has been extrapolated according to the port doubling and 58% premium cost criterion considered also in [60].

In this analysis, we consider both SDM-ROAMs presented in subsection 5.1, namely, with and without spatial conversion, and we include as a benchmark scenario the JoS SDM-ROADM. This latter SDM-ROADM, as shown in Fig. 2.7, is based on the R&S scheme because of the high splitting ratio it needs. In fact, if B&S scheme would have been applied to JoS SDM-ROADM, an integrated SDM power splitters would be necessary to be developed like the prototype $1 \cdot 7{:}2 \cdot 7$ MCF splitter presented in [131]; otherwise individual power splitters per spatial channel should

be placed (increasing the complexity and cost). For this reason, we also take into account the R&S scheme for the rest of SDM-ROADMs for fair comparison purposes. First, for the two topologies DT12 and EON16, we quantify the number of SSSs per node and their required size, based on the previously presented Table 2.1 and Table 5.11, in order to obtain the node-wide cost. Then, the total network-wide cost (i.e., the sum of all costs per node) is computed and its results are shown in Table 5.12 for 7/19/30 spatial channels (as example cases) in the both reference topologies. This results show that the most expensive solution (considering the bypass part of the ROADMs) is the SDM-ROADM with spatial conversion, followed by the SDM-ROADM without spatial conversion, while the cheapest one appears to be the JoS SDM-ROADM solution. We determine that the SDM-ROADM with spatial conversion solution is more and more expensive as the spatial channel count increases. Thus, for S=7, it can be up to 2.9-fold and 2.5-fold more expensive for DT12 and EON16 networks, respectively, while for S=30 these difference raise up to 7.1-fold and 6.3-fold. Similarly, the SDM-ROADM without spatial conversion solution is more and more expensive than the JoS one as S increases. Cost increments up to 1.6-fold and 2-fold are reported for S=7 in DT12 and EON16 networks, respectively, while for S=30 these differences raise up to around 3-fold for both networks.

Table 5.11. Normalized Cost per SSS [60]

SSS Size	Normalized Cost
1x5	0.63
1x9	1
1x20	1.58
1x40	2.50
1x80	3.95
1x160	6.25
1x320	9.87

In conclusion, the cost of the bypass part in SDM-ROADMs without spatial conversion is reduced to a large extent compared to the one with spatial conversion support, while the throughput capabilities remain very similar, with differences up to 14% when Spe-SChs are allocated in large continental networks. Moreover, when Spa-SChs are allocated, it is necessary to validate if the throughput gains obtained by deploying SDM-ROADMs without spatial conversion versus the solution with JoS SDM-ROADMs justify the extra cost of the network nodes. For instance in Fig. 5.9.b, when S=30 a throughput gain of 40% should be analysed in detail to determine if a 3-fold factor network cost increment with the SDM-ROADM without spatial conversion is justified; otherwise, for these scenarios the JoS SDM-ROADM solution could become the best option, as it is for $S \in [7,12]$ interval in the same Fig. 5.9.b. In addition, it is worth mentioning that, Spa-SChs against Spe-SChs can reduce the cost of the BVTs, resulting from the absence of frequency combs or AWGs, the use of common laser sources and joint digital signal processing at the

receivers, as we mentioned in chapter 2. According to [58], this reduction can be around 5-20% for Spa-SChs with 2-10 Sb-Chs.

Table 5.12. Network-wide cost

SDM-ROADM	**Network-wide cost** (arbitrary units) for S=7/19/30	
	DT12	**EON16**
w/o spatial conversion	106/287/454	141/383/604
w/ spatial conversion	301/1325/3222	352/1511/3771
JoS	66/113/165	71/140/200

5.3 Conclusions

In this chapter, we exhaustively evaluate the impact of the spatial conversion on network performance and cost under planning and operation scenarios. To this end, we use different network topologies, traffic profiles and SDM fiber types (with crosstalk and crosstalk-free).

For planning scenarios, RTSSA ILPs and lightweight LS-based heuristic with good accuracy have been presented. Results have revealed three main conclusions: (i) A minimal penalty in terms of throughput by restricting the spatial conversion at network nodes was found. Specifically, less than 1% penalties were observed when spatial conversion is not supported against nodes with spatial conversion. This places such SDM-ROADMs without spatial conversion, as a favorable cost-performance alternative for Flex-Grid/SDM networks. (ii) The effect of the introduced ICXT in MCFs can be relevant, as the case of 19-core MCF considered in this thesis, especially in networks with a diameter similar to its TR (iii) The network economic efficiency study shows that 7 and 12-core MCFs present a good compromise for scaling the network capacity of future transport networks.

Regarding operation scenarios, we have analyzed the impact of spatial conversion by considering the allocation of Spe- and Spa-SChs. For this purpose, we have also proposed a RMSSA heuristic with execution times in the order of the ms. In particular, throughput penalties between 0% (the minimum obtained when Spa-SChs are allocated) and 14% (the maximum obtained when Spe-SChs are allocated) have been reported when spatial conversion is not supported at SDM-ROADMs. In contrast, SDM-ROADMs without spatial conversion allows carrying up to 40% extra throughput than the JoS SDM-ROADMs. However, we have found that the network performance (as stated in [57]) is not only influenced by the traffic profile, but also by the spatial multiplicity, thus extending its dependency on both parameters allocating either Spe-SChs or Spa-SChs.

It is worth highlighting that ICXT does not contribute to performance degradation when SCC is considered and the results obtained in network operation scenarios are in the order of the ones obtained in planning scenarios. This fact supports, even more, the adoptation of SDM-ROADMs without spatial conversion at expenses of careful analysis of the cost-performance trade-off with JoS SDM-ROADMs, which report the lowest network cost from the bypass point of view. In fact, according to our analysis, we have shown that SDM-ROADMs without spatial conversion becomes a cheaper solution than those SDM-ROADM with spatial conversion support, reducing the network cost down to 86% with minimum throughput penalties (as stated before). In contrast, they can be up to 3-fold more expensive than the JoS SDM-ROADMs. Finally, we have found that the cost of SDM-ROADMs is also influenced by the spatial multiplicity. For instance, the cost of SDM-ROADMs with spatial conversion is from 2.5-fold to 7.1-fold higher than the ones without spatial conversion for a same 4.3-fold spatial multiplicity increase.

Chapter 6

6 Final Discussion and Future Work

This PhD thesis has addressed various strategies for the network planning and operation of high capacity optical networks driven by SDM. Specifically, two SDM fiber types have been considered, namely, bundle of SMFs and weakly-coupled MCFs. The main contributions of this thesis are per chapter summarized as follows:

- Chapter 3 presented a TR estimation method for both bundle of SMFs and MCFs considering the minimum transmission distance between inter- and intra-core impairments, leveraging the well-known GN-model for uncompensated coherent transmission links. Besides, allocation strategies, restrictions, requirements and capacity of spatially fixed Flex-Grid/SDM networks were largely investigated. These aspects led to study, thereby, the characteristics for the configuration of Spa-SChs. Based on the results of Spa-SChs' GBs impact on network performance, we proposed a GB width representing an affordable compromise between hardware and network performance. Moreover, we proposed a methodology called PSA strategy to configure Spa-SChs, as a cost-effective solution when flexible baud-rate per OC is considered. Indeed, it allows to save transceivers (therefore, CapEx) without affecting the network performance regarding the straightforward FSA strategy to be applied. The capacity of spatially fixed Flex-Grid/SDM networks is affected by (i) Spa-SCh configuration and (ii) switching strategy. The first aspect is related with the overhead caused by GBs and the second one with the reservation of a spectrum portion over a rigid number of spatial channels. Both aspects caused that spatially fixed Flex-Grid/SDM networks do not have a strict correspondence between spatial multiplicity and capacity scalability. To counteract this issue, a *dynamic* e2e-grooming strategy was proposed in order to reuse some lightpaths during provisioning, thus increasing the network throughput. In this chapter, we considered various weakly-coupled MCF prototypes available in the literature. Some of them have revealed that, although they present low ICXT, this one limits the TR causing some significant penalties in the network performance versus a crosstalk-free SDM solution depending on the network size. Therefore, in this chapter we proposed a strategy to cancel the negative effects of ICXT by applying MIMO-DSP to the least amount of Spa-SChs, thus saving cost and computational complexity. For this purpose, MIMO assignment sub-problem has been incorporated into RMSA problem by means of ILP and metaheuristic, thus giving rise to a joint RMMSA problem applied to spatially fixed Flex-Grid/SDM optical networks.

- Chapter 4 largely studied allocation strategies, requirements and capacity of SS-FONs. Taking into account flexibility in both spectral and spatial domains for configuring SChs, this chapter proposed a novel methodology called WSSA in order to explore different SCh allocation options ranging from the one with the shortest to the one with the largest spatial resources. Each specific SCh configuration has a trade-off between network performance and hardware complexity especially from BVTs point of view. As a contribution of this methodology, it was demonstrated that the optimal setting of an input parameter in the WSSA method yields a maximum throughput with relaxed hardware requirements. This optimal setting is not always related to the pure Spe-SCh allocation (the solution with the best-expected results), but rather it might comprise a mix allocation of Spe-SCh with SC/MC Spa-SChs. Significant cost reductions can be provided by adapting such input parameter of the WSSA method, taking into account the trade-off with the correspondent network capacity. Regarding this latter aspect, in SS-FONs the spatial multiplicity factor and throughput increment have a more strict correspondence than the one obtained in spatially fixed Flex-Grid/SDM, but at expenses of a more complex switching scheme implemented at SDM-ROADMs supporting space and wavelength switching granularity. Nevertheless, the network capacity scalability driven by spatial multiplicity in SS-FONs strongly depends on SCh configuration. This chapter and the previous one have demonstrated the feasibility implementation of weakly-coupled MCFs in long-haul transport networks given their extremely low ICXT, knowing also that prototypes are each time improved in the laboratory with techniques aimed at reducing ICXT as much as required in layouts with moderate core counts.
- Chapter 5 largely studied the impact of spatial conversion at SDM-ROADMs on the network performance and cost. For this purpose, this chapter proposed ILP formulations and lightweight heuristic to solve RTSSA problem with and without spatial conversion. The major contribution of this chapter is that it was demonstrated that performance penalties without spatial conversion are minimal regarding scenarios where it is allowed under both planning and operation scenarios, and when both Spe- and Spa-SChs are allocated. Moreover, it was found that the restriction of the spatial conversion is the cheapest switching solution at SDM-ROADMs for SS-FONs. In contrast, it is more expensive than the JoS strategy used in spatially fixed Flex-Grid/SDM networks. Again, an important outcome is that the trade-off between hardware complexity (therefore, cost) and performance has to be analyzed in detail in order to propose an overall solution, even more since it was demonstrated that the two parameters strongly depend on spatial multiplicity, while the network performance on the traffic profile as well. In any case, contrasting the network performance with (the best-expected performance under SDM-ROADM with the highest flexibility) versus without spatial conversion, this chapter demonstrated that such SDM-ROADMs without spatial

conversion are a promising solution with good cost-benefit relationship. Finally, when weakly-coupled MCFs are considered, their low ICXT does not contribute to performance degradation when spatial conversion is not allowed.

Future works can be addressed by following some research lines stated in this thesis. Specifically, regarding spatially fixed Flex-Grid/SDM networks planning scenarios can be studied for determining the capacity aware of other input parameters like the number of client interfaces in the A/D modules of SDM-ROADMs, transceiver-constrained BVTs, e2e-grooming, etc.. In addition, the non-monotonically increasing behavior of network throughput with the spatial multiplicity can be analyzed in greater detail in order to determine if there exist mechanisms to change this tendency. As for SS-FONs, it is also pending to evaluate their scalability in network planning scenarios. Moreover, dynamic SCh configurations for each traffic demand can be explored aimed at deepening in the optimal SCh configuration in terms of assigned spectral and spatial resources yielding reasonable cost-performance trade-offs. Concerning SDM-ROADMs, internal losses can be analyzed in a further TR model. Moreover, enhanced TR models can consider (i) online computation, i.e., at moment of establishing lightpaths aware of the network and lightpaths status; (ii) a unified GN-model considering ICXT, as an additional Gaussian noise source, interesting to be developed and tested. Additionally, future cost models of SDM networks can consider more network elements, like A/D SDM-ROADM modules, SDM amplifiers, BVTs, etc..

Finally, the RA stratagies proposed in this thesis can be tested/extended in an SDN-based controller taking into account that there are several programmable parameters in Flex-Grid as well as in SDM networks. In addition, other SDM fiber types can be also evaluated in order to explore the DSDM region, e.g., by means of FM-MCFs. Indeed, leveraged in the research internship realized in the *Centre Tecnològic Telecomunicacions Catalunya* (CTTC), first results with this fiber type have been obtained and they are in the process to be published.

Appendix A

A Reference transport networks

Different RA strategies tested throughout this PhD thesis has been carried out by using various well-known reference transport networks in the research community. Specifically, different national and continental backbone networks have been considered and they are shown from Fig. A.1 to Fig. A.6. The main characteristics of these networks are detailed in Table A.1. There, networks appear ordered by the network diameter (i.e., the longest shortest path between any pair of nodes). Other characteristics are the number of nodes ($|\mathcal{N}|$), the number of unidirectional links ($|\mathcal{E}|$), the average link length in km, the nodal degree and the network connectivity obtained by *natural connectivity* definition presented in [119].

Table A.1: Main characteristics of reference backbone networks

Network ($\|\mathcal{N}\|, \|\mathcal{E}\|$)	**Avg. Link Length [km]**	**Network diameter [km]**	***D*** **Min/Avg/Max**	**Network connectivity**
DT (12, 40)	243	1,019	2/3.33/5	4.99
TEST1 (6, 16)	460	1,160	2/2.67/3	3.60
EON (16, 46)	486	2,663	2/2.88/5	4.41
US (26, 84)	469	3,660	2/3.23/4	4.75
TEST2 (9, 26)	1,063	4,116	2/2.88/4	4.11
NSF (15, 46)	1,022	4,688	2/2.88/4	4.60

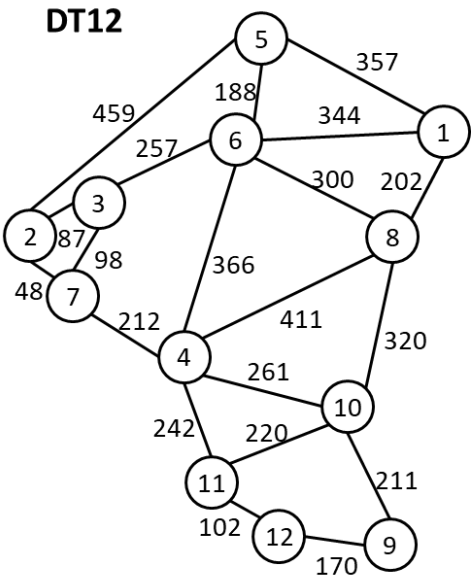

Fig. A.1. Deutsche Telekom National backbone network (DT12)

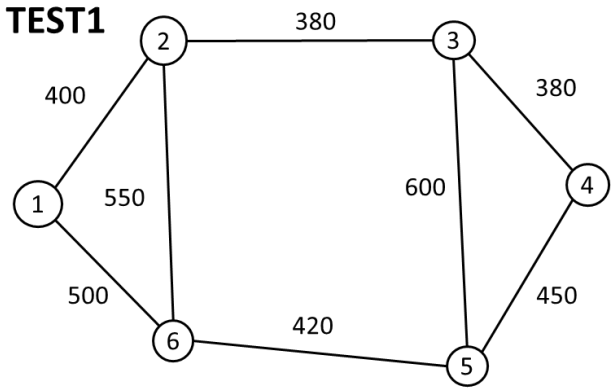

Fig. A.2. TEST1 optical backbone network

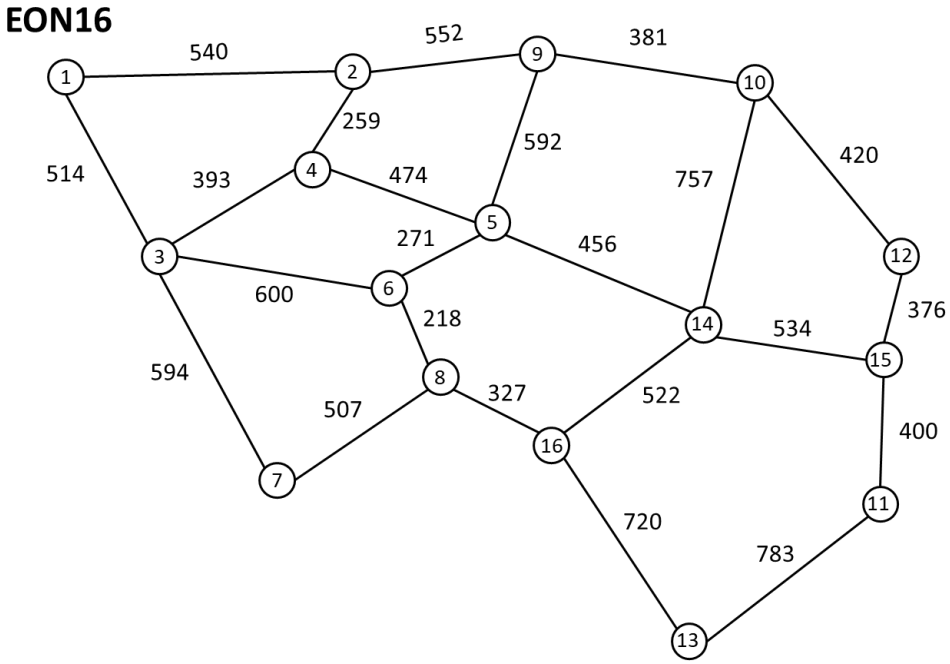

Fig. A.3. Continental European Optical Backbone Network (EON16)

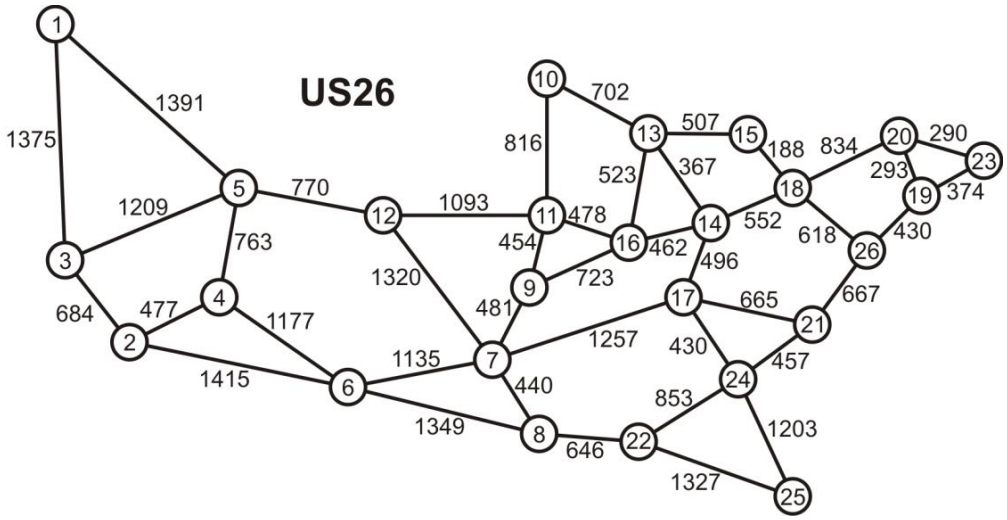

Fig. A.4. Continental US optical backbone network (US26)

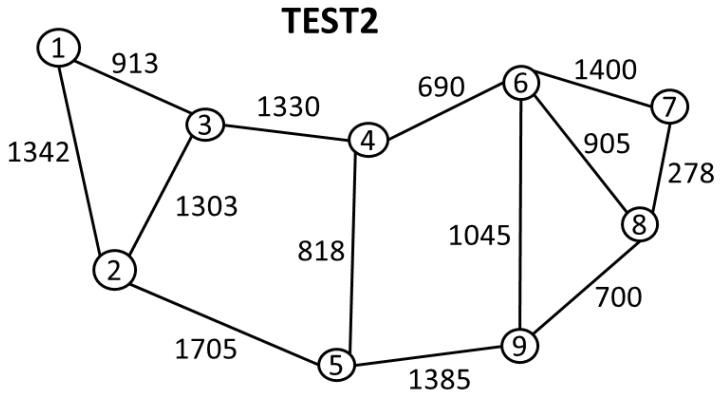

Fig. A.5. TEST2 optical backbone network

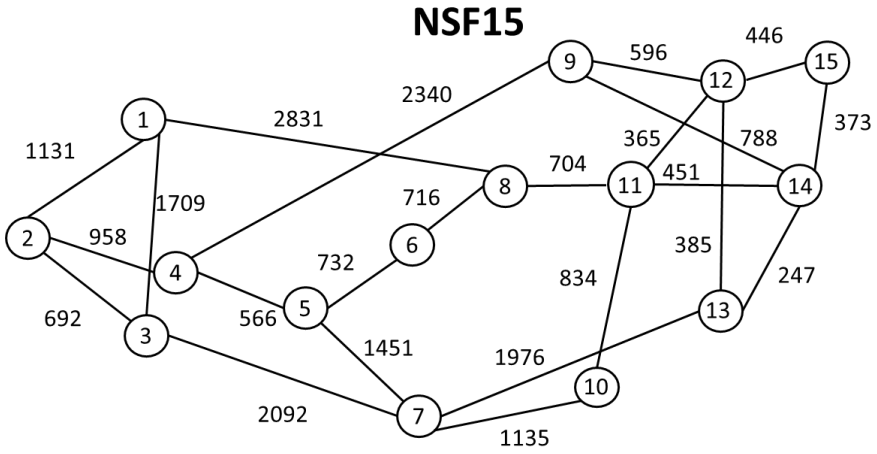

Fig. A.6. Continental National Science Foundation optical backbone network (NSF15)

Appendix B

B Publication List

B.1 Publications in Journals

1. **R. Rumipamba-Zambrano**, J. Perelló, J. M. Gené, and S. Spadaro, "On the scalability of dynamic Flex-Grid/SDM optical core networks," *Computer Networks*, vol. 142, pp. 208–222, Sept. 2018. JCR (2017): 2.522, Q1.
2. **R. Rumipamba-Zambrano**, F.-J. Moreno-Muro, J. Perelló, P. Pavón-Mariño, and S. Spadaro, "Space continuity constraint in dynamic Flex-Grid/SDM optical core networks: An evaluation with spatial and spectral super-channels," *Computer Communications*, vol. 126, pp. 38–49, Aug. 2018. JCR (2017): 2.613, Q2.
3. **R. Rumipamba-Zambrano**, J. Perelló, and S. Spadaro, "Route, Modulation Format, MIMO and Spectrum Assignment in Flex-Grid/MCF Transparent Optical Core Networks," *Journal of Lightwave Technologies*, vol. 36, no. 16, pp. 3534–3546, Aug. 2018. JCR (2017): 3.652, Q1.
4. **R. Rumipamba-Zambrano**, J. Perelló, J. M. Gené, and S. Spadaro, "Cost-effective spatial super-channel allocation in Flex-Grid/MCF optical core networks," *Optical Switching and Networking*, vol. 27, pp. 93–101, Jan. 2018. JCR (2017): 1.113, Q3.
5. F.-J. Moreno-Muro, **R. Rumipamba-Zambrano**, P. Pavón-Mariño, J. Perelló, J. M. Gené, and S. Spadaro, "Evaluation of Core-Continuity-Constrained ROADMs for Flex-Grid/MCF Optical Networks," *Journal of Optical Communication Networking*, vol. 9, no. 11, p. 1041, Nov. 2017. JCR (2017): 2.742, Q1.

B.2 Publications in Conferences

1. P. Lechowicz, **R. Rumipamba-Zambrano**, J. Perelló, S. Spadaro, and K. Walkowiak, "Inter-Core Crosstalk Impact on Migration Planning from Elastic Optical Networks to Spectrally-Spatially Flexible Optical Networks," in *Proceedings of Optical Fiber Communications Conference and Exhibition (OFC 2019)*, San Diego (USA), March 2019.
2. **R. Rumipamba-Zambrano**, J. Perelló, and S. Spadaro, "Dynamic Traffic Grooming in Joint Switching (JoS)-enabled Flex-Grid/SDM Optical Core Networks," in *Proceedings of European Conference on Optical Communication* (*ECOC 2018*), Rome (Italy), September 2018.

3. P. Lechowicz, **R. Rumipamba-Zambrano**, J. Perelló, S. Spadaro, and K. Walkowiak, "Migration Planning from Elastic Optical Networks to Spectrally-Spatially Flexible Optical Networks," in *Proceedings of Photonics in Switching and Computing (PSC 2018)*, Limassol (Cyprus), September 2018.
4. **R. Rumipamba-Zambrano**, F.-J. Moreno-Muro, P. Pavon-Marino, J. Perelló, S. Spadaro, and J. Sole-Pareta, "Assessment of Flex-Grid/MCF Optical Networks with ROADM limited core switching capability," in *Proceedings of 21st International Conference on Optical Network Design and Modeling (ONDM 2017)*, Budapest (Hungary), May 2017.
5. **R. Rumipamba-Zambrano**, J. Perelló, J. M. Gené, and S. Spadaro, "Capacity quantification of joint-switching-enabled Flex-grid/SDM optical backbone networks," in *Proceedings of Optical Fiber Communications Conference and Exhibition (OFC 2017)*, Los Angeles (USA), March 2017.
6. **R. Rumipamba-Zambrano**, J. Perelló, A. Pagès, J. M. Gené, and S. Spadaro, "Influence of the spatial super channel guard-band width on the performance of dynamic Flex-Grid/SDM optical Core networks," in *Proceedings of International Conference on Transparent Optical Networks (ICTON 2016)*, Trento (Italy), July 2016.

Bibliography

[1] D. J. Richardson, J. M. Fini, and L. E. Nelson, “Space Division Multiplexing in Optical Fibres,” *Nat. Photonics*, vol. 7, pp. 354–362, 2013.

[2] G. Ellbrock and J. X. Tiejun, “The Road to 100G Deployment,” *IEEE Commun. Mag.*, vol. 48, no. 3, pp. S14–S18, 2010.

[3] X. Yangzhang, V. Aref, S. T. Le, H. Buelow, and P. Bayvel, “400 Gbps Dual-polarisation Non-linear Frequency-division Multiplexed Transmission with b-Modulation,” in *ECOC - European Conference and Exhibition on Optical Communication*, 2018, no. 2, pp. 1–3.

[4] M. Jinno, H. Takara, B. Kozicki, Y. Tsukishima, Y. Sone, and S. Matsuoka, “Spectrum-efficient and scalable elastic optical path network: architecture, benefits, and enabling technologies,” *IEEE Commun. Mag.*, vol. 47, no. 11, pp. 66–73, Nov. 2009.

[5] O. Gerstel, M. Jinno, A. Lord, and S. J. Ben Yoo, “Elastic optical networking: A new dawn for the optical layer?,” *IEEE Commun. Mag.*, vol. 50, no. 2, pp. 12–20, 2012.

[6] P. J. Winzer, “Making spatial multiplexing a reality,” *Nat. Photonics*, vol. 8, no. 5, pp. 345–348, Apr. 2014.

[7] A. R. Chraplyvy, “Plenary paper: The coming capacity crunch,” *2009 35th Eur. Conf. Opt. Commun.*, p. 8007, 2009.

[8] P. J. Winzer, “Optical Networking Beyond WDM,” *IEEE Photonics J.*, vol. 4, no. 2, pp. 647–651, 2012.

[9] H. Takara *et al.*, “1.01-Pb/s (12 SDM/222 WDM/456 Gb/s) Crosstalk-managed Transmission with 91.4-b/s/Hz Aggregate Spectral Efficiency,” *Eur. Conf. Opt. Commun.*, 2012.

[10] I. Tomkos, B. Shariati, J. M. Rivas-Moscoso, D. M. Marom, and D. Klonidis, “New frontiers in optical communication networking,” *2017 19th Int. Conf. Transparent Opt. Networks*, no. July, pp. 1–2, 2017.

[11] P. Pavon-Marino and J.-L. Izquierdo-Zaragoza, “Net2Plan : An open-source network planning tool for bridging the gap between academia and industry,” in *Optical Network Design and Modelling*, 2014, no. October, pp. 90–96.

[12] International Telecommunication Union - ITU-T, “G.694.1 (02/2012), Spectral grids for WDM applications: DWDM frequency grid,” *Ser. G.694.1*, pp. 1–16, 2012.

[13] M. Dallaglio, N. Sambo, F. Cugini, and P. Castoldi, “Control and Management of

Transponders With NETCONF and YANG," *J. Opt. Commun. Netw.*, vol. 9, no. 3, p. B43, Mar. 2017.

[14] N. Sambo, A. Giorgetti, F. Cugini, and P. Castoldi, "Sliceable transponders: pre-programmed OAM, control, and management," *J. Light. Technol.*, vol. 8724, no. c, pp. 1–1, 2017.

[15] M. Svaluto Moreolo *et al.*, "SDN-Enabled Sliceable BVT Based on Multicarrier Technology for Multiflow Rate/Distance and Grid Adaptation," *J. Light. Technol.*, vol. 34, no. 6, pp. 1516–1522, 2016.

[16] O. G. De Dios *et al.*, "Experimental demonstration of multivendor and multidomain EON with data and control interoperability over a Pan-European test bed," *J. Light. Technol.*, vol. 34, no. 7, pp. 1610–1617, 2016.

[17] P. J. Winzer, "High-spectral-efficiency optical modulation formats," *J. Light. Technol.*, vol. 30, no. 24, pp. 3824–3835, Dec. 2012.

[18] P. J. Winzer, "Spatial Multiplexing : The Next Frontier in Network Capacity Scaling," *Eur. Conf. Exhib. Opt. Commun.*, p. We.1.D.1, 2013.

[19] P. J. Winzer, "Energy-Efficient Optical Transport Capacity Scaling Trough Spatial Multiplexing," *Ieee Photonics Technol. Lett.*, vol. 23, no. 13, pp. 851–853, 2011.

[20] P. J. Winzer and D. T. Neilson, "From Scaling Disparities to Integrated Parallelism: A Decathlon for a Decade," *J. Light. Technol.*, vol. 35, no. 5, pp. 1099–1115, 2017.

[21] P. J. Winzer, D. A. T. N. Eilson, A. N. R. C. Hraplyvy, N. B. Labs, and H. Road, "Fiber-optic transmission and networking : the previous 20 and the next 20 years [Invited]," *Opt. Express*, vol. 26, no. 18, pp. 24190–24239, 2018.

[22] G. M. Saridis, D. Alexandropoulos, G. Zervas, and D. Simeonidou, "Survey and evaluation of space division multiplexing: From technologies to optical networks," *IEEE Commun. Surv. Tutorials*, vol. 17, no. 4, pp. 2136–2156, 2015.

[23] A. M. Ortiz and R. L. Sáez, "Multi-Core Optical Fibers: Theory, Applications and Opportunities," *Sel. Top. Opt. Fiber Technol. Appl.*, no. February, 2018.

[24] K. Saitoh and S. Matsuo, "Multicore fiber technology," *J. Light. Technol.*, vol. 34, no. 1, 2016.

[25] T. Hayashi, T. Taru, O. Shimakawa, T. Sasaki, and E. Sasaoka, "Design and fabrication of ultra-low crosstalk and low-loss multi-core fiber," *Opt. Express*, vol. 19, no. 17, p. 16576, 2011.

[26] T. Hayashi, T. Taru, O. Shimakawa, T. Sasaki, and E. Sasaoka, "Ultra-low-crosstalk multi-core fiber feasible to ultra-long-haul transmission," *2011 Opt. Fiber Commun. Conf. Expo. Natl. Fiber Opt. Eng. Conf.*, pp. 1–3, 2011.

[27] J. Sakaguchi *et al.*, "Space division multiplexed transmission of 109-Tb/s data signals using homogeneous seven-core fiber," *J. Light. Technol.*, vol. 30, no. 4, pp. 658–665, 2012.

[28] A. Sano *et al.*, "409-Tb/s + 409-Tb/s crosstalk suppressed bidirectional MCF transmission over 450 km using propagation-direction interleaving.," *Opt. Express*, vol. 21, no. 14, pp. 16777–16783, 2013.

[29] J. Sakaguchi *et al.*, "19-core MCF transmission system using EDFA with shared core pumping coupled via free-space optics.," *Opt. Express*, vol. 22, no. 1, pp. 90–5, 2014.

[30] B. J. Puttnam *et al.*, "2.15 Pb/s transmission using a 22 core homogeneous single-mode multi-core fiber and wideband optical comb," in *2015 European Conference on Optical Communication (ECOC)*, 2015, pp. 1–3.

[31] Y. Amma *et al.*, "High-density Multicore Fiber with Heterogeneous Core Arrangement," in *Optical Fiber Communication Conference*, 2015, p. Th4C.4.

[32] S. Matsuo *et al.*, "High-Spatial-Multiplicity Multicore Fibers for Future Dense Space-Division-Multiplexing Systems," *J. Light. Technol.*, vol. 34, no. 6, pp. 1464–1475, Mar. 2016.

[33] T. Mizuno *et al.*, "Long-Haul Dense Space-Division Multiplexed Transmission over Low-Crosstalk Heterogeneous 32-Core Transmission Line Using a Partial Recirculating Loop System," *J. Light. Technol.*, vol. 35, no. 3, pp. 488–498, 2017.

[34] S. K. Korotky, "Price-Points for Components of Multi-Core Fiber Communication Systems in Backbone Optical Networks," *J. Opt. Commun. Netw.*, vol. 4, no. 5, p. 426, 2012.

[35] Y. Li, N. Hua, and X. Zheng, "CapEx advantages of multi-core fiber networks," *Photonic Netw. Commun.*, vol. 31, no. 2, pp. 228–238, 2016.

[36] R. Proietti *et al.*, "3D Elastic Optical Networking in the Temporal , Spectral , and Spatial Domains," *IEEE Commun. Mag.*, no. February, pp. 79–87, 2015.

[37] M. Yang, Q. Wu, and Y. Zhang, "Joint Assignment of Spatial Granularity, Routing, Modulation, and Spectrum in SDM-EONs: Minimizing the Network CAPEX Considering Spectrum, WSS, and Laser Resources," *J. Light. Technol.*, vol. 36, no. 18, pp. 4153–4166,

2018.

[38] M. Yaghubi-Namaad, A. G. Rahbar, and B. Alizadeh, “Adaptive modulation and flexible resource allocation in space-division- multiplexed elastic optical networks,” *J. Opt. Commun. Netw.*, vol. 10, no. 3, pp. 240–251, 2018.

[39] S. Fujii, H. Tode, Y. Hirota, and H. Tode, “Dynamic Resource Allocation with Virtual Grid for Space Division Multiplexed Elastic Optical Network,” *Eur. Conf. Opt. Commun.*, pp. 2–4, 2013.

[40] H. M. N. S. Oliveira and N. L. S. da Fonseca, “Protection, Routing, Modulation, Core and Spectrum Allocation in SDM Elastic Optical Networks,” *IEEE Commun. Lett.*, vol. PP, no. c, pp. 1–1, 2018.

[41] A. Muhammad, G. Zervas, and R. Forchheimer, “Resource Allocation for Space-Division Multiplexing: Optical White Box Versus Optical Black Box Networking,” *J. Light. Technol.*, vol. 33, no. 23, pp. 4928–4941, Dec. 2015.

[42] Y. Zhao *et al.*, “Super-channel oriented routing, spectrum and core assignment under crosstalk limit in spatial division multiplexing elastic optical networks,” *Opt. Fiber Technol.*, vol. 36, pp. 249–254, 2017.

[43] H. Tode and Y. Hirota, “Routing, Spectrum, and Core and/or Mode Assignment on Space-Division Multiplexing Optical Networks [Invited],” *J. Opt. Commun. Netw.*, vol. 9, no. 1, p. A99, Jan. 2017.

[44] J. Zhu and Z. Zhu, “Physical-Layer Security in MCF-based SDM-EONs: Would Crosstalk-Aware Service Provisioning be Good Enough,” *J. Light. Technol.*, vol. 8724, no. c, pp. 1–11, 2017.

[45] M. Yang, Y. Zhang, and Q. Wu, “Routing , Spectrum , and Core Assignment in SDM-EONs With MCF : Node-Arc ILP / MILP Methods and an Efficient XT-Aware Heuristic Algorithm,” *J. Opt. Commun. Netw.*, vol. 10, no. 3, pp. 195–208, Mar. 2018.

[46] M. Ruiz *et al.*, “Planning fixed to flexgrid gradual migration: Drivers and open issues,” *IEEE Commun. Mag.*, vol. 52, no. 1, pp. 70–76, 2014.

[47] M. M. Filer and S. Tibuleac, “N-degree ROADM Architecture Comparison: Broadcast-and-Select versus Route-and-Select in 120 Gb/s DP-QPSK Transmission Systems,” in *Optical Fiber Communication Conference*, 2014, p. Th1I.2.

[48] B. Collings, “New devices enabling software-defined optical networks,” *IEEE Commun. Mag.*, vol. 51, no. 3, pp. 66–71, Mar. 2013.

[49] D. M. Marom and M. Blau, "Switching solutions for WDM-SDM optical networks," *IEEE Commun. Mag.*, vol. 53, no. 2, pp. 60–68, 2015.

[50] D. M. Marom *et al.*, "Survey of Photonic Switching Architectures and Technologies in Support of Spatially and Spectrally Flexible Optical Networking [Invited]," *J. Opt. Commun. Netw.*, vol. 9, no. 1, p. 1, Jan. 2017.

[51] L. E. Nelson *et al.*, "Spatial superchannel routing in a two-span ROADM system for space division multiplexing," *J. Light. Technol.*, vol. 32, no. 4, pp. 783–789, 2014.

[52] S. Ben-Ezra *et al.*, "First WDM-SDM Optical Network with Spatial Sub-Group Routing ROADM Nodes Supporting Spatial Lane Changes," in *Advanced Photonics 2018 (BGPP, IPR, NP, NOMA, Sensors, Networks, SPPCom, SOF)*, 2018, p. NeTh1F.3.

[53] N. Amaya *et al.*, "Fully-elastic multi-granular network with space/frequency/time switching using multi-core fibres and programmable optical nodes," *Opt. Express*, vol. 21, no. 7, p. 8865, Apr. 2013.

[54] N. Amaya *et al.*, "Software defined networking (SDN) over space division multiplexing (SDM) optical networks: features, benefits and experimental demonstration.," *Opt. Express*, vol. 22, no. 3, pp. 3638–3647, 2014.

[55] P. Sayyad Khodashenas *et al.*, "Comparison of Spectral and Spatial Super-channel Allocation Schemes for SDM Networks," *J. Light. Technol.*, vol. 8724, no. c, pp. 1–1, 2016.

[56] B. Shariati *et al.*, "Evaluation of the Impact of Different SDM Switching Strategies in a Network Planning Scenario," *Opt. Fiber Commun. Conf.*, no. 1, pp. 6–8, 2016.

[57] B. Shariati, D. Klonidis, D. Siracusa, F. Pederzolli, and L. Velasco, "Impact of Traffic Profile on the Performance of Spatial Superchannel Switching in SDM Networks," *42nd Eur. Conf. Exhib. Opt. Commun.*, no. M.1.F.1, pp. 73–75, 2016.

[58] J. M. Rivas-Moscoso, B. Shariati, A. Mastropaolo, D. Klonidis, and I. Tomkos, "Cost Benefit Quantification of SDM Network Implementations based on Spatially Integrated Network Elements," *42nd Eur. Conf. Exhib. Opt. Commun.*, no. M.1.F.4, pp. 82–84, 2016.

[59] F. Pederzolli, D. Siracusa, B. Shariati, J. M. Rivas-Moscoso, E. Salvadori, and I. Tomkos, "Improving Performance of Spatially Joint-Switched Space Division Multiplexing Optical Networks via Spatial Group Sharing," *J. Opt. Commun. Netw.*, vol. 9, no. 3, p. B1, Mar. 2017.

[60] J.-M. Rivas-Moscoso *et al.*, "Comparison of CD (C) ROADM Architectures for Space

Division Multiplexed Networks," *Opt. Fiber Commun. Conf.*, no. C, pp. 3–5, Mar. 2017.

[61] B. Shariati *et al.*, "Impact of spatial and spectral granularity on the performance of SDM networks based on spatial superchannel switching," *J. Light. Technol.*, vol. 35, no. 13, pp. 2559–2568, 2017.

[62] I. Tomkos, D. Klonidis, P. Zakynthinos, D. M. Marom, and D. Siracusa, "Concept paper of INSPACE project D7.1," 2015.

[63] "Lumentum: TrueFlex Twin 1x35 WSS." [Online]. Available: https://www.lumentum.com/en/products/trueflex-twin-1x35-wavelength-selective-switch. [Accessed: 28-Oct-2018].

[64] N. K. Fontaine *et al.*, "Heterogeneous Space-Division Multiplexing and Joint Wavelength Switching Demonstration," *Opt. Fiber Commun. Conf.*, p. Th5C.5, 2015.

[65] D. Klonidis *et al.*, "Spectrally and spatially flexible optical network planning and operations," *IEEE Commun. Mag.*, vol. 53, no. 2, pp. 69–78, 2015.

[66] E. Palkopoulou, G. Bosco, A. Carena, D. Klonidis, P. Poggiolini, and I. Tomkos, "Nyquist-WDM-Based Flexible Optical Networks: Exploring Physical Layer Design Parameters," *J. Light. Technol.*, vol. 31, no. 14, pp. 2332–2339, Jul. 2013.

[67] J. M. Rivas-Moscoso *et al.*, "Cost and power consumption model for flexible super-channel transmission with all-optical sub-channel add/drop capability," *Int. Conf. Transparent Opt. Networks*, vol. 2015–Augus, pp. 1–4, 2015.

[68] M. D. Feuer *et al.*, "Joint Digital Signal Processing Receivers for Spatial Superchannels," *IEEE Photonics Technol. Lett.*, vol. 24, no. 21, pp. 1957–1960, Nov. 2012.

[69] H. Zang, J. P. Jue, B. Mukherjee, H. Zang, and J. P. Jue, "A Review of Routing and Wavelength Assignment Approaches for Wavelength Routed Optical WDM Networks," *Opt. NETWORKS Mag.*, vol. 1, pp. 47--60, 2000.

[70] B. Jaumard, C. Meyer, B. Thiongane, and A. L. Formulation, "ILP Formulations and Optimal Solutions for the RWA Problem," in *IEEE Global Telecommunications Conference, 2004. GLOBECOM '04*, 2004, pp. 1918–1924.

[71] G. N. Rouskas, "Routing and Wavelength Assignment in Optical WDM Networks," in *Wiley Encyclopedia of Telecommunications*, Hoboken, NJ, USA: John Wiley & Sons, Inc., 2003.

[72] A. E. Ozdaglar and D. P. Bertsekas, "Routing and wavelength assignment in optical networks," *IEEE/ACM Trans. Netw.*, vol. 11, no. 2, pp. 259–272, 2003.

[73] K. Christodoulopoulos, I. Tomkos, and E. a Varvarigos, “Elastic Bandwidth Allocation in Flexible OFDM- based Optical Networks,” *J. Light. Technol.*, vol. 29, no. 9, pp. 1354–1366, 2011.

[74] J. Y. Yen, “Finding the K shortest loopless paths in a network,” *Manage. Sci.*, vol. 17, no. 11, Jul. 1971.

[75] M. Klinkowski and K. Walkowiak, “Routing and spectrum assignment in spectrum sliced elastic optical path network,” *IEEE Commun. Lett.*, vol. 15, no. 8, pp. 884–886, 2011.

[76] M. Dallaglio, A. Giorgetti, N. Sambo, L. Velasco, and P. Castoldi, “Routing , Spectrum , and Transponder Assignment in Elastic Optical Networks,” *J. Light. Technol.*, vol. 33, no. 22, pp. 4648–4658, 2015.

[77] C. Rottondi, P. Boffi, P. Martelli, and M. Tornatore, “Routing, Modulation Format, Baud Rate and Spectrum Allocation in Optical Metro Rings with Flexible Grid and Few-Mode Transmission,” *J. Light. Technol.*, vol. 35, no. 1, pp. 61–70, Jan. 2017.

[78] N. Sambo *et al.*, “Routing Code and Spectrum Assignment (RCSA) in Elastic Optical Networks,” *J. Light. Technol.*, vol. 33, no. 24, pp. 5114–5121, Dec. 2015.

[79] D. J. Ives, P. Bayvel, and S. J. Savory, “Routing, modulation, spectrum and launch power assignment to maximize the traffic throughput of a nonlinear optical mesh network,” *Photonic Netw. Commun.*, vol. 29, no. 3, pp. 244–256, Jun. 2015.

[80] D. Siracusa, F. Pederzolli, D. Klonidisz, V. Lopezy, and E. Salvadori, “Resource allocation policies in SDM optical networks (Invited paper),” *2015 Int. Conf. Opt. Netw. Des. Model.*, pp. 168–173, 2015.

[81] H. Tode and Y. Hirota, “Routing, spectrum and core assignment for space division multiplexing elastic optical networks,” *2014 16th Int. Telecommun. Netw. Strateg. Plan. Symp.*, 2014.

[82] A. Muhammad, G. Zervas, D. Simeonidou, and R. Forchheimer, “Routing , Spectrum and Core Allocation in Flexgrid SDM Networks with Multi-core Fibers,” in *Optical Network Design and Modelling*, 2014, pp. 19–22.

[83] M. Klinkowski, P. Lechowicz, and K. Walkowiak, “Survey of resource allocation schemes and algorithms in spectrally-spatially flexible optical networking,” *Opt. Switch. Netw.*, vol. 27, no. August 2017, pp. 58–78, 2018.

[84] P. Pavon-Marino, *Optimization of Computer Networks : Modeling and Algorithms. A Hands-On Approach*. Wiley, 2016.

[85] J. Perelló, J. M. Gené, A. Pagès, J. A. Lazaro, and S. Spadaro, "Flex-Grid/SDM Backbone Network Design with Inter-Core XT-Limited Transmission Reach," *J. Opt. Commun. Netw.*, vol. 8, no. 8, p. 540, Aug. 2016.

[86] K. Walkowiak, P. Lechowicz, M. Klinkowski, and A. Sen, "ILP modeling of flexgrid SDM optical networks," in *2016 17th International Telecommunications Network Strategy and Planning Symposium (Networks)*, 2016, pp. 121–126.

[87] P. Lechowicz, K. Walkowiak, and M. Klinkowski, "Selection of spectral-spatial channels in SDM flexgrid optical networks," *2017 21st Int. Conf. Opt. Netw. Des. Model.*, 2017.

[88] M. Klinkowski, G. Zalewski, and K. Walkowiak, "Optimization of Spectrally and Spatially Flexible Optical Networks with Spatial Mode Conversion," in *2018 International Conference on Optical Network Design and Modeling (ONDM)*, 2018, no. May, pp. 148–153.

[89] R. Ramaswami, K. N. Sivarajan, and G. H. Sasaki, *Optical networks: a practical perspective*. 2009.

[90] B. C. B. C. Chatterjee, S. Ba, and E. Oki, "Fragmentation Problems and Management Approaches in Elastic Optical Networks: A Survey," *IEEE Commun. Surv. Tutorials*, vol. 20, no. 1, pp. 1–1, 2017.

[91] A. Rosa, C. Cavdar, S. Carvalho, J. Costa, and L. Wosinska, "Spectrum allocation policy modeling for elastic optical networks," *High Capacit. Opt. Networks Emerging/Enabling Technol.*, 2012.

[92] Y. Sone, A. Hirano, A. Kadohata, M. Jinno, and O. Ishida, "Routing and Spectrum Assignment Algorithm Maximizes Spectrum Utilization in Optical Networks," *37th Eur. Conf. Expo. Opt. Commun.*, 2011.

[93] Y. Yin, M. Zhang, Z. Zhu, and S. J. B. Yoo, "Fragmentation-Aware Routing, Modulation and Spectrum Assignment Algorithms in Elastic Optical Networks," in *Optical Fiber Communication Conference/National Fiber Optic Engineers Conference 2013*, 2013.

[94] A. Castro, L. Velasco, M. Ruiz, M. Klinkowski, J. P. Fernández-Palacios, and D. Careglio, "Dynamic routing and spectrum (re)allocation in future flexgrid optical networks," *Comput. Networks*, vol. 56, no. 12, pp. 2869–2883, Aug. 2012.

[95] F. Cugini *et al.*, "Push-pull defragmentation without traffic disruption in flexible grid optical networks," *J. Light. Technol.*, 2013.

[96] M. Zhang, Y. Yin, R. Proietti, Z. Zhu, and S. J. B. Yoo, "Spectrum Defragmentation

Algorithms for Elastic Optical Networks using Hitless Spectrum Retuning Techniques," *Opt. Fiber Commun. Conf. Fiber Opt. Eng. Conf. 2013*, no. c, p. OW3A.4, 2013.

[97] S. Fujii, Y. Hirota, H. Tode, and K. Murakami, "On-demand spectrum and core allocation for reducing crosstalk in multicore fibers in elastic optical networks," *IEEE/OSA J. Opt. Commun. Netw.*, vol. 6, no. 12, Dec. 2014.

[98] S. Fujii, Y. Hirota, H. Tode, and K. Murakami, "On-Demand Spectrum and Core Allocation for Multi-Core Fibers in Elastic Optical Network," in *Optical Fiber Communication Conference/National Fiber Optic Engineers Conference 2013*, 2013, pp. 6–8.

[99] K. Walkowiak, M. Klinkowski, and P. Lechowicz, "Dynamic Routing in Spectrally Spatially Flexible Optical Networks with Back-to-Back Regeneration," *J. Opt. Commun. Netw.*, vol. 10, no. 5, p. 523, May 2018.

[100] P. Poggiolini, G. Bosco, A. Carena, V. Curri, Y. Jiang, and F. Forghieri, "The GN-Model of Fiber Non-Linear Propagation and its Applications," *J. Light. Technol.*, vol. 32, no. 4, pp. 694–721, Feb. 2014.

[101] A. Carena, G. Bosco, V. Curri, Y. Jiang, P. Poggiolini, and F. Forghieri, "EGN model of non-linear fiber propagation," *Opt. Express*, vol. 22, no. 13, p. 16335, Jun. 2014.

[102] P. J. Winzer, a. H. Gnauck, a. Konczykowska, F. Jorge, and J.-Y. Dupuy, "Penalties from in-band crosstalk for advanced optical modulation formats," *2011 37th Eur. Conf. Exhib. Opt. Commun.*, no. 1, pp. 1–3, 2011.

[103] F. Fidler, P. J. Winzer, M. K. Thottan, and K. Bergman, "Impairment-Aware Optical Networking Using Cross-Layer Communication," *J. Opt. Commun. Netw.*, 2013.

[104] B. Li *et al.*, "The Role of Effective Area in the Design of Weakly Coupled MCF: Optimization Guidance and OSNR Improvement," *IEEE J. Sel. Top. Quantum Electron.*, vol. 22, no. 2, 2016.

[105] M. N. Dharmaweera, L. Yan, M. Karlsson, and E. Agrell, "Nonlinear-Impairments- and Crosstalk-Aware Resource Allocation Schemes for Multicore-Fiber-based Flexgrid Networks," in *42nd European Conference and Exhibition on Optical Communications (ECOC 2016)*, 2016, no. 1, pp. 1223–1225.

[106] S. J. Savory, "Digital Coherent Optical Receivers: Algorithms and Subsystems," *IEEE J. Sel. Top. Quantum Electron.*, vol. 16, no. 5, pp. 1164–1179, 2010.

[107] R. Ryf, S. Chandrasekhar, S. Randel, D. T. Neilson, N. K. Fontaine, and M. Feuer,

"Physical layer transmission and switching solutions in support of spectrally and spatially flexible optical networks," *IEEE Commun. Mag.*, vol. 53, no. 2, pp. 52–59, Feb. 2015.

[108] N. Goldshtein *et al.*, "Fine Resolution Photonic Spectral Processor Using a Waveguide Grating Router With Permanent Phase Trimming," *J. Light. Technol.*, vol. 34, no. 2, pp. 379–385, Jan. 2016.

[109] T. Mizuno, H. Takara, K. Shibahara, A. Sano, and Y. Miyamoto, "Dense space division multiplexed transmission over multicore and multimode fiber for long-haul transport systems," *J. Light. Technol.*, vol. 34, no. 6, pp. 1484–1493, 2016.

[110] T. Tanaka *et al.*, "Demonstration of Single-Mode Multicore Fiber Transport Network with Crosstalk-Aware In-Service Optical Path Control," *J. Light. Technol.*, vol. 8724, no. c, 2017.

[111] R. Ryf *et al.*, "MIMO-based crosstalk suppression in spatially multiplexed 3 × 56-Gb/s PDM-QPSK signals for strongly coupled three-core fiber," *IEEE Photonics Technol. Lett.*, vol. 23, no. 20, pp. 1469–1471, 2011.

[112] Y. Li, N. Hua, and X. Zheng, "Routing, wavelength and core allocation planning for multi-core fiber networks with MIMO-based crosstalk suppression," *2015 Opto-Electronics Commun. Conf. OECC 2015*, vol. 2, pp. 2–4, 2015.

[113] S. Randel, P. J. Winzer, M. Montoliu, and R. Ryf, "Complexity Analysis of Adaptive Frequency-Domain Equalization for MIMO-SDM Transmission," *39th Eur. Conf. Exhib. Opt. Commun. (ECOC 2013)*, pp. 801–803, 2013.

[114] Y. Li, N. Hua, and X. Zheng, "A Capacity Analysis for Space Division Multiplexing Optical Networks with MIMO Equalization," *Opt. Fiber Commun. Conf.*, p. Th2A.15, 2017.

[115] N. P. Diamantopoulos, B. Shariati, and I. Tomkos, "On the Power Consumption of MIMO Processing and its Impact on the Performance of SDM Networks," *Opt. Fiber Commun. Conf.*, p. Th2A.18, 2017.

[116] Y. Wang, X. Cao, and Y. Pan, "A study of the routing and spectrum allocation in spectrum-sliced Elastic Optical Path networks," *Proc. - IEEE INFOCOM*, pp. 1503–1511, 2011.

[117] S. Kirkpatrick, C. D. Gelatt, and M. P. Vecchi, "Optimization by simulated annealing.," *Science*, vol. 220, no. 4598, pp. 671–80, May 1983.

[118] IBM, "IBM ILOG CPLEX Optimizer." [Online]. Available: https://www.ibm.com/products/ilog-cplex-optimization-studio.

[119] J. Wu, M. Barahona, Y. Tan, and H. Deng, "Robustness of random graphs based on graph spectra," *Chaos An Interdiscip. J. Nonlinear Sci.*, vol. 22, no. 4, p. 043101, Dec. 2012.

[120] T. Mizuno *et al.*, "12-core x 3-mode Dense Space Division Multiplexed Transmission over 40 km Employing Multi-carrier Signals with Parallel MIMO Equalization," in *Optical Fiber Communication Conference: Postdeadline Papers*, 2014, p. Th5B.2.

[121] T. Sakamoto *et al.*, "Experimental and numerical evaluation of inter-core differential mode delay characteristic of weakly-coupled multi-core fiber," *Opt. Express*, vol. 22, no. 26, pp. 31966–31976, 2014.

[122] M. Klinkowski, P. Lechowicz, and K. Walkowiak, "A Study on the Impact of Inter-Core Crosstalk on SDM Network Performance," in *2018 International Conference on Computing, Networking and Communications (ICNC)*, 2018.

[123] T. Sakamoto *et al.*, "Low-loss and Low-DMD Few-mode Multi-core Fiber with Highest Core Multiplicity Factor," *Opt. Fiber Commun. Conf. Postdeadline Pap.*, vol. 1, pp. 20–22, Mar. 2016.

[124] T. Hayashi, Y. Tamura, T. Hasegawa, and T. Taru, "Record-Low Spatial Mode Dispersion and Ultra-Low Loss Coupled Multi-Core Fiber for Ultra-Long-Haul Transmission," *J. Light. Technol.*, vol. 35, no. 3, pp. 450–457, 2017.

[125] R. G. H. Van Uden, C. M. Okonkwo, R. H. G. Van Uden, H. De Waardt, and A. M. J. Koonen, "The impact of bit-width reduced MIMO equalization for few mode fiber transmission systems," *Eur. Conf. Opt. Commun. ECOC*, pp. 2–4, 2014.

[126] S. Randel *et al.*, "First real-time coherent MIMO-DSP for six coupled mode transmission," *2015 IEEE Photonics Conf. IPC 2015*, 2015.

[127] "Net2Plan - The open-source network planner." [Online]. Available: http://www.net2plan.com. [Accessed: 20-Oct-2018].

[128] L. Velasco *et al.*, "Modeling the routing and spectrum allocation problem for flexgrid optical networks," *Photonic Netw. Commun.*, vol. 24, no. 3, pp. 177–186, Dec. 2012.

[129] "SNDlib." [Online]. Available: http://sndlib.zib.de. [Accessed: 20-Oct-2018].

[130] "JOM - The Java Optimization Modeler." [Online]. Available: http://www.net2plan.com/jom. [Accessed: 20-Oct-2018].

[131] E. Awad, "Multicore optical fiber Y-splitter," *Opt. Express*, vol. 23, no. 20, p. 25661, 2015.